The Dissertation Committee for Erica Lynn Belmont certifies that this is the approved version of the following dissertation:

Controlling Parameters of Excess Enthalpy Combustion

Committee:

Janet L. Ellzey, Supervisor

Noel T. Clemens

Ofodike A. Ezekoye

Carlos H. Hidrovo

Li Shi

Controlling Parameters of Excess Enthalpy Combustion

by

Erica Lynn Belmont, B.S.Ch.E.; M.S.

Dissertation

Presented to the Faculty of the Graduate School of

The University of Texas at Austin

in Partial Fulfillment

of the Requirements

for the Degree of

Doctor of Philosophy

The University of Texas at Austin

May 2014

Controlling Parameters of Excess Enthalpy Combustion

Erica Lynn Belmont, Ph.D.

The University of Texas at Austin, 2014

Supervisor: Janet L. Ellzey

Excess enthalpy combustion utilizes heat recirculation, in which heat is transferred from hot products to cold reactants to effectively preheat the reactants, in order to achieve improved combustion performance through the extension of flammability limits and increased burning rate. This research examines the effect of key parameters in excess enthalpy combustion on combustion stability, fuel conversion, and product species production through experimental and numerical investigation. Operating condition parameters that are studied include inlet reactant equivalence ratio and inlet velocity, and reactor geometry parameters that are studied include reactor channel height and length. Premixed reactants, including gaseous and liquid fuels, are investigated at rich and lean conditions. The examination of liquid fuels and the ability of a reactor to support rich and lean combustion of both gaseous and liquid fuels is a significant demonstration of a reactor's flexibility for practical applications.

This research experimentally and numerically examines excess enthalpy combustion in a counter-flow reactor. First, the counter-flow reactor, previously used for thermal partial oxidation of gaseous hydrocarbon fuels, is used in experiments to reform a liquid hydrocarbon fuel, heptane, to syngas. The effect of inlet operating conditions, including reactant equivalence ratio and inlet velocity, on combustion stability and product composition is explored. Second, lean combustion is demonstrated through experiments in the same counter-flow reactor previously used in reforming studies. The effect of inlet operating conditions, including reactant equivalence ratio and inlet velocity, on combustion stability and pollutant concentrations in combustion products is studied. An analytical model, previously developed for rich combustion, is adapted to qualitatively predict the behavior of the counter-flow reactor in response to changes in lean operating conditions. Third, lean combustion in the counter-flow reactor is further studied by examining the combustion of increasingly complex gaseous and liquid fuels. Again, the effect of inlet operating conditions, including reactant equivalence ratio and inlet velocity, on combustion stability and pollutant concentrations in combustion products is studied. Fourth and finally, a computational scaling study examines the impact of counter-flow reactor channel geometry on combustion stability, temperature increase above adiabatic values, heat recirculation, and fuel and product species conversion efficiency.

Table of Contents

List of Tables

List of Figures

x

1   INTRODUCTION

Premixed combustion is the rapid, exothermic reaction of thoroughly mixed fuel and oxidizer reactants. One of the most important characteristics of premixed combustion is the concept of upper and lower flammability limits, defined as the maximum and minimum concentrations of a given fuel in an oxidizer required for self-sustained combustion. Flammability limits of fuel and oxidizer mixtures are experimentally determined, for example by monitoring temperature, pressure or radiation as a premixed flame propagates in a tube or spherical enclosure. Since flammability limits are sensitive to specific experimental conditions, standard protocols have been established. Under all standards, a mixture is considered to be flammable if a flame is observed to propagate a significant distance from the ignition source.

Conventional flammability limits are based upon the conditions of the unburned reactants, including the temperature and pressure of the mixture. Reactant mixtures beyond conventional flammability limits may be made flammable with no net energy addition to the reactor system through a technique called superadiabatic combustion. This research studies the superadiabatic combustion of reactant mixtures that are near or beyond the conventional flammability limits of the fuels. The influence of controlling parameters on superadiabatic combustion characteristics, including combustion stability, fuel conversion and product species production, are studied.

1.1 Fundamentals of superadiabatic combustion

Equilibrium and flame temperatures of combustion products under adiabatic reaction conditions are dependent upon a number of factors, including the composition of the reactants and their initial temperature. Addition of energy to fuel/air reactants in the form of preheating will translate to a change in product composition as well as an increase in equilibrium and flame temperatures. One available source of the energy needed to preheat reactants is hot combustion products, from which heat can be recirculated to preheat reactants prior to combustion. The idea of heat recirculation from combustion products to preheat reactants was proposed by Weinberg in 1971 [1], who suggested that temperatures in excess of adiabatic flame temperatures, called superadiabatic temperatures, may be achieved without any net addition of energy to the system. Such a process is known as superadiabatic or excess enthalpy combustion.

Figure 1 shows the sensible enthalpy of combustion gases as they progress along the flow coordinate, and convert from reactant species to product species through combustion. In a combustion scenario without heat recirculation, shown by a dashed line in Figure 1, the sensible enthalpy of the reactant gases does not change in the flow direction until combustion occurs; the enthalpy of combustion is released within the flame and the sensible enthalpy of the products increases by that amount. The combustion gases are then mostly or completely converted to product species, and their enthalpy is maximized. Following combustion, the enthalpy of the product gases remains at this maximum value if the system is adiabatic and there are no external losses. If there are losses, as in any

practical system, the enthalpy of the product species will decrease by some amount equal

to the losses, as shown in Figure 1.
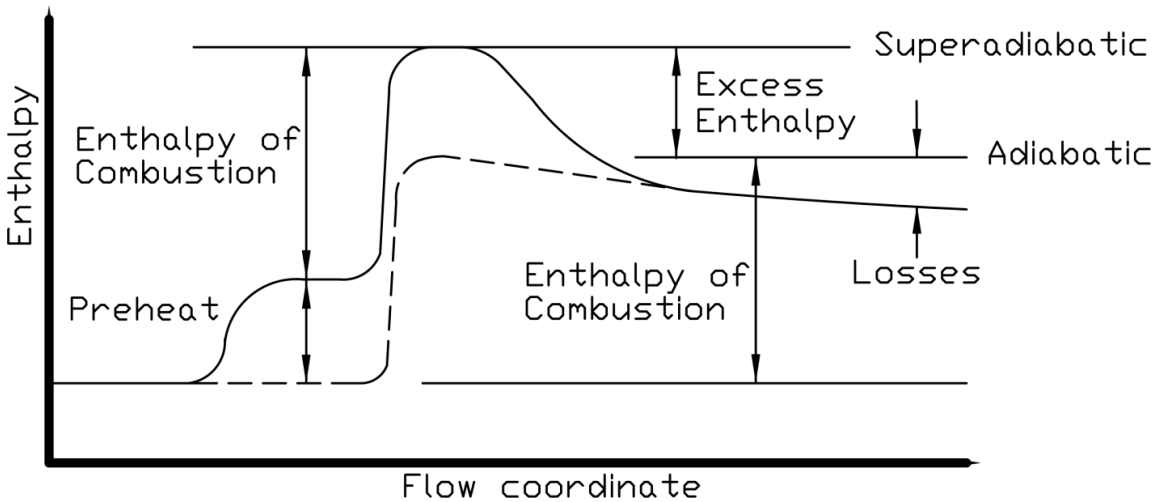
Figure 1. Combustion gas sensible enthalpy along flow coordinate with (solid line) and without (dashed line) heat recirculation

In a combustion scenario with heat recirculation, as shown by the solid line in Figure 1, the sensible enthalpy of the reactant gases increases prior to the release of the enthalpy of combustion in the flame. This pre-combustion increase is due to energy recirculated by heat transfer from hot combustion products to cold incoming reactants. The effect of this energy recirculation and enthalpy addition is an increase in the temperature of the reactant gases – the reactants are preheated prior to combustion. Following this region of preheat, the reactants combust and the enthalpy of combustion is released. The sensible enthalpy of the product gases increases by the same amount as in the scenario without heat recirculation – that amount is the enthalpy of combustion – but the peak sensible

enthalpy of the gases is now higher than it would be without heat recirculation. The peak sensible enthalpy of the product gases is now greater than the adiabatic value by the amount of preheat enthalpy, and the gases are at *superadiabatic* conditions. Following combustion and in the absence of external heat losses, the enthalpy of the product gases decreases to adiabatic values as the excess enthalpy of the gases is recirculated to continue preheating cold reactants. In a practical system, the enthalpy of the product gases will decrease to below adiabatic values due to heat losses.

1.2   Effects of excess enthalpy on combustion

Rich and lean flammability limits denote the high and low limits, respectively, of fuel-to-air ratios that will burn under given conditions. Flammability limits are dependent upon a number of factors, including reactant species, pressure and temperature. Figure 2, reproduced from [2], shows the qualitative effect of initial reactant temperature on flammability limits. As the temperature of combustion reactants is increased, flammability limits on both the fuel-lean and fuel-rich sides of stoichiometry are extended. For example, a reactant mixture with fuel (or combustible) concentration and temperature indicated by point A in Figure 2 is below the lower flammability limit, and therefore not flammable. If, however, the reactant mixture with the same fuel concentration is heated to a higher temperature, so that its properties are given by point B in Figure 2, the reactant mixture is now above the lower flammability limit, and is therefore flammable. The reactant mixtures in this study are at temperatures above their respective saturation points and below their auto-ignition temperatures.
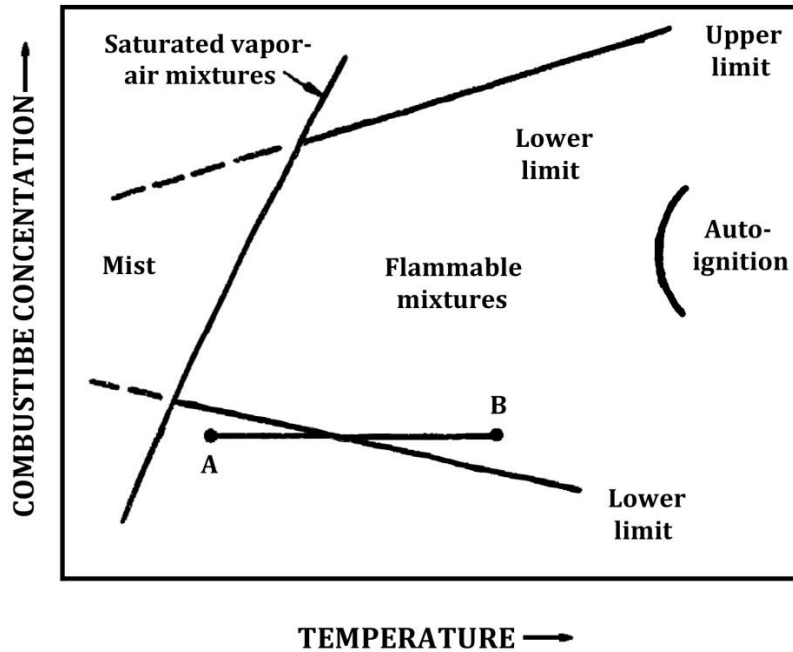
Figure 2. Effect of reactant temperature on rich and lean flammability limits, reproduced from [2]

Superadiabatic combustion effectively preheats reactants with no external or net addition of energy to the reactor, and the flammability limits of a fuel/air reactant mixture can be extended beyond their conventional limits based upon inlet conditions. Theoretical work on mixtures flowing through porous media has shown that any fuel/oxidizer mixture should react with sufficient energy addition or heat recirculation [3]. In practice, heat loss and material properties limit the amount of heat recirculation achievable; however, the operating range can be dramatically broader than that predicted by conventional flammability limits based upon initial reactant condition. The US Bureau of Mines

published data that detailed known initial temperature effects on flammability limits for over 200 combustible species [2]. Hustad and Sonju [4] studied the effect of elevated temperature on the lower flammability limit for upward propagating methane/air flames in a 1.8 m tube and showed that with no preheating, the lean flammability limit of reactants at 25°C was ~5.5% methane by volume. At a temperature of 300°C, the limit was lowered to ~3.8%. Wierzba and Wang [5] showed similar results for the lower flammability limit of methane at 300°C, and an extension of the rich limit from 14% at 25°C to 17% at 300°C. Fan et al. [6] studied quenching mechanisms of methane/air in microscale quartz channels and observed extension of the lower flammability limit to approximately an equivalence ratio (ϕ) of 0.4 as well as a decrease in the quenching diameter with increasing wall temperature. More extreme levels of preheating were achieved by Maruta et al. [7] who studied combustion in microchannels with channel wall temperatures up to 1000°C. Flames were stabilized for equivalence ratios of ϕ = 0.05-1.9 and over a wide range of inlet velocities (u).

A second aspect of superadiabatic combustion that makes it potentially advantageous is the effect of excess enthalpy on burning velocity. An increase in burning velocity occurs with an increase in initial reactant temperature [8-11]. This has been described by a number of proposed correlations of the form given by Equation 1

$$s_L = s_{Lo} \left(\frac{T}{T_o}\right)^a \tag{1}$$

where S_{Lo} is the burning velocity at the reference temperature T_o, S_L is the burning velocity at the unburned reactant temperature of interest T, and a is a value determined by data fitting. Konnov [12] reports a number of values in the literature for a for stoichiometric methane/air which range from 1.42 to 2.4. Therefore, superadiabatic reactor operation may permit increased burning rates, which equates to higher reactor throughput.

1.3   Heat recirculating reactors

Combustion of reactant mixtures beyond conventional flammability limits can be accomplished by a number of methods, including catalytic and non-catalytic techniques. Some heat-recirculating reactors utilize catalyst to increase reaction rates while operating at moderate temperatures. Non-catalytic reactors, which are the focus of this research, utilize elevated temperatures to increase reaction rates. They do not have the same fuel purity requirements and temperature limits as catalytic reactors, which are restricted by a catalyst surface that is prone to damage.

Non-catalytic superadiabatic combustion is a technique that relies on energy addition to reactant mixtures in order to elevate reaction temperatures, thereby increasing the rate of chemical conversion. Figure 3 illustrates how reactors operate with and without heat recirculation. The schematic of a reactor operating without heat recirculation (Figure 3a) shows cold reactants entering from the top, reacting in the combustion zone, and leaving the reactor in the form of combustion products and at the adiabatic equilibrium

7

temperature, assuming no external losses from the reactor. In contrast, the schematic of a reactor operating with heat recirculation (Figure 3b) also shows cold reactants entering from the top, but those reactants are preheated by heat transfer from hot combustion products in the reactor prior to reacting in the combustion zone. The preheated reactants then react in the combustion zone, and leave the combustion zone at temperatures in excess of the adiabatic equilibrium temperature, or superadiabatic temperatures. The superadiabatic combustion products then transfer their excess enthalpy to incoming cold reactants, thereby continuing the steady state heat recirculation, and leave the reactor in the form of combustion products and at the adiabatic equilibrium temperature, again assuming no external losses from the reactor.

The addition of energy to reactants can be achieved internally or externally. This study focuses on internal heat recirculation reactors, in which energy in transferred internally by conduction, radiation and convection within the solid and gaseous phases of the reactor from hot combustion products to incoming reactants. As a result of this heat recirculation, reactants are preheated and peak temperatures within the combustion zone can significantly exceed the adiabatic equilibrium temperature, or the temperature predicted by chemical equilibrium. This is known as excess enthalpy combustion at superadiabatic temperatures [1].
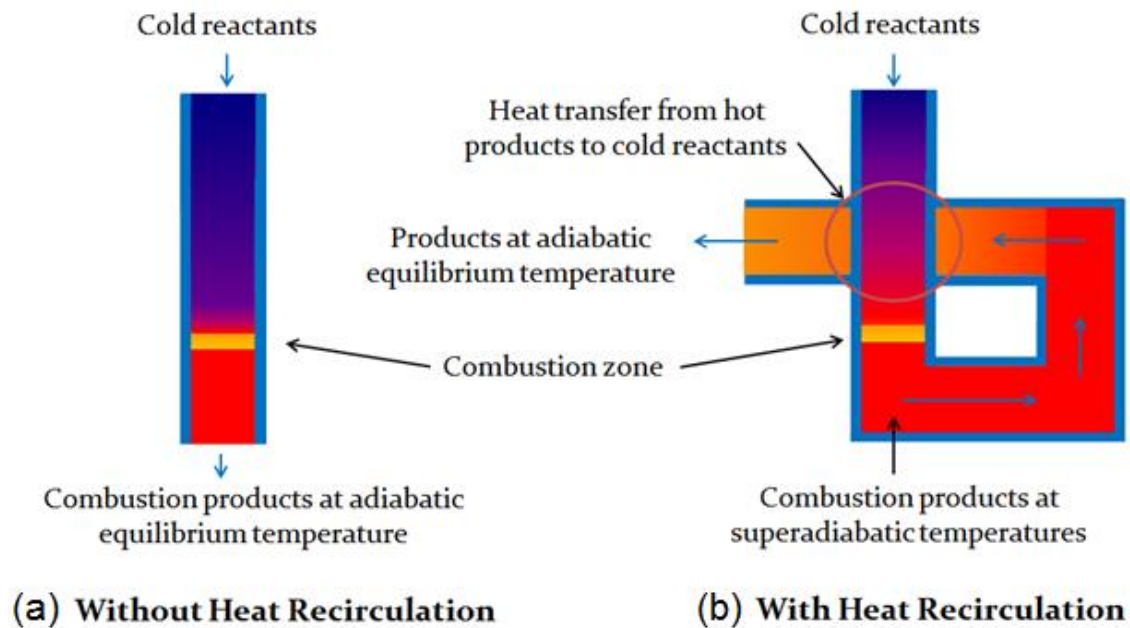
Figure 3. Schematics illustrate generic reactor operating (a) without heat recirculation, and (b) with heat recirculation

Various non-catalytic reactors achieve internal heat recirculation through the solid material of the reactor itself. In some reactor designs, the combustor consists of a solid matrix, such as a reticulated foam or packed bed of spheres [13-17]. This type of reactor is called a filtration reactor, and some of these designs do not have a means of stabilizing the reaction front which may propagate through the solid matrix. When the front propagates downstream, it passes over preheated solid and the gas gains additional energy, resulting in significantly superadiabatic temperatures. These high temperatures increase reaction rates and potentially result in high fuel conversion efficiencies [18, 19]. A disadvantage of this design is that the wave ultimately reaches the end of the reactor

requiring periodic restarting or reversal of the flow [20]. Porous media reactors have been used in numerous lean and rich combustion studies [13, 21].

Other reactor designs have a means of stabilizing the reaction front, but these designs typically do not achieve temperatures as high as those achieved under propagating reaction front conditions. A two section porous media reactor can support a stationary combustion zone, and this design has been used to combust lean and rich fuel mixtures including methanol, methane, octane and automotive-grade petrol [22, 23]. Alternatively, a diverging section of porous media permits stabilized reaction zones for fuel reforming and has been used successfully in several studies [24-26].

A Swiss roll reactor [27-29] has been used for both reforming and thermal oxidation [8]. In this reactor design, a central combustion chamber is surrounded by alternating inlet and outlet flow channels that wrap around the combustion chamber. Cold incoming reactants and hot combustion products flow through these channels, and heat from the exhaust is transferred through the walls to the incoming reactants. The same basic principle is applied in the design of the counter-flow reactor used in this research. This reactor consists of straight channels with no predetermined combustion zone location within the channels, which simplifies the geometry as compared to other reactor designs and permits a wide range of stable operating conditions. Theoretical analyses and experimental studies of channel reactors have shown that superadiabatic temperatures, increased burning velocities, and broadened flammability limits can be achieved [8, 30-33].

1.4   Counter-flow reactor

The counter-flow reactor is a heat recirculating reactor design consisting of parallel channels that recirculate heat from hot products to cold reactants through the walls of adjacent channels [34]. Figure 4 is a schematic of the operating principle of the counter-flow reactor. The flow direction alternates in adjacent channels so that energy from hot combustion products is transferred to cold incoming reactants. The preheated reactants may reach temperatures in the combustion zone that are superadiabatic.

Ju et al. [30, 31], using both numerical analysis and experiments of flames in mesoscale channels, in which the flame scale is on the order of a few millimeters, achieved broadened flammability limits and burning velocities greater than those of adiabatic flames. The counter-flow reactor design has been proposed analytically [31, 34, 35] and previously validated in experimental studies on the reforming of methane [36] and propane [37]. This work expanded upon those initial experimental studies to examine the reforming of heptane [38], as well as combustion of lean methane [39], propane and heptane [40].
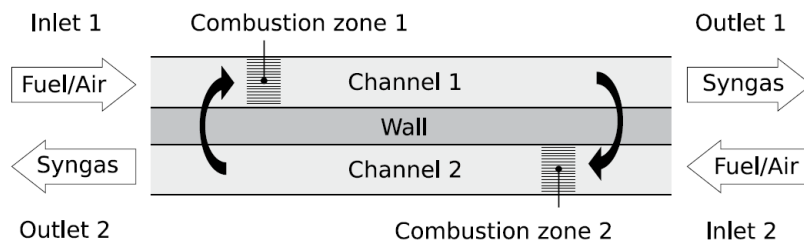
Figure 4. Counter-flow reactor utilizes heat transfer from hot combustion products through channel walls to preheat incoming reactants

Figure 5 shows the counter-flow reactor used in this research, which is the same design used in previous experimental studies on reforming of methane and propane [36, 37]. Ceramic walls, end plugs and porous foam inserts are constructed of silicon carbide. Dimensions, including channel width and length, are shown for the reactor utilized in the experimental portions of this work. The experimental reactor consists of four 4 mm high parallel channels constructed of 1 mm thick silicon carbide (SiC) walls. The reactor is 17.3 cm long, with a 91.5 mm long main section and two 40.8 mm long reactor heads where inlets and outlets are located. Also located in the reactor heads are end plugs, which prevent the mixing of combustion products and unreacted fuel/air mixture, and two 6.4 mm wide sections of SiC porous foam (17.7 pores/cm, 9% density) which act as flow straighteners and flame arresters. Two alumina walls spaced 33.6 mm apart enclose the SiC channels. Fine wire B-type thermocouples are inserted into the channels through the alumina insulation 10 mm apart. They sit flush with the channel wall in order to prevent flame holding. The entire reactor is shrouded in alumina insulation in order to minimize

heat losses from the system. Further details about the reactor construction can be found in Schoegl and Ellzey [36].
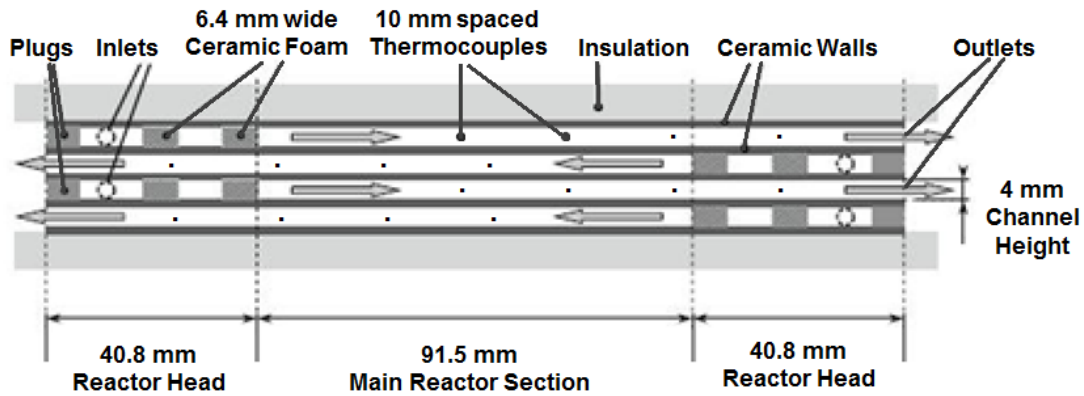
Figure 5. Counter-flow reactor schematic with components and dimensions

The counter-flow reactor design is distinguished from many other heat-recirculating reactors by its lack of a predetermined reaction zone or combustion chamber. As a result, operation over a broad range of operating conditions can be achieved, as well as stable, non-propagating flame fronts which permit continuous operation over long time spans.

1.5   Applications of micro- and meso-scale heat recirculating reactor

The extension of flammability limits, achievable through heat recirculation and superadiabatic combustion, can be advantageous for a variety of applications. Figure 6 shows the results of equilibrium composition calculations of methane/air mixtures over a

range of equivalence ratios performed by Schoegl [41]. Although equilibrium is not necessarily an accurate predictor of the actual magnitudes of species concentrations that will be found in combustion products of practical reactors, it is an adequate predictor of trends. In the lean regime, at equivalence ratios below stoichiometry but above the lean flammability limit, equilibrium predicts nearly complete oxidation of product species, and therefore maximum fuel efficiency, but also the formation of undesirable pollutants such as nitrogen oxides (NO_x) and carbon monoxide (CO) due to high reaction temperatures. In the ultra-lean regime, at equivalence ratios below the conventional lean flammability limit of reactants based upon their initial conditions, the reactor is a thermal oxidizer in which a gaseous stream containing methane or other fuel species in very low concentrations reacts and the reactant species, which may be trace pollutants, are converted to non-toxic or less polluting compounds. In the rich regime, at equivalence ratios above stoichiometry but below the rich flammability limits, products are incompletely, or partially, oxidized, and increasing concentrations of H_2 and CO are observed with increasing equivalence ratio. In the rich regime and the ultra-rich regime, at equivalence ratios above the conventional rich flammability limit of reactants based upon their initial conditions, the reactor is a fuel reformer and converts the rich fuel/air mixture to a gaseous mixture consisting of H_2, CO, and other species; this gaseous product mixture is known as synthesis gas, or syngas. Syngas can be utilized as a fuel in stationary, portable, or remote power systems. Syngas may be used directly, or purified to isolate the hydrogen that it contains, and reacted in devices such as generators or fuel cells to produce power [42]. Hydrogen-based technologies have been proposed as an

alternative to petroleum-based power sources, where the hydrogen can be derived from renewable sources.
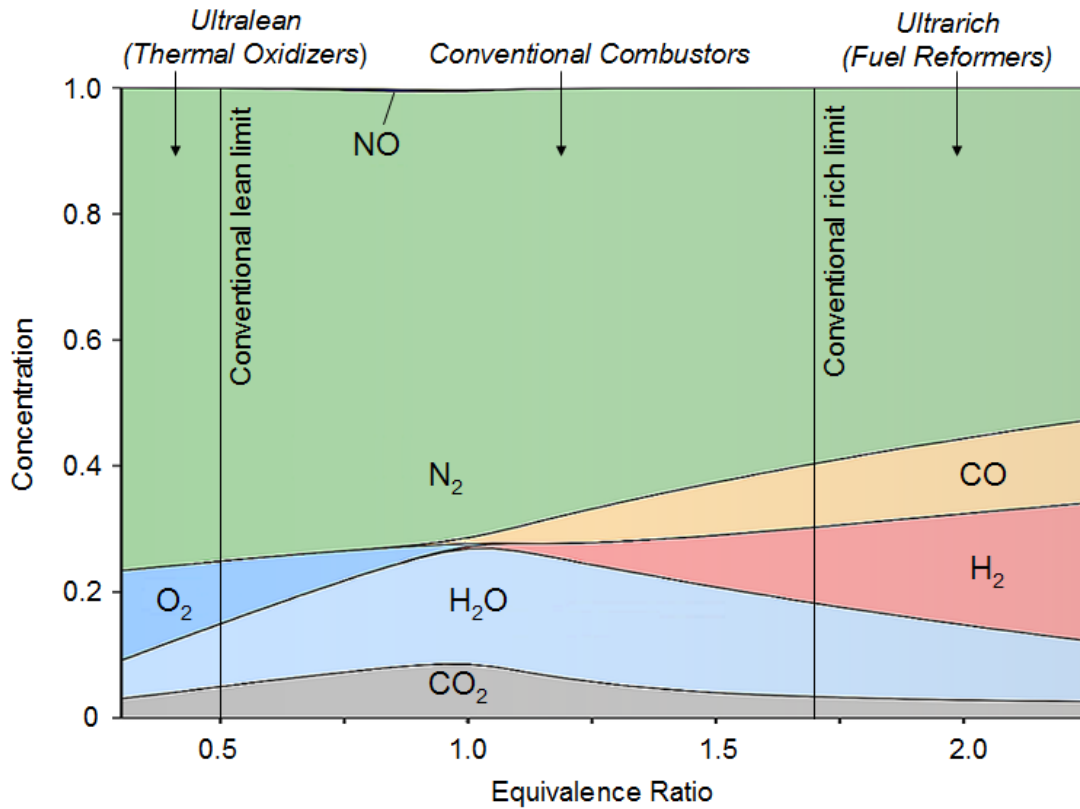
Figure 6. Equilibrium concentrations of major product species of methane/air combustion for a range of equivalence ratios [41]

The extension of flammability limits and increase in burning rates, which equates to higher reactor throughput, achievable by superadiabatic reactor operation has important implications for combustion across a wide range of equivalence ratios, including the regions highlighted in Figure 6 where ultra-lean thermal oxidizers and ultra-rich fuel reformers operate, and the intermediate region where conventional combustors operate.

Extended flammability limits and increased throughput would permit thermal oxidizers to process trace pollutants, fuel reformers to produce syngas or hydrogen, and combustors to provide hot product gases to drive turbines, thermoelectrics, or other energy conversion devices [43], at higher rates.

1.5.1 Lean combustors

Demands for small scale and portable power sources are increasing for a wide variety of applications, including propulsion and electricity generation. As personal and portable power systems become increasingly important, there is a need for compact, durable and lightweight components that can support these demands. Hydrocarbon fuels currently have higher energy density than even the most advanced batteries, therefore combustion-derived power continues to be preferable for many applications. Small scale combustors have been proposed for use in conjunction with mechanical or electrical conversion devices, such as micro-turbines and thermoelectrics, to address the increasing need for portable power [44-47]. Lean reactant mixtures are desirable in these combustors to achieve high system conversion efficiencies because they can permit increased levels of fuel conversion and thermal efficiencies as compared to reactant mixtures nearer to stoichiometric. There is a tradeoff, however, because progressively leaner mixtures result in lower temperatures and reduced heat losses, but require higher volumetric throughput to achieve the same input power as their less lean counterparts. Because of this, the optimal lean equivalence ratio is dependent on the details of the particular system [46].

There is, therefore, a demand on compact power system combustors to operate under varied lean equivalence ratios and with optimal efficiency.

There are also applications for small scale thermal oxidizers capable of rendering trace amounts of hydrocarbons or other VOCs into less harmful product species. A good example of one such application has been proposed by Chen and Ronney [48] who proposed the use of a Swiss roll reactor in a gas mask to eliminate air contaminants at concentrations well below the conventional lean flammability limit.

1.5.2   Rich reformers

Another potential application for small scale non-catalytic heat recirculating reactors is local syngas or hydrogen production at the site of use. In recent years interest has increased in hydrogen-based technologies, such as fuel cells, to replace petroleum-dependent power generation. Syngas or hydrogen can be used directly in internal combustion engines and solid-oxide fuel cells (SOFC), or processed to separate hydrogen for other applications such as proton exchange membrane (PEM) fuel cells [42]. One of the largest impediments to the implementation of such technologies, however, is the lack of infrastructure for the production and distribution of hydrogen [42]. There are currently significant cost and safety challenges associated with large-scale hydrogen storage and distribution. There is currently a limited hydrogen pipeline network, and hydrogen is expensive to store and transport in either gaseous or liquid form. Hydrogen gas has low volumetric energy density at standard conditions, and a significant amount of energy

must be expended to compress it to a density suitable for transportation. Liquid hydrogen requires cryogenic systems, and a large amount of energy is required for liquefaction and storage. These challenges are overcome if hydrogen is produced at the site of use from fuels that are more readily transported. Therefore, onboard or localized reforming of more readily transported or locally procured fuels may be a practical solution [49]. These include natural gas and liquid hydrocarbon fuels [50, 51]. An abundance of hydrogen is bound in organic fuels such as natural gas, petroleum-based fuels, and biofuels, and the syngas or molecular hydrogen needed for fuel cells can be generated from such sources. Liquid fuels, in particular, are generally readily transported and have high volumetric energy density, making them a favorable fuel option for field applications [50, 51].

Known methods of syngas production include steam reforming and partial oxidation, of which steam reforming currently accounts for the majority of hydrogen generation in the US. One major limitation of steam reforming is the use of a catalyst, which is both expensive and prone to degradation and poisoning, thereby limiting the process to relatively narrow operating conditions, moderate temperatures, and high quality reactants [52]. Another major limitation of steam reforming is that it is less economical at small scales, meaning hydrogen produced at the site of use is more expensive than fuel that can be delivered through conventional means such as gasoline [53]. Therefore, small scale non-catalytic reformers have the potential to meet hydrogen production needs in small field or portable power applications. The ability to reform liquid fuels on a small scale and at the site of use therefore has the potential to replace or supplement batteries for energy storage.

1.5.3   *Other systems*

Finally, it is important to note that research into excess enthalpy combustion has relevance to combustion systems that are not specifically designed to incorporate heat recirculation from hot combustion products to cold reactants. Conventional combustors, often constructed of highly conductive materials and radiative enclosures, are potentially conducive to heat recirculation. Therefore, the findings of the current research may be pertinent to understanding fuel conversion and operational stability in those systems as well.

1.6   Objectives

The primary objective of this research is to further the understanding of non-catalytic combustion of fuel- and oxidizer-enriched, or rich and lean, hydrocarbon fuel mixtures, in which heat recirculation is utilized to increase the enthalpy of the reaction zone in order to extend flammability limits and increase burning rates. In particular, the effects of operating conditions, including equivalence ratio and inlet velocity of incoming reactants, and reactor geometry on combustion stability and fuel conversion to product species in heat recirculating reactors are examined.

This research objective is accomplished through experiments and computations of rich and lean combustion in a non-catalytic counter-flow reactor. The non-catalytic counter-

flow reactor is utilized because of its geometric simplicity compared to other heat-recirculating reactors. Additionally, the counter-flow reactor has significant potential for utilization in portable power applications; therefore, the characterization of its operation on a variety of fuels and over a wide range of operating conditions, as well as the impact of geometric scaling, significantly advances the technology towards industrial implementation.

Experiments include the examination of multiple fuels, including gaseous and liquid fuels, and comparison of data to previously-acquired and published experimental data, calculations of equilibrium composition based upon initial reactant conditions, and one-dimensional flame simulations. Gaseous fuels that are tested in this study include methane, which is the simplest hydrocarbon, has well-understood chemistry, and is therefore favorable as a research fuel; and propane, which is a more complex hydrocarbon than methane, and has more widespread usage. The liquid fuel examined in this study is *n*-heptane, which is an important surrogate component for logistical fuels.

The counter-flow reactor utilized in this research consists of multiple reactor channels. Combustion in channels or tubes has widespread importance and is the subject of extensive research. Therefore, the impact of counter-flow reactor channel geometric scaling on combustion has significant implications for the optimization of numerous reactor designs. Computations in this study examine rich combustion in the non-catalytic

counter-flow reactor as a function of reactor channel geometry. Computational modeling allows for time- and resource-efficient examination of multiple reactor geometries and a wide range of operating conditions. Additionally, characteristic values can be quantified in computations that are not readily measured in experiments. Methane is utilized in this study because its chemistry is well-understood, and can be accurately modeled.

1.7   Methodology

Experiments were performed using three hydrocarbon fuels: methane, propane and *n*-heptane. Methane and propane are gaseous at ambient conditions, which makes the premixing and feeding of reactants to the reactor relatively straightforward. Liquid fuels, including *n*-heptane, are more difficult to use in experimentation than gaseous fuels due to the required heating and vaporization of liquid fuels prior to premixing and combustion of reactant mixtures. Heating and vaporization were performed external to the counter-flow reactor, and a vaporization and premixing chamber was designed and constructed for this study.

Rich combustion of *n*-heptane to produce hydrogen-rich syngas was performed in the counter-flow reactor, and this is described in detail in Chapter 2. This was the first liquid fuel to be reformed in the counter-flow reactor, and the results of this study supplement previous studies of rich methane and propane combustion in the counter-flow reactor, to reveal common trends of combustion stability, fuel conversion and product species

production as a function of operating conditions. Data was also compared to calculations of equilibrium composition based upon initial reactant conditions, and previously-published experimental data obtained using a different type of heat recirculating reactor, called a filtration reactor.

Lean combustion of methane, propane and *n*-heptane was performed in the counter-flow reactor. This study was the first investigation of lean combustion using the counter-flow reactor. Initially, methane was examined experimentally, and a previously developed analytical model was adapted to simulate changes in flame front location and temperature profiles in response to changes in lean reactor operating conditions. Data was also compared to calculations of equilibrium composition based upon initial reactant conditions. This work in described in Chapter 3.

Following the study of lean methane combustion using the counter-flow reactor, lean combustion of more complex fuels, propane and liquid *n*-heptane, was examined experimentally and is described in detail in Chapter 4. The data obtained for lean combustion of all three fuels was compared to reveal common trends of combustion stability, fuel conversion and pollutant species production as a function of operating conditions. Data was also compared to calculations of equilibrium composition based upon initial reactant conditions.

Finally, a computational study was performed to study the impact of reactor geometric scaling on rich methane combustion stability, fuel conversion and syngas production. Scaled reactors were modeled in ICEM CFD, and simulations were conducted in ANSYS FLUENT using full methane combustion kinetics mechanism GRI 2.11. Several user-defined functions were utilized to supplement ANSYS FLUENT capabilities. A range of channel heights and lengths were tested, and the computational results were compared to equilibrium calculations and one-dimensional flame simulations performed using Cantera. This study is described in detail in Chapter 5.

2   SYNGAS PRODUCTION FROM HEPTANE IN A NON-CATALYTIC COUNTER-FLOW REACTOR

The focus of this study was the demonstration and quantification of liquid fuel reforming in the counter-flow reactor. This work is described below, and was published as *E.L. Belmont, S.M. Solomon, J.L. Ellzey, Combust. Flame 159 (2012) 3624-3631.*

2.1   Introduction

One of the compelling characteristics of non-catalytic reactors is their ability to operate on a wide variety of fuels. There have been numerous studies on the production of syngas from gaseous fuels [52, 54-56], but fewer have done so from liquid fuels. In this study, the first liquid fuel reforming in the counter-flow reactor was established, using heptane as fuel. The results augment those obtained on an identical reactor using methane [36] and propane [37]. Heptane is a particularly interesting liquid fuel as it is often used as a single-component, or one element of a multi-component, surrogate for commercial fuels [57-60]. Dixon et al. [61] presented experimental and numerical analyses of syngas production from heptane in a porous media reactor. Equivalence ratio (ϕ) and inlet velocity (u) were varied, and exhaust gas hydrogen concentrations were found to increase with both of these parameters. These trends are similar to those found in previous filtration combustion studies [23, 62]. In the results of Dixon et al. [61], maximum hydrogen conversion efficiencies of approximately 80% were achieved at ϕ between 2.5 and 3.5 at $u = 60$ cm/s, and at the highest tested inlet velocity of 80 cm/s and $\phi = 2.5$.

Maximum CO conversion efficiencies of approximately 90% were observed at similar conditions. Pastore and Mastorakos [62] reformed heptane to syngas in a two-section porous burner and obtained comparable results to Dixon et al. [61] at some operating conditions but with a more limited stable burner range. Al-Hamamre [63] numerically studied the thermal partial oxidation of heptane by equilibrium and kinetic analyses over a range of equivalence ratios and preheat temperatures, and found a maximum reforming efficiency of 87% at $\phi = 3.1$ and preheat temperatures of 1300K or greater. Furthermore, reforming efficiency for all tested equivalence ratios was observed to increase with reactant preheat temperature up to approximately 1100K, above which reforming efficiency remained nearly constant with further increases in preheat temperatures.

The earlier study of the porous media reactor operating on heptane provided guidance for this work. In that study [61], the reactor operated near the conventional flammability limits of heptane without prohibitive soot formation causing any observed degradation in performance. At more extreme conditions, soot buildup did pose a challenge, and Dixon et al. [61] developed a regeneration procedure that is utilized in this study as well, in which soot depositions can be removed by purging the reactor with air. The non-catalytic surfaces of the counter-flow reactor imply that small amounts of soot deposits should not degrade the performance as long as the channel dimensions and wall properties are not significantly changed due to buildup, thus opening the possibility of using fuels that may produce more soot.

In this work, we focused on conversion of heptane to syngas in the counter-flow reactor. The stable operating limits were determined as a function of reactant equivalence ratio and inlet velocity. Additionally, concentrations of major product species, including hydrogen and carbon monoxide, and minor hydrocarbon product species, including methane, acetylene and ethylene, were quantified over a wide range of reactant equivalence ratios and inlet velocities. Hydrogen species, hydrogen energy, and total energy conversion efficiencies were determined as a function of operating conditions, including equivalence ratio and inlet velocity. These quantities were compared to previously obtained data for the same reactor operating on rich methane [36] and rich propane [37].

2.2   Experimental approach

2.2.1   *Experimental apparatus*

Liquid fuel is vaporized and premixed with air, prior to being introduced to the counter-flow reactor, via a custom-designed and built vaporization and mixing chamber. *n*-Heptane (Fisher Scientific, HPLC grade) is pumped to an atomizing nozzle mounted inside the mixing chamber. Air is fed to the mixing chamber using a Hastings mass flow controller. Downstream of the controller but upstream of the mixing chamber, the total air is split between the atomizing nozzle and a heater by a control valve. The heated air is introduced into the annular space surrounding the nozzle in order to vaporize the

26

atomized heptane and prevent condensation of heptane on the mixing chamber walls. The atomized fuel/air mixture exits the vaporization and mixing chamber where it is vaporized and mixed with the heated air, and fuel/air reactant mixture is then fed into a manifold that splits the flow among the four channels. The delivery system, from the mixing chamber to the inlet ports, is wrapped in heat tape and monitored using K-type thermocouples to maintain the system above 150 °C. Figure 7 is a schematic that shows the vaporization and mixing chamber, as well as the manifold piping that feeds premixed fuel and air to the counter-flow reactor.
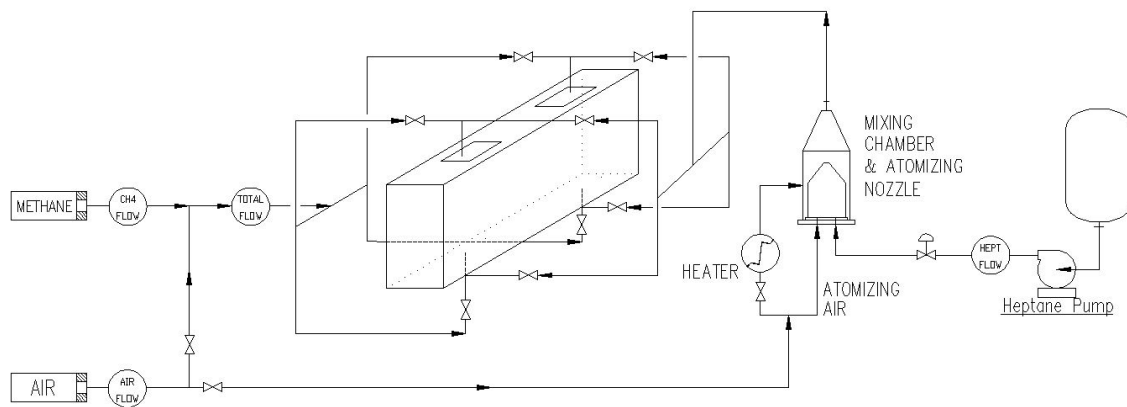
Figure 7. Vaporization and mixing chamber, and manifold piping to reactor inlets

Exhaust gas composition is analyzed using a Varian CP 4900 gas chromatograph (GC) with three columns: a molecular sieve (Molsieve) measures diatomic hydrogen (H_2), nitrogen (N_2), oxygen (O_2), carbon monoxide (CO) and methane (CH_4); a porous polymer unit (PPU) gives concentrations of carbon dioxide (CO_2), ethylene (C_2H_4), ethane (C_2H_6),

27

acetylene (C_2H_2) and propane (C_3H_8); and a CP-SIL column detects larger hydrocarbons (*i-,n-*) butane, (*i-,n-*) pentane, *n*-hexane and *n*-heptane. In order to quench reactions outside of the reactor and prevent moisture accumulation in the GC, exhaust samples are drawn from the reactor exhaust through a quartz probe. The sample then passes through inert Silco Steel tubing and a filter before entering the GC. Previous findings [37] showed slightly lower H_2 and CO product concentrations from outside channels and minimal variation of composition with position within a single channel except near the alumina walls. Exhaust samples in this study were taken from the center channels, which are expected to be most representative of interior channels in scaled up reactors, and the sample probe was placed at the middle of the channel exit.

2.2.2   *Experimental method*

The start-up procedure began with warming the system to above 150 °C using both heating tape and heated air flowing through the reactant delivery system and the reactor. A slightly rich, vaporized, premixed heptane/air mixture was then introduced to the system and ignited at the channel outlets at an inlet velocity of 50 cm/s. Flame fronts propagated upstream in the reactor channels until they stabilized downstream of the porous SiC flow straighteners. Operating conditions were gradually adjusted to $\phi = 3.0$ and $u = 125$ cm/s, where the reactor was operated until temperatures stabilized. The initial warm-up phase took approximately 30-45 minutes.

Experiments included determination of stable operating conditions, and studying the effect of inlet velocity and equivalence ratio variation on exhaust gas composition. Test conditions were considered stable if combustion could be sustained in the main reactor section for ten minutes. Alumina reactor wall temperatures in each of the four channels were monitored throughout the experiments. Gas temperatures were not directly measured due to the tendency of thermocouples inserted into the channels to act as flame holders; however, an analytical model of the counter-flow reactor predicts peak gas temperatures significantly above the maximum wall temperatures [35]. Peak temperatures were recorded after the reactor stabilized at a given set point, and showed less than $\pm 5\,°C$ variation during the time of continuous operation at that set point and while exhaust gas samples were taken. All data presented in this study were taken at operating points that met the above criterion for stability, and no directional drift in measured temperatures or species concentrations was observed with repeated sampling.

Inlet velocity and equivalence ratio were changed in steps of $\Delta u = 15$ cm/s and $\Delta\phi = 0.1$, respectively, and the inlet velocity was specified at standard conditions of 25 °C and 1 atm. Results were obtained for variation of inlet velocity from 50-200 cm/s with equivalence ratio held constant at 3.0, and variation of equivalence ratio from 2.9-3.8 with inlet velocity held constant at 125 cm/s. The inlet velocity range was restricted at the upper limit in order to avoid damage to the reactor due to wall temperatures approaching 1300 °C, while the lower limit was determined by flame instability and extinction. The equivalence ratio range was limited by flashback on the lean end of the tested range, in which the flame propagated upstream into the porous SiC foam in the reactor channel,

and blow-off on the rich end, where the flame front propagated out the end of the reactor. Significant deposits of soot and pyrolytic graphite [64] were observed during extended periods of operation at the highest tested equivalence ratios and inlet velocities. For all experimental conditions reported in this paper, the soot build-up was prevented by briefly interrupting the fuel and purging the reactor with air for 10-20 seconds before continuing the experiments. At high equivalence ratio and inlet velocity operating points, where soot buildup was most likely, the reactor was purged approximately every 20 minutes.

At each operating point, five consecutive GC measurements were taken and the first two were discarded to ensure that any residual gases in the sample line had been eliminated. Each operating point was tested twice, giving a total of six data points. Total uncertainty was calculated at each operating point as the root-sum-square of the contributing uncertainties. Therefore the uncertainty of GC results is due to repeatability of measurements, calculated using a student-t distribution, calibration gases, with specified uncertainties of 1-5%, and the GC itself with uncertainty of 1% of the maximum calibrated value for each species. The error bars shown in plotted results represent average uncertainties for each set of operating conditions. Inlet velocity uncertainty is due to uncertainties of 1% of the air flow controller maximum flow rate and 2% of the rotameter maximum flow rate, as well as an estimated 5% tolerance of the channel cross-sectional area. Equivalence ratio uncertainty is due to contributions from the air flow controller and rotameter. Inlet velocity uncertainty increases with increasing u, where δu = ±4.0 cm/s at u = 50 cm/s and δu = ±10.3 cm/s at u = 200 cm/s. Equivalence ratio

uncertainty increases slightly with increasing ϕ but more significantly with decreasing u, with $\delta\phi = \pm0.05$ at $u = 200$ cm/s and $\delta\phi = \pm0.20$ at $u = 50$ cm/s.

2.3   Results and Discussion

2.3.1   *Operating range*

One of the critical aspects of the counter-flow reactor is the ability to recirculate heat from the hot products in one channel to the incoming reactants in the neighboring channel. The preheating increases the burning rate for a reactant mixture compared to standard conditions. The combustion zone stabilizes at a position in the reactor where the burning rate is balanced by the local velocity. For example, increasing the equivalence ratio from 3.2 to 3.6 at a fixed inlet velocity results in lower heat release and the stable position for the flame is further downstream in the channel where the heat recirculation is more significant. Ultimately as the equivalence ratio is increased further, heat release and recirculation are insufficient compared to heat losses and the flame blows off. If instead heat release is increased compared to heat losses, for example by lowering the equivalence ratio from 3.2 to 2.8 at a constant inlet velocity, then the combustion zone will migrate upstream to a stable position where heat recirculation is reduced. With further reduction in equivalence ratio the flame will propagate into the porous flow straighteners and flash back.

31

Figure 8 shows the stable operating conditions for premixed rich heptane/air reactants. As the velocity increases, flashback occurs at leaner conditions. For example, flashback occurs at $\phi = 2.9$ at an inlet velocity of 50 cm/s. At $u = 200$ cm/s, where heat release and the burning rate are greater, flashback occurs at the leaner condition of $\phi = 2.7$. Similarly, blow-off occurs at $\phi = 4.0$ when the inlet velocity is 50 cm/s and $\phi = 3.6$ when the inlet velocity is 200 cm/s. Extinction occurs at inlet velocities below 50 cm/s due to excessive heat losses relative to heat release rates. The two sets of test conditions at which exhaust gas composition were evaluated, $\phi = 3.0$ with inlet velocity varied from 50-200 cm/s and $u = 125$ cm/s with equivalence ratio varied from 2.9-3.8, are highlighted in the figure. These values were selected because the reactor operating range is relatively large and equilibrium predicts that the conversion of heptane to hydrogen is maximum at an equivalence ratio of 2.9.
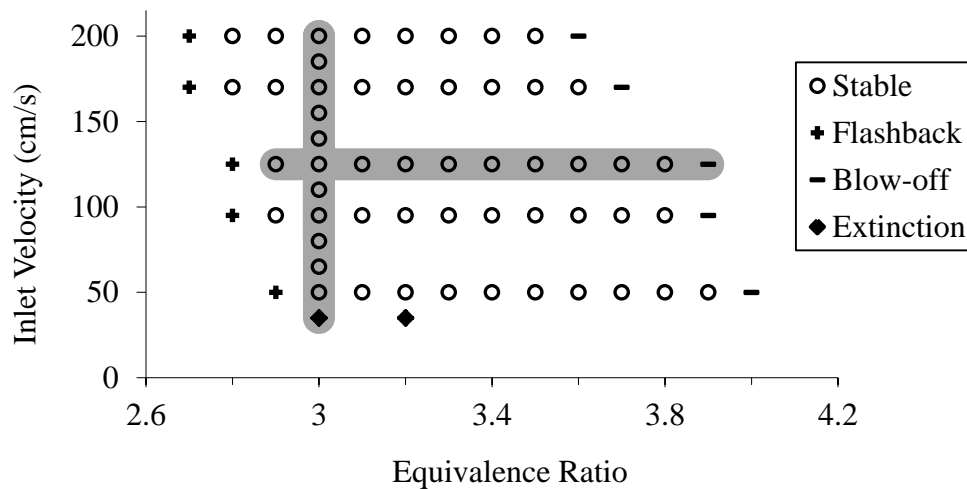
Figure 8. Stable and unstable operating conditions, with highlighted operating points where exhaust gas composition was analyzed

32

2.3.2   *Combustion temperature and exhaust gas composition*

Although equilibrium calculations should not necessarily predict the products of the reactor, they do form a standard for comparison of trends as well as degree of reaction progression. In Table 1, equilibrium values are determined for a constant pressure, adiabatic system. Wet and dry equilibrium values are tabulated for $\phi = 3.0$ and $\phi = 3.5$, where dry values do not include water in the equilibrium composition and will be used for comparison against experimental results. Oxygen, heptane, and most other hydrocarbons including C_2H_2, C_2H_6 and C_3H_8 are not present in significant amounts in the equilibrium composition. Methane is the only unburned hydrocarbon present in non-negligible amounts, and its concentration increases with increasing equivalence ratio. Another compositional change that correlates to an increasing ϕ is the appearance of solid carbon. The adiabatic equilibrium temperature is predicted to decrease from 808.9 °C to 774.6 °C as equivalence ratio increases from $\phi = 3.0$ to $\phi = 3.5$.

ϕ	3.0	3.0	3.5	3.5
	WET	**DRY**	**WET**	**DRY**
T (°C)	808.9	808.9	774.6	774.6
H2 [%]	26.61	26.82	28.00	28.33
H2O	0.75	--	1.15	--
CO	23.46	23.64	20.51	20.75
CH4	0.29	0.29	0.49	0.49
C2H2	<1E-5	<1E-5	<1E-5	<1E-5
C2H6	<1E-5	<1E-5	<1E-5	<1E-5
C3H8	<1E-5	<1E-5	<1E-5	<1E-5
N2	48.17	48.54	44.50	45.01
C(s)	0.00	0.00	4.35	4.40

Table 1. Equilibrium values of adiabatic equilibrium temperature and product composition for premixed heptane/air reactant mixtures of $\phi = 3.0$ and $\phi = 3.5$

Figure 9 and Figure 10, and Figure 11 and Figure 12, show experimental measurements of exhaust gas composition and peak reactor wall temperatures as functions of equivalence ratio and inlet velocity, respectively. A key feature of heat recirculating reactors is their ability to produce superadiabatic temperatures, which are necessary to increase reaction rates and achieve high conversion efficiency [61, 65]. Figure 9 and Figure 11 illustrate that the peak wall temperature for all cases is superadiabatic. Temperatures follow the trend of equilibrium and exceed the adiabatic equilibrium temperature by 190-460 °C in constant equivalence ratio tests, and 290-380 °C in constant inlet velocity tests.

Figure 9 also shows the impact of varying equivalence ratio on major exhaust components H_2 and CO. Experimental measurements of CO concentration show little change over the range of tested equivalence ratios, and results are within the average

uncertainty. In contrast to equilibrium values, experimental measurements of H_2 concentrations decrease with increasing equivalence ratio. Despite peak reactor temperatures in excess of theoretical adiabatic temperatures, both H_2 and CO concentrations are below equilibrium values. This is attributed to a significant amount of unconverted hydrocarbons and is indicative that the reactions did not proceed to equilibrium within the residence time of the reactor. Such results have been suggested in calculations done previously by Al-Hamamre et al. [25] for methane, in which an initial sharp increase in product concentration is observed, followed by a more gradual increase towards equilibrium over time scales that are significantly longer than those that exist in the present experiments.

Figure 10 shows experimental values of intermediate hydrocarbons in the reactor. Total unburned hydrocarbons (UHC) increase monotonically from 5.2% to 9.8% with increasing equivalence ratio. Methane and ethylene, with H/C ratios of 4 and 2 respectively, both increase with equivalence ratio while acetylene, with an H/C ratio of 1, decreases. This shows that hydrogen is increasingly bound in hydrocarbons rather than in diatomic hydrogen. Ethane, propane and *i*-butane concentrations increase with increasing equivalence ratio, but are at all points present in amounts less than 0.2% and are not shown. At high equivalence ratios, the results show carbon monoxide near equilibrium and measured UHC in excess of equilibrium. The amount of carbon in exhaust species that are not measured by GC can be estimated using a carbon balance. Based on the species that are measured by GC, with carbon numbers up to C_7, it is expected that the unmeasured species are larger hydrocarbons and possibly soot. At the highest

35

equivalence ratio of 3.8, the experimental carbon balance shows that ~11% of incoming carbon is contained in species not measured by the GC. In contrast, equilibrium predicts that ~25% of incoming carbon goes to form solid carbon product. Therefore, in experiments there are higher values of measured UHC than equilibrium predicts but lower values of higher hydrocarbons and soot.

Combustion chemistry literature provides insight into oxidation of rich hydrocarbon mixtures and aids in interpretation of these trends. n-Heptane oxidation is initiated via H abstraction by H, O or OH radicals. The resultant heptyl radical is then susceptible to breakdown by β-scission to produce ethylene and pentyl radical. The latter undergoes repeated further β-scission to produce ethylene and a methyl radical. Ethylene may react with an O radical to form a methyl radical and HCO, or in fuel rich mixtures ethylene undergoes further H abstraction by H and OH radicals to produce a vinyl radical, which quickly reacts to form acetylene. Therefore acetylene appears as a product further along in the progression of the complex hydrocarbon breakdown process. Methane can form through multiple pathways, both as an early and a late breakdown product [66]. Constant inlet velocity results show via the correlation of methane with ethylene trends that its formation is not predominantly due to further reduction of acetylene.

Although hydrocarbons larger than C_7 were not measured, soot formation was observed at high equivalence ratios and inlet velocities. The data are too limited to draw conclusions about the pathway of polycyclic aromatic hydrocarbons (PAH) formation, but it is interesting to note that acetylene, which is present at all operating points in

excess of equilibrium concentrations, participates in the chemistry of formation of PAH, a precursor to soot [66].
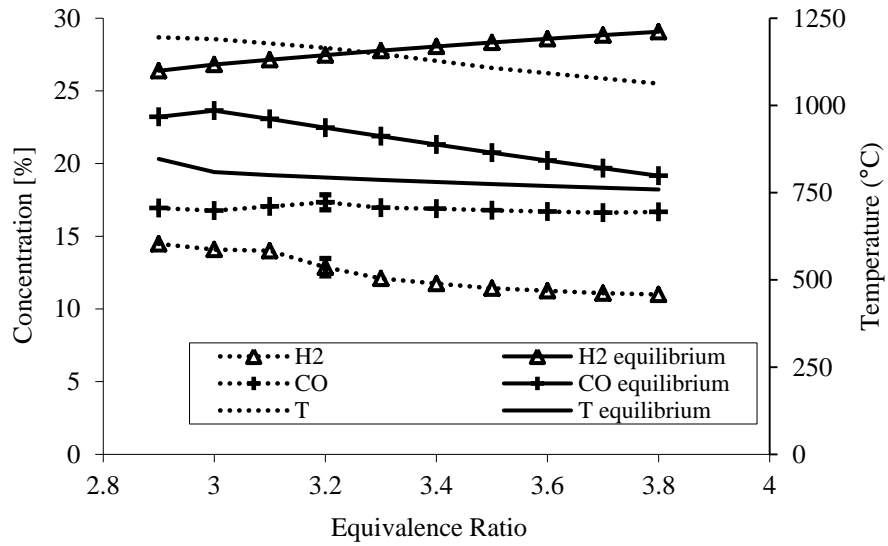
Figure 9. Exhaust gas and equilibrium concentrations of H_2 and CO, and peak wall and adiabatic equilibrium temperatures for u = 125 cm/s and varying ϕ
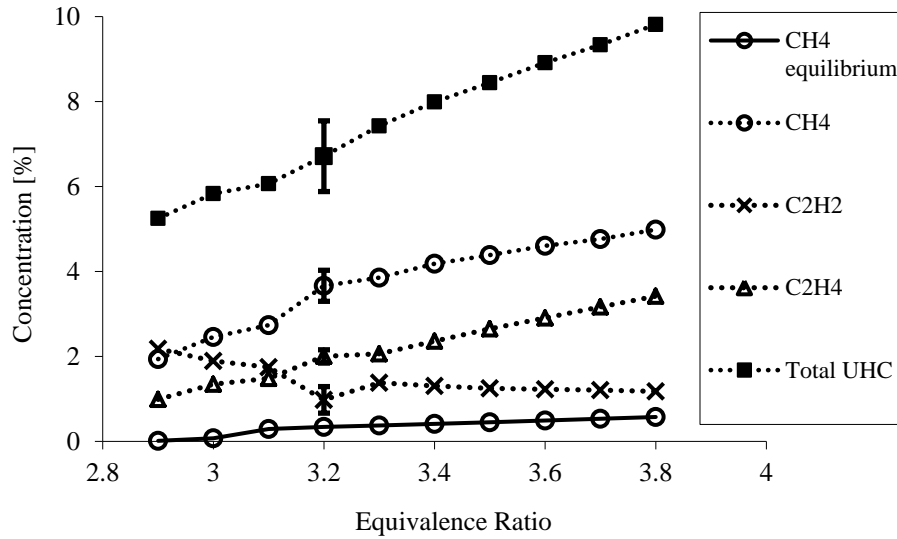
Figure 10. Exhaust gas concentrations of CH$_4$, C$_2$H$_2$, C$_2$H$_4$ and total UHC, and equilibrium concentrations of CH$_4$ (equilibrium concentrations of C$_2$H$_2$ and C$_2$H$_4$ are negligible and not shown) for $u = 125$ cm/s and varying ϕ

Figure 11 shows the impact of inlet velocity on peak reactor wall temperature and on the concentrations of H$_2$ and CO. Equilibrium values are shown for comparison. In experiments with increasing velocity, the volumetric heat release rate increases resulting in higher peak temperatures. The H$_2$ concentration is influenced by two competing effects in this system. Higher temperatures increase the reaction rate and result in faster fuel conversion [36, 61], however, increased velocities imply shorter residence times which may counteract the influence of the higher temperatures [37]. These competing effects are reflected in experimental values of H$_2$ concentrations, which increase initially at velocities up to 80 cm/s and then remain nearly constant. CO concentrations show minimal change with inlet velocity. The increase in H$_2$ and UHC (Figure 12) with no

38

corresponding increase in carbon monoxide at lower inlet velocities suggests that larger intermediate hydrocarbons not measured by the GC may be present at the lowest u. Molecular hydrogen is formed as those species are further broken down, while carbon remains bound in the smaller intermediate hydrocarbon species.

Figure 12 shows exhaust gas concentrations of CH_4, C_2H_2 and C_2H_4, as well as total UHC, for $\phi = 3.0$ and varying u. All other measured hydrocarbons are present in levels less than 0.1%. Total unburned hydrocarbons remain constant within the margin of uncertainty at an average value of 5.5% up to an inlet velocity of 155 cm/s, above which the total decreases monotonically to 4.4% at 200 cm/s. Acetylene, which is a species formed late in hydrocarbon breakdown, initially increases in concentration with increasing inlet velocity up to 80 cm/s and subsequently decreases at higher inlet velocities. Methane and ethylene increase with inlet velocity up to $u = 155$ cm/s, above which concentrations decrease with further increase in velocity. Ethylene is less reduced than acetylene and forms earlier in hydrocarbon breakdown. The existence of a peak acetylene value followed by ethylene and methane maxima at higher inlet velocities suggests that fuel breakdown is diminished by decreased residence time. At the highest inlet velocities, ethylene and methane concentrations as well as total measured unburned hydrocarbons decrease. In conjunction with no increase in H_2 levels and visual observation of significant soot formation, the results suggest that fuel breakdown is promoted by high temperatures but intermediate species may form larger soot precursors instead of further reduction at the highest inlet velocities.
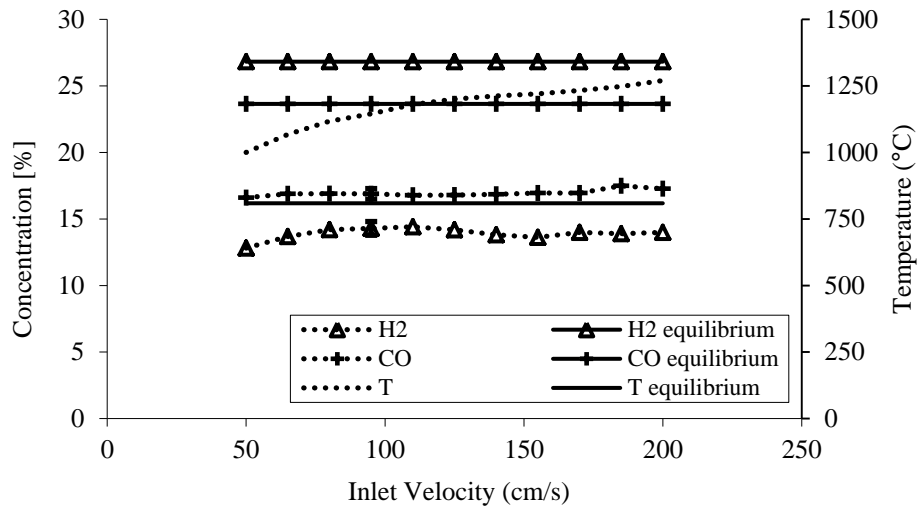
Figure 11. Exhaust gas and equilibrium concentrations of H_2 and CO, and peak wall and adiabatic equilibrium temperatures for $\phi = 3.0$ and varying u
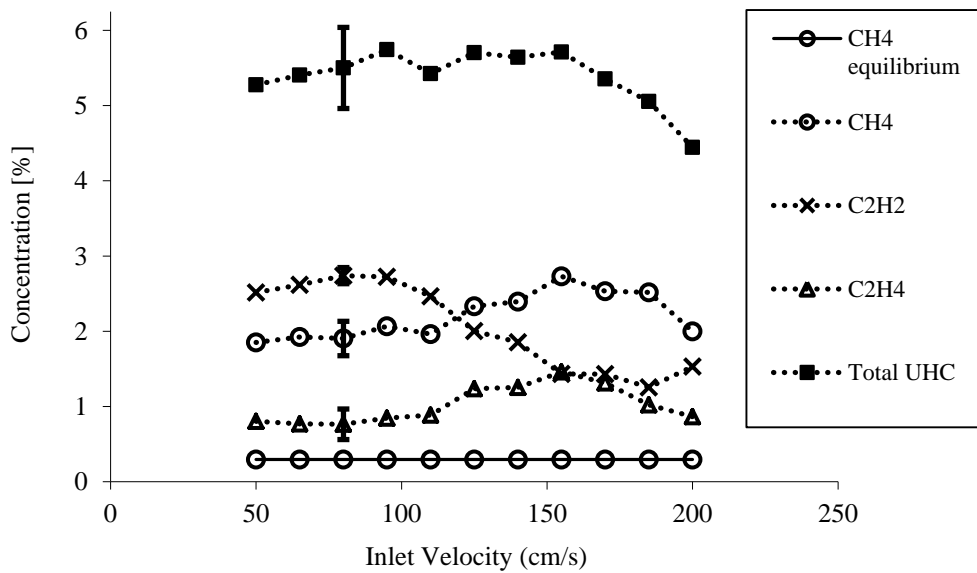
Figure 12. Exhaust gas concentrations of CH_4, C_2H_2, C_2H_4 and UHC, and equilibrium concentrations of CH_4 (equilibrium concentrations of C_2H_2 and C_2H_4 are negligible and not shown) for $\phi = 3.0$ and varying u

2.3.3   Fuels comparisons

The conversions of methane [36] and propane [37] to syngas were investigated in earlier studies using the counter-flow reactor design. The current results for heptane are compared to those from the previous publications using three metrics: species conversion efficiency, and species and total energy conversion efficiencies.

Species conversion efficiency, also called species yield, compares actual species production to the theoretical maximum based on the amount of that species' components bound in the reactant fuel stream. Equation 2 gives H_2 conversion efficiency, which is the number of moles generated compared to the number of moles of hydrogen bound in the heptane feedstock.

$$\eta_{H_2} = \frac{\dot{N}_{H_2}}{\dot{N}_{H_2,\text{max}}} = \frac{\dot{N}_{H_2}}{8\dot{N}_{C_7H_{16}}} \qquad (2)$$

Species energy conversion efficiency represents the amount of chemical energy bound in a product species compared to the total chemical energy in the reactant fuel. Chemical energy is represented by the lower heating value (LHV) in kJ/kmol at standard conditions. Equation 3 gives H_2 energy conversion efficiency.

$$\eta_{Energy,H_2} = \frac{\dot{N}_{H_2} LHV_{H_2}}{\dot{N}_{C_7H_{16},in} LHV_{C_7H_{16}}} \qquad (3)$$

Total energy conversion efficiency compares the chemical energy bound in all of the energy containing product species to the initial chemical energy of the reactant fuel. The difference between the two is the sum of energy lost to surroundings and sensible enthalpy of the product gas. Equation 4 gives total energy conversion efficiency.

$$\eta_{Energy,total} = \frac{\sum_{out} \dot{N}_i LHV_i}{\dot{N}_{C_7H_{16},in} LHV_{C_7H_{16}}} \qquad (4)$$

Figure 13, Figure 14 and Figure 15 show experimental and equilibrium results of methane, propane and heptane reforming in terms of the above three metrics for experiments in which inlet velocity was held constant at 125 cm/s and equivalence ratio was varied. Experiments were conducted over different equivalence ratio ranges because of differences in stability when operating the reactor with the three fuels. As previously discussed, the combustion zone is stable within the reactor when the local velocity equals the burning rate, which is a function of temperature and reactant species. Variation in temperature between the three studies is due to differences in the adiabatic equilibrium temperatures of different reactant species, equivalence ratios, and levels of preheat. Heptane and propane have higher adiabatic equilibrium temperatures than methane. In addition, heptane is preheated to maintain the vapor phase; therefore preheated heptane has a higher adiabatic equilibrium temperature than propane. For example, the adiabatic

equilibrium temperatures of propane and heptane at 25 °C for $\phi = 2.9$ are 850 °C and 847 °C, whereas the equilibrium temperature of heptane increases to 934 °C when the reactants are preheated to 150 °C. Due to these differences, an equivalence ratio and velocity combination that is in the stable range but near the flashback limit for methane will be outside the stable range for propane. The same is true for propane and heptane. A comparison of burner maps for the three studies [36, 37] further illustrates these stability differences.

Methane is the only one of the three fuels that shows a maximum value in the experimental results of hydrogen species (Figure 13) and energy (Figure 14) conversion efficiencies under the tested conditions. Methane, propane and heptane efficiencies decrease with increasing equivalence ratio above $\phi = 2.2$, and experimental conversion efficiencies are significantly less those predicted by equilibrium at these points, despite a peak hydrogen conversion efficiency for heptane predicted at $\phi = 2.9$ by equilibrium. The occurrence of peak conversion efficiency at equivalence ratios below those predicted by equilibrium is consistent with the results of Al-Hamamre et al. [25] for methane, in which incomplete conversion occurs on counter-flow reactor timescales. This suggests that propane and heptane might also produce peak H_2 at a leaner operating point if such stable operation were possible but, as discussed in Section 2.3.1, leaner operation is limited by flashback and therefore these points could not be tested. The results also indicate that the current reactor design does not permit complete fuel conversion at high equivalence ratios.
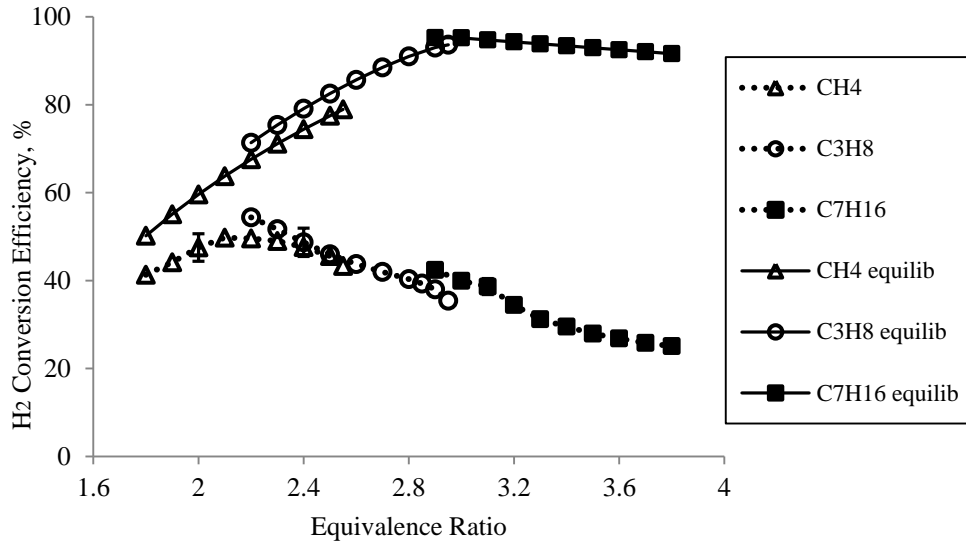
Figure 13. Experimental and equilibrium values of H₂ conversion efficiencies of methane [36], propane [37] and heptane reforming with constant *u* = 125 cm/s and varying equivalence ratio
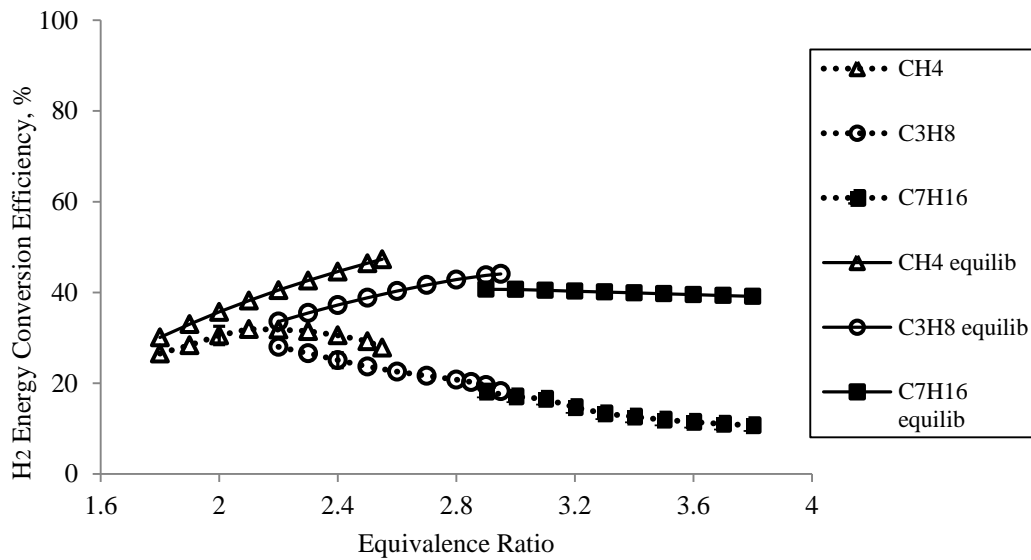
Figure 14. Experimental and equilibrium H₂ energy conversion efficiencies of methane [36], propane [37] and heptane reforming with constant *u* = 125 cm/s and varying equivalence ratio

Experimental values of total energy conversion efficiencies show trends and values similar to equilibrium (Figure 15) for the three data sets. In each case, unburned hydrocarbon concentrations increase with increasing equivalence ratio [36, 37], and the chemical energy bound in those hydrocarbons contributes significantly to the total. Peak reactor temperatures decrease with increasing equivalence ratio for all three fuels [36, 37]. This lessens convective and radiative losses to the environment as well as energy required to increase product gas enthalpy.
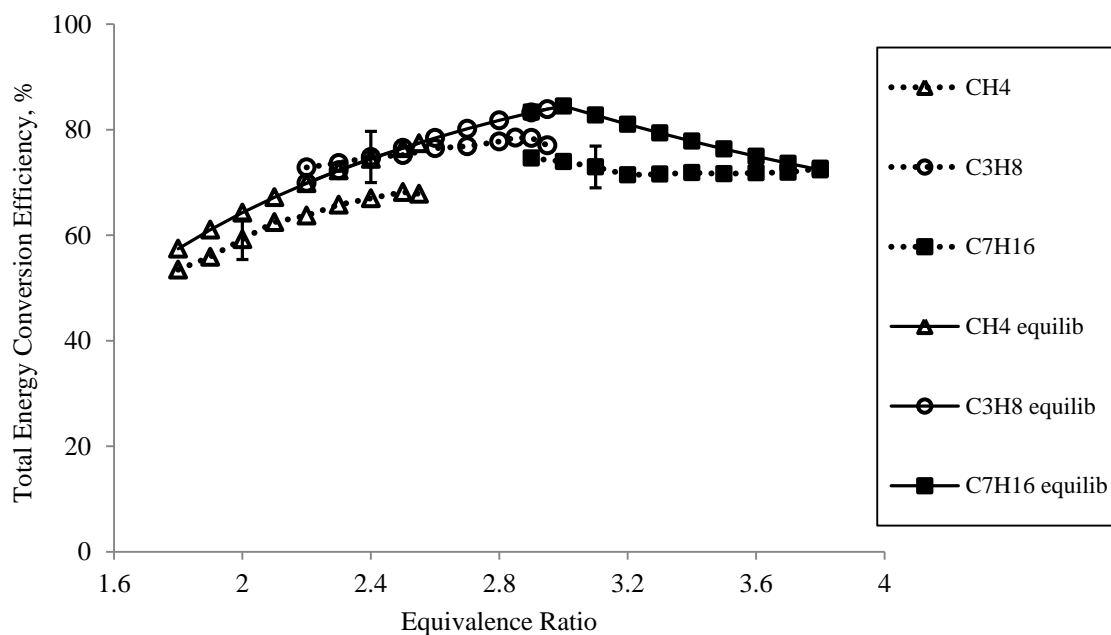
Figure 15. Experimental and equilibrium total energy conversion efficiencies of methane [36], propane [37] and heptane reforming with constant *u* = 125 cm/s and varying equivalence ratio

Figure 16 shows the results of methane, propane and heptane reforming in terms of species and energy conversion efficiencies for experiments in which inlet velocity was varied from 50-200 cm/s and equivalence ratio was held constant at $\phi = 2.2$ for methane, $\phi = 2.4$ for propane and $\phi = 3.0$ for heptane. All conversion efficiencies, with the exception of methane total energy conversion efficiency, increase initially with inlet velocity and show little change at higher u. The initial increase supports the discussion above for heptane that conversion improves with increased energy release rates and resultant higher peak temperatures. The marginal change over the remainder of the tested inlet velocity range suggests that product composition is affected by competing effects of increased temperature, which promotes conversion, and reduced residence time, which inhibits conversion. The decrease in total energy conversion efficiency of heptane at the highest u is attributed to the formation of soot, which consists of high chemical energy species that are not accounted for by GC measurements.

Heptane conversion has also been studied in filtration reactors consisting of a column of porous media, which showed a broader operating range of 1.4-3.8 in comparison to the stable range of 2.8-3.9 in the counter-flow reactor [61]; however both reactors were tested at or near an equivalence ratio of 2.9, where peak hydrogen conversion efficiency is estimated from equilibrium calculations to occur. The tested range in the current study also partially overlaps the equivalence ratio range of 2.5-3.5 that was estimated by Dixon et al. [61] to be favorable conditions for heptane reforming in a filtration reactor. Pastore and Mastorakos [62] reported that the peak conversion efficiencies for heptane occurred at equivalence ratios of 1.8- 2.5 depending on the reactor. These differing values of the

optimum equivalence ratio indicate that conversion is sensitive to the details of the reactor and operating conditions.

Peak H_2 conversion efficiencies from the counter-flow reactor were less than those obtained in porous media, from which efficiencies of greater than 80% were obtained. Hydrocarbon product concentrations in the porous reactor were significantly lower than those measured in the counter-flow reactor, at less than 1% compared to 5.8%, indicating more complete fuel breakdown. Peak temperatures in porous media were in excess of 1400 °C at $\phi = 3.0$ and $u = 60$ cm/s, compared to 1190 °C at $\phi = 3.0$ and $u = 125$ cm/s in the counter-flow reactor. Residence times for the porous media and counter-flow reactors were approximately the same at these operating conditions, with both on the order of 100 ms. The difference in conversion efficiency is attributed to higher peak temperatures in the porous media reactor [37, 67].
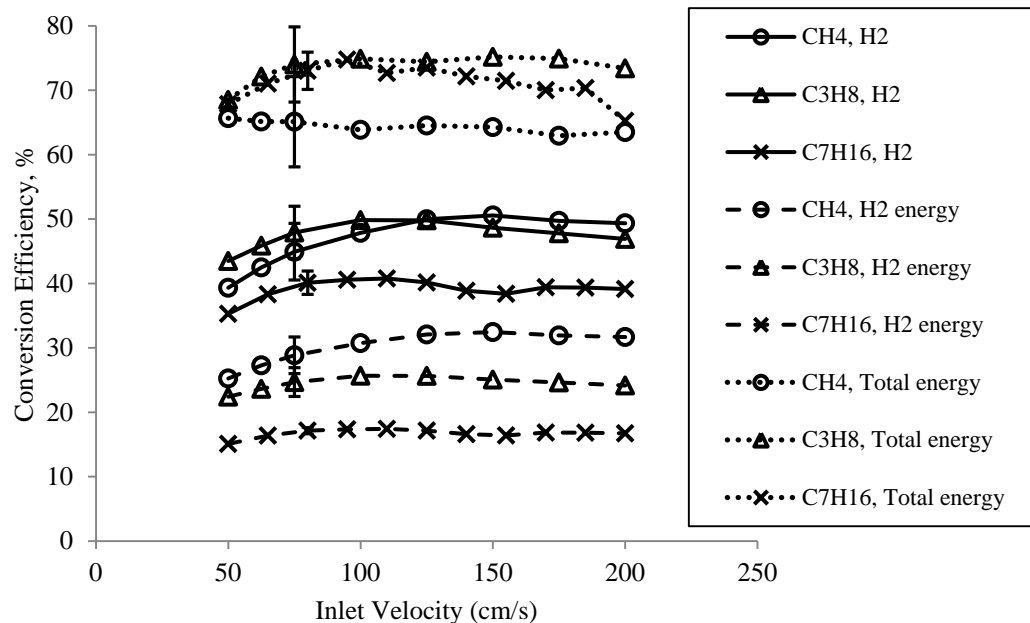
Figure 16. H₂, H₂ energy and total energy conversion efficiencies of methane ($\phi =$ 2.2) [36], propane ($\phi = 2.4$) [37] and heptane ($\phi = 3.0$) with varying inlet velocity

2.4   Conclusions

In this study we examined, experimentally, non-catalytic reforming of heptane to produce hydrogen-rich syngas in a counter-flow reactor. A key advantage of this reactor is that the reaction zones are stationary, which permits continuous operation and practical applications. Stable operation of the reactor with premixed heptane/air reactants was established for equivalence ratios between 2.8 and 3.9 and inlet velocities between 50 cm/s and 200 cm/s. Peak wall temperatures were monitored throughout reactor operation and were at all points in excess of the adiabatic equilibrium temperature, thus excess-enthalpy flames were achieved through internal heat recirculation.

Exhaust gas composition was measured using gas chromatography for two sets of tests: equivalence ratio was varied from 2.9-3.8 with inlet velocity held constant at 125 cm/s, and equivalence ratio was held constant at 3.0 with inlet velocity varied from 50-200 cm/s. H_2 concentration decreased with increasing equivalence ratio from a maximum of 14.5% to a minimum of 10.6%, while CO concentration remained nearly constant around 17.0%. Both H_2 and CO concentrations showed little dependence overall on inlet velocity, with the former varying from 12.8-14.4% and the latter varying between 16.6-17.5%. The largest effect of inlet velocity was found at the lower end of the tested range where rates of heat release and temperatures are lower.

In all cases, unburned hydrocarbons were measured in excess of concentrations predicted by equilibrium composition. Total unburned hydrocarbon levels increased with increasing equivalence ratio. Soot was noted with significant formation observed at higher equivalence ratios and inlet velocities. These results and observations strongly suggested that the extent of fuel breakdown is reduced by insufficient reaction rate and residence time.

The results of this study showed trends similar to previously published studies on syngas production from methane and propane using the counter-flow reactor [36, 37]. Each fuel had H_2 species and energy conversion efficiencies below equilibrium values, but total conversion efficiencies were comparable to equilibrium. In addition, energy-dense unburned hydrocarbon concentrations were in excess of equilibrium with concentrations

an order of magnitude higher than predicted by equilibrium at the highest tested equivalence ratios in this study. The comparison between the different fuels indicates that, although the stable operating range for heptane does include the theoretically optimal value as predicted by hydrogen conversion efficiencies calculated from equilibrium, the current reactor design does not permit complete fuel conversion at high equivalence ratios. In addition, the formation of soot at some conditions suggests the importance of operating at more moderate conditions for optimal performance.

This study demonstrated the fuel flexibility of the counter-flow reactor by reforming a liquid fuel, and results supplemented previous reforming studies on the counter-flow reactor. Peak H_2 conversion efficiency was significantly lower than that attained via filtration combustion in porous media, an alternate method of non-catalytic reforming. Differences were attributed to higher peak temperatures in the porous media reactor, which has higher specific surface area for heat transfer as compared to the counter-flow reactor under investigation. Furthermore, although the tested equivalence ratio range in this study does include $\phi = 2.9$, where peak conversion efficiency is predicted to occur by equilibrium, previous studies predict peak conversion efficiencies over a range of $\phi = 1.8$ to $\phi = 3.5$. The results of hydrogen conversion in this study indicate that the optimum equivalence ratio might be outside the operating range of the counter-flow reactor. The parametric study of reactor geometry, described in Chapter 5, gives insight into optimization of the counter-flow to improve reactor performance.

3 EXPERIMENTAL AND ANALYTICAL INVESTIGATION OF LEAN PREMIXED METHANE/AIR COMBUSTION IN A MESOSCALE COUNTER-FLOW REACTOR

The second focus of this research was the first demonstration of lean combustion in the counter-flow reactor. This work is described below, and was published as *E.L. Belmont, I. Schoegl, J.L. Ellzey, Proc. Combust. Inst. 34 (2013) 3361–3367.*

3.1 Introduction

Various lean combustor designs rely on heat recirculation for increased reaction rates. A review of lean methane combustion in porous media was conducted by Wood and Harris [13]. Numerous studies have utilized a monolith or packed bed to achieve the combustion of lean and ultra-lean reactant mixtures. Mathis and Ellzey [22] used a two section porous burner to stabilize combustion of methane/air mixtures with equivalence ratios of 0.6-0.75 and inlet velocities (*u*) of 40-190 cm/s, which correspond to firing rates of 834-3961 kW/m^2. Exhaust emissions of carbon monoxide (CO), nitrogen oxides (NOx) and unburned hydrocarbons (UHCs) were below 35, 10 and 25 ppm, respectively, for all operating points. Smucker and Ellzey [68] computationally and experimentally investigated the combustion of lean propane/air and methane/air mixtures in a similar but larger diameter burner over a range of equivalence ratios from 0.6-0.7 and inlet velocities

from 20-120 cm/s for methane. Emissions of CO, NOx and UHCs were less than 35, 15 and 5 ppm, respectively.

Other heat recirculating reactor designs have been utilized in the study of lean combustion. One design utilizes annular porous media to vaporize and preheat lean fuel and air entering a combustor [69]. Another category of heat recirculating reactors, constructed of mesoscale flow channels, has been used to study lean combustion. An investigation of one reactor of this type, a Swiss roll combustor [33], demonstrated that the lean flammability limit of propane was extended from 0.51 to 0.18 at mixture inlet velocities significantly in excess of adiabatic laminar flame speeds [8]. The analytical model of channel combustors by Ronney [32] illustrated the influence of heat recirculation on operating limits.

In this study, the straight-channel counter-flow reactor is investigated as a combustor and thermal oxidizer. This study is the first demonstration of its use to stabilize flames at lean equivalence ratios. Methane is studied experimentally and analytically, where the latter was achieved through modification of a previously developed analytical model [35]. The stable combustion limits of lean methane in the counter-flow reactor are determined as a function of reactant equivalence ratio and inlet velocity. Additionally, concentrations of major pollutant species, including NO_x, CO, and unburned hydrocarbons (UHCs) are quantified over a range of reactant equivalence ratios and inlet velocities. Emissions indices of CO and NO_x as a function of firing rates are presented.

3.2 Experimental method

3.2.1 Experimental apparatus

Methane and air are metered using mass flow controllers, and premixed prior to being introduced to the counter-flow reactor. Exhaust concentrations of CO, NO_x and UHCs were measured using Rosemount Analytical analyzers. Samples were drawn from the reactor exhaust through an uncooled quartz probe with an inner diameter of 2 mm and inert tubing, and dried before analysis. Previous findings [37] showed slightly lower concentrations of product species from outside channels and minimal variation of composition with position within a single channel except near the alumina walls. Exhaust samples in this study were taken from the center channels, which are expected to be most representative of interior channels in scaled up reactors, at the middle of the channel exit.

3.2.2 Experimental method

The start-up procedure began by burning a near-stoichiometric methane/air mixture at the reactor outlets at an inlet velocity of 50 cm/s. Once the reactor heads warmed, the reaction fronts propagated upstream in the channels until they stabilized downstream of the porous SiC flow straighteners. Operating conditions were gradually adjusted to $\phi = 0.44$ and $u = 125$ cm/s, where the reactor was operated until temperatures stabilized. The initial warm-up phase took approximately 30-45 minutes.

Experiments included the determination of stable operating conditions, and the effect of inlet velocity and equivalence ratio variation on exhaust gas concentrations of CO, NOx and UHCs. Test conditions were considered stable if combustion was sustained in the main reactor section for ten minutes at constant temperatures. Alumina reactor wall temperatures in each of the four channels were monitored throughout the experiments. Gas temperatures were not directly measured due to the tendency of thermocouples inserted into the channels to act as flame holders. Peak wall temperatures were recorded after the reactor stabilized at a given operating point, and showed less than ± 5 °C variation during the time of continuous operation at that point and while exhaust gas samples were taken.

Inlet velocity was specified at standard conditions of 25 °C and 1 atm. Emissions results were obtained for variation of inlet velocity from 60 to 225 cm/s with equivalence ratio held constant at 0.44, and variation of equivalence ratio from 0.41 to 0.48 with inlet velocity held constant at 125 cm/s. The tested range corresponds to firing rates of 664 to 2490 kW/m^2. Emissions concentrations in parts per million (ppm) are reported as measured on a dry basis. Emission indices for CO and NOx were calculated using the molecular weight of NO as representative of NOx. Peak wall temperatures were limited to under 1300 °C in order to avoid damage to the reactor, thus the inlet velocity range was restricted at the upper limit and some operating points were not tested for stability at high inlet velocities.

Each operating point was tested twice. Total uncertainty was calculated at each point as the root-sum-square of the contributing uncertainties. Therefore the uncertainty of emissions results is due to repeatability of measurements, calculated using a student-t distribution, calibration gases and the analyzers. Average uncertainty for CO and NOx is equal to +/- 10 ppm and +/- 2 ppm, respectively, and average uncertainty for UHCs is +/- 16 ppm. Inlet velocity uncertainty is due to uncertainties of the air and methane flow controllers, as well the channel cross-sectional area. Equivalence ratio uncertainty is due to contributions from the air and methane flow controllers. Average uncertainties for inlet velocity and equivalence ratio are +/- 10.3 cm/s and +/- 0.03, respectively. Temperature uncertainty is attributed to contributions from repeatability of measurements, the thermocouples, and the data acquisition system, and average uncertainty is estimated to be +/- 12 °C.

3.3   Analytical model

An analytical model was developed by Schoegl and Ellzey [35] to investigate the operating principle of the reactor and obtain qualitative predictions of its behavior in response to changes in rich combustion operating conditions. A complete description of the model can be found in [35] where it was developed for analysis of the counter-flow reactor as a fuel reformer. A summary of the model and description of its recalibration for lean reactants is described below.

The purpose of the one-dimensional model is to provide insight into the general performance of the counter-flow reactor. The model assumes constant thermophysical properties, and combustion is modeled using activation energy asymptotics. Radiative heat losses are included through a boundary condition in the wall temperature solution. The model solves for non-dimensional wall temperature (T_w) and gas temperature (T_i) along a normalized x coordinate. The location of the reaction zone is determined indirectly to be where the local reaction rate produces a burning speed that is equal to the local velocity, which is the condition for stability. Operating conditions are specified by equivalence ratio, inlet temperature T_o, and ambient temperature T_∞. Properties of the reactor are specified using non-dimensional parameters which can be found in [35].

The gas temperatures in two adjacent channels are coupled by heat transfer through a common conducting wall. Equation 5 gives the normalized steady-state energy conservation equations and includes conduction and convection, transport, external losses and chemical reactions, given by

$$\frac{d^2 T_w}{dx^2} = \frac{\mu}{\kappa \epsilon^2}\left[(1 + \chi)T_w - \frac{1}{2}(T_1 + T_2) - \chi T_\infty\right] \tag{5a}$$

$$\frac{d^2 T_i}{dx^2} = \pm \frac{\mu}{\epsilon}\frac{dT_i}{dx} + \frac{\mu}{\epsilon^2}(T_i - T_w) + \frac{T_{ad} - T_\infty}{\epsilon^2}w_i \tag{5b}$$

where indices $i = 1,2$ denote individual channels and T_{ad} is the normalized adiabatic flame temperature. Equation 6 is the species conservation equation which includes

56

diffusion, transport and reactions, and gives the concentration of the limiting reactant species y_i as

$$\frac{1}{Le}\frac{d^2 y_i}{dx^2} = \pm \frac{u}{\epsilon}\frac{dy_i}{dx} - \frac{1}{\epsilon^2}w_i \qquad (6)$$

where Le is the Lewis number and u is the inlet velocity non-dimensionalized by the adiabatic flame speed of the reference case. Equation 7 represents the reaction terms w_i, which are modeled as point sources using activation energy asymptotics [70] by

$$w_i \approx \epsilon\delta(x - x_{c.i})exp\left(\frac{\beta(T_i - T_{ad})}{2T_i/T_{ad}}\right) \qquad (7)$$

where $\delta(x - x_{c,i})$ are Dirac delta functions at the combustion locations $x_{c,i}$. The normalized activation energy β is equal to Ze/γ, where the Zeldovich number Ze is given by $E_a'\Delta T_{ad}'/R'T_{ad}'^2$, the prime (′) denotes a dimensional quantity, E_a' is the activation energy, $\Delta T_{ad}'$ is the adiabatic temperature rise of a mixture over the unburned mixture T_u', and R' is the universal gas constant. The scaling factor γ is equal to $\Delta T_{ad}'/T_{ref}'$ where T_{ref}' is the adiabatic equilibrium temperature of the reference case.

Chemical reactions are modeled using single-step, first-order, irreversible Arrhenius kinetics. The activation energy is calibrated for lean methane/air mixtures using laminar flame speeds for various preheating levels at the equivalence ratios of interest calculated with Cantera [71] and GRI 3.0 [72]. Adiabatic flame temperature and flame speed at the

57

reference condition $\phi = 0.5$ and $T'_o = 177.0\ °C$ are used for the non-dimensionalization of the model. Equation 8 is utilized to obtain the activation energy by fitting β at each equivalence ratio

$$|u_i| = exp\frac{\beta(T_{c,i} - T_{ad})}{2T_{c,i}/T_{ad}} \tag{8}$$

where $T_{c,i}$ are adiabatic flame temperatures normalized by the reference temperature. The normalized adiabatic flame temperature T_{ad} is equal to 1 at $\phi = 0.50$; at other equivalence ratios, it is the adiabatic flame temperature resulting in a mass flux equal to the reference case in detailed simulations, which matches flame speeds within the context of the constant density approximation used for this model. Table 2 gives the conditions resulting in constant mass flux and the resultant values for the calibrated activation energies.

Table 2. Calibrated activation energies derived from calculated temperatures and flame speeds

ϕ	T'_u	T'_{ad}	$\Delta T'_{ad}$	u'	
	(°C)	(°C)	(°C)	(cm/s)	E'_a (kJ/mol)
0.42	316	1285	696	20.2	249.7
0.44	281	1295	741	19.1	247.2
0.46	247	1305	786	17.9	244.2

Due to the simplifications used in the analytical model, its use is limited to qualitative predictions of reactor behavior. It is, however, able to illustrate the stabilization mechanism of the reactor and the trends of temperature and reaction zone location in response to variations in reactant equivalence ratio and inlet velocity.

3.4   Results and Discussion

3.4.1   Operating range

Figure 17 shows the stable operating range of the reactor in terms of inlet velocity and both standard and normalized equivalence ratio [66]. The combustion process becomes unstable due to either flashback, in which the reaction front propagates upstream past a section of porous flow straightener in the reactor channel, blow-off, in which the reaction front propagates out of the outlet of the reactor channel, or extinction. In addition to the data presented in this paper for operation in the lean regime, data from an earlier study [36] on rich methane/air mixtures is also shown. The stable operating points on both the rich and lean sides are beyond the conventional flammability limits.
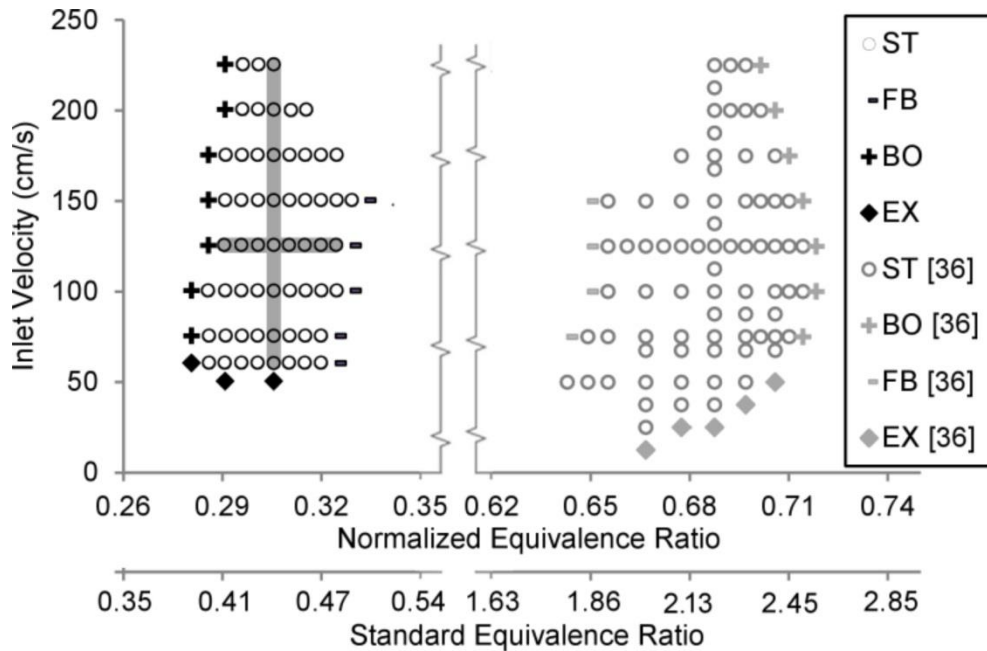
Figure 17. Stability map for counter-flow reactor operating on lean (this study) and rich ([36]) methane/air reactants, with both stable (ST) and unstable points due to flashback (FB), blow-off (BO) and extinction (EX) shown as a function of inlet velocity and both standard and normalized equivalence ratios

In terms of standard equivalence ratio, the stable operating range on the lean side is considerably narrower than that on the rich side. Stability is strongly influenced by the temperature of the products and the resultant preheating of the reactants in the neighboring channel. It is known that in comparison to the rich side of stoichiometric, the temperature of the products changes more rapidly with standard equivalence ratio on the lean side resulting in a smaller range of stable conditions. Due to the asymmetry inherent in the standard equivalence ratio definition, the stability range is also presented in terms of normalized equivalence ratio. In normalized form, the width of the stable range in the

rich regime is approximately 60% broader than the lean, which is attributed to differences in chemical kinetics between the two regimes.

3.4.2   Analytical model

The stable operating range (Figure 17) shows that equivalence ratio and inlet velocity can be changed independently while stability is maintained within the reactor. There are no predetermined flame stabilization points within the channel; therefore the combustion zone freely adjusts to a new position within the channel following a change in equivalence ratio or inlet velocity. The combustion zone moves to a position where sufficient heat is gained from the adjacent channel and reactants are preheated to the point where the burning velocity equals the local velocity, and stability is maintained.

Figure 18 shows the results of the analytical model for gas and wall temperature profiles for varying equivalence ratio from 0.42 to 0.46 with inlet velocity held constant at 125 cm/s, as well as experimental temperature measurements taken along the axial length of a reactor channel while operating at these conditions, normalized by axial position and overlaid onto the analytical domain. Figure 19 shows the results of the model and experimental measurements for varying inlet velocity from 75 to 175 cm/s with equivalence ratio held constant at 0.44.
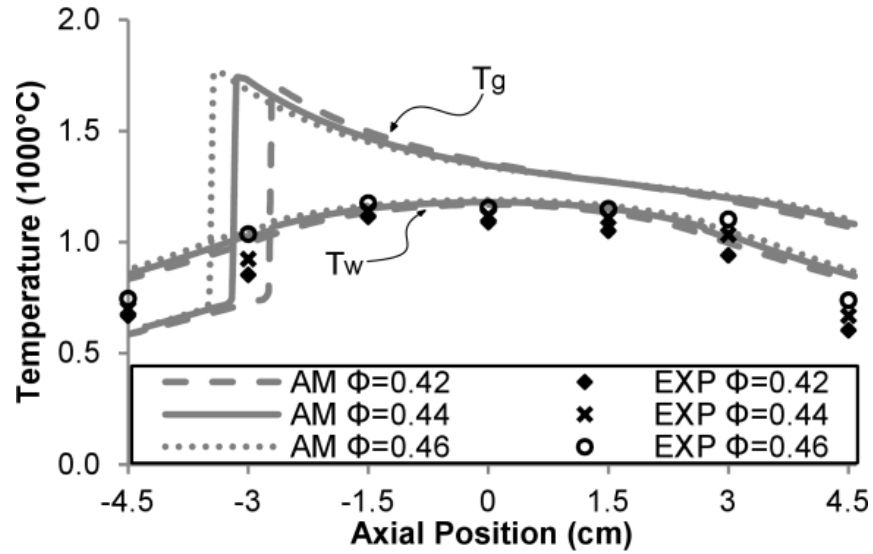
Figure 18. Analytical model (AM) gas (T$_g$) and wall (T$_w$) temperatures and experimental (EXP) temperatures measured along axial position in channel for varying ϕ and u = 125 cm/s
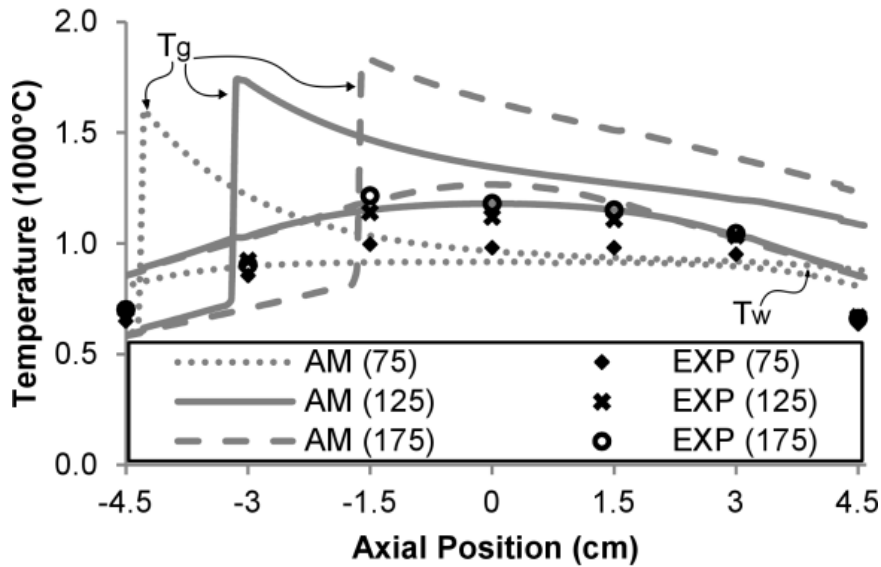
Figure 19. Analytical model (AM) gas (T$_g$) and wall (T$_w$) temperatures and experimental (EXP) temperatures measured along axial position in channel for varying u and ϕ = 0.44

In both cases, the inlet temperature was specified at 577 °C to account for preheating that occurs in the reactor heads. The combustion zone is identified by a sharp increase in gas temperature, while the wall temperature shows a broader profile. The combustion zone adjusts its location towards the center of the reactor following a decrease of ϕ or an increase in u in Figure 18 and Figure 19, respectively. For increasing ϕ (at fixed u), the temperature of the flame increases and less preheat is required for the mixture to react and so the flame stabilizes nearer the entrance than for the cases at lower ϕ which require greater preheating (Figure 18). For increasing u (at fixed ϕ), the reactants travel further into the channel before reaching the critical temperature for combustion (Figure 19). Through this adjustment in combustion zone location a burning velocity is attained that equals the local velocity.

Wall temperatures also respond to changes in ϕ or u, both in magnitude and broadness of temperature profile. As ϕ is increased (Figure 18) or u is decreased (Figure 19) and the combustion zone shifts upstream, hot products flow over the remaining length of the channel. This condition, as well as conduction through the wall, results in the broad profile predicted by the model. Similarly, as ϕ is decreased or u is increased and the reaction zone shifts towards the center of the reactor, the central portion of the wall receives more heat and the peak temperature zone in the wall is narrower. Experimental temperature measurements are in qualitative agreement with the results of the analytical model in terms of relative values at the tested operating points.

While the analytical results can only be interpreted qualitatively due to simplifications in the model, they do accurately capture temperature trends and the general conditions under which flashback and blow-off occur, which are at high ϕ-low u and low ϕ-high u, respectively. The results of this study can also be compared to a previous study in which the counter-flow reactor was operated as a fuel reformer, and the analytical model was used to predict its behavior under fuel rich conditions [35]. In that study the model similarly predicted changes in combustion zone location in response to changes in ϕ and u. In the case of fuel rich conditions the combustion zone migrated downstream for increases in u, as in this study. However, the zone migrated downstream for increases in ϕ because more preheating is required to attain the same peak reaction temperature as a rich mixture becomes progressively richer, analogous to the case for a lean mixture becoming progressively leaner. Therefore the model indicates that the stabilization method for rich and lean mixtures in the counter-flow reactor is similar.

3.4.3 Emissions

Figure 20 shows the variation of CO, NOx and UHC concentrations measured in the reactor exhaust, peak reactor channel wall temperatures, and calculated adiabatic equilibrium flame temperature for varying equivalence ratio with inlet velocity held constant at 125 cm/s.

Peak reactor wall temperatures are above the adiabatic flame temperatures, or superadiabatic, for each of the tested equivalence ratios. The measured wall temperatures

in these experiments are less than 1300 °C. However, the results of the analytical model suggest that peak gas temperatures are significantly higher, with gas temperatures predicted by the model to be as much as 780 °C higher than peak wall temperatures. Therefore, NOx is expected to form through the thermal and prompt NO mechanisms in these experiments [66].

The concentration of CO is observed to increase with decreasing equivalence ratio. This is in contrast to the product composition that is predicted by thermodynamic equilibrium, which suggests a decrease in CO concentration with decreasing ϕ. However, the results of this study are in agreement with those attained previously by Xu et al. [73] for experiments in porous media, in which CO concentrations rose from under 100 ppm at equivalence ratios of 0.49 and higher, to over 200 ppm at the lowest tested equivalence ratio of 0.42. Similarly, Francisco et al. [74] reported a significantly higher CO emission index for methane/air mixtures of $\phi = 0.45$ as compared with higher equivalence ratios, although stable velocity operating ranges differed slightly as well. Other studies have noted the importance of temperature in promoting consecutive oxidation of methane to CO and CO_2 [75, 76]. This is seen in the experimental results of this study, where temperature decreases from 1203 °C at $\phi = 0.48$ to 1108 °C at $\phi = 0.41$.
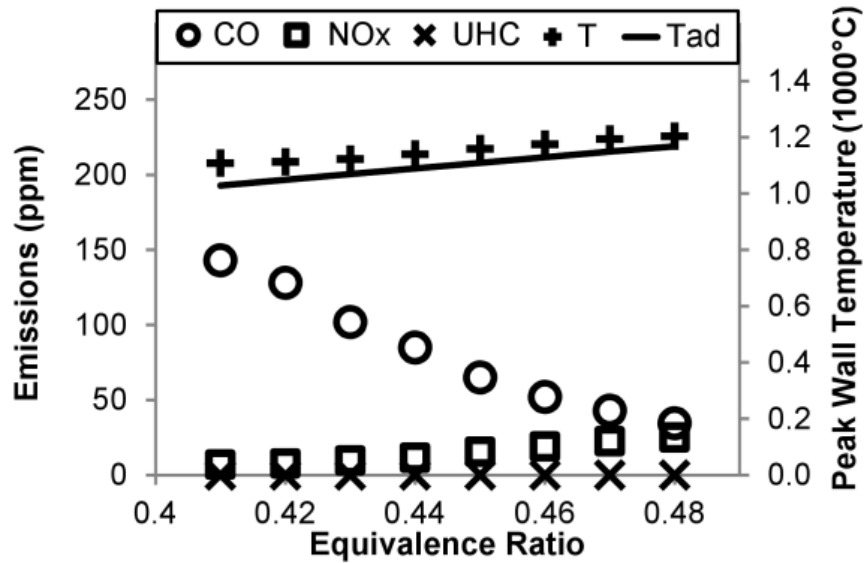
Figure 20. CO, NOx and UHC concentrations and peak wall temperature measurements (T), as well as adiabatic equilibrium temperature (T_{ad}), for varying ϕ with $u = 125$ cm/s

Figure 21 shows CO, NOx and UHC concentrations, peak wall temperatures, and calculated adiabatic equilibrium flame temperature in the reactor exhaust for varying inlet velocity with equivalence ratio held constant at $\phi = 0.44$. Consistent with results for other reactors of this scale, peak temperatures decrease with inlet velocity as the heat losses to ambient dominate over the rate of chemical energy release within the reactor [36, 37]. Peak wall temperatures range from 912 to 1272 °C at the lowest and highest tested inlet velocities, respectively. These wall temperatures are superadiabatic at inlet velocities above 100 cm/s.

NOx concentrations are below 13 ppm at all tested points. At the lowest tested inlet velocities of 50 and 75 cm/s, the CO concentration drops from the peak value that occurs at 100 cm/s. UHCs are detected at and below an inlet velocity of 100 cm/s, and measured UHC concentrations increase with decreasing inlet velocity from 5 to 110 ppm at 100 and 60 cm/s, respectively. The results indicate that some fuel is not broken down at these low temperature conditions. No UHCs are detected at inlet velocities above 100 cm/s, indicating that the fuel is broken down and the conversion becomes more complete with lower CO values at the higher velocity and temperature conditions.
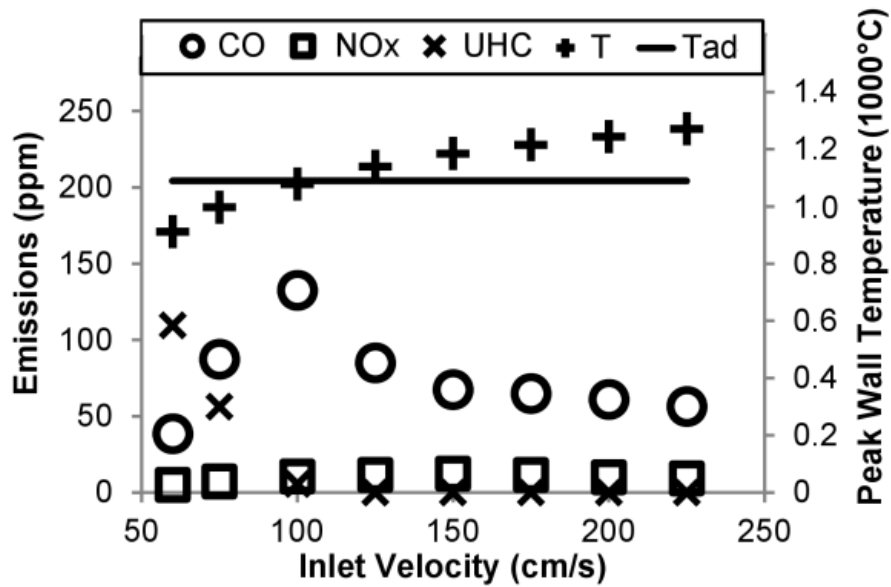
Figure 21. CO, NOx and UHC concentrations and peak wall temperature measurements (T), as well as adiabatic equilibrium temperature (T_{ad}), for varying u and $\phi = 0.44$

Both sets of data, for varying ϕ and u, can be further understood by examining the dependence of pollutant formation and peak temperature on firing rate. Figure 22 shows these dependencies, with CO and NOx emissions presented in terms of emission index (EICO and EINOx, respectively), defined as mass flow rate of a pollutant species of interest (in grams) divided by the mass flow rate of fuel (in kilograms). EICO and EINOx are plotted separately for the variation of inlet velocity or equivalence ratio, while peak temperature data sets have been combined. EICO shows a negative correlation with firing rate for operating points where no UHCs are detected, however the correlation differs depending on which parameter, u or ϕ, is being varied. EINOx, on the other hand, shows a positive correlation with firing rate as a function of ϕ, but generally decreases with increasing firing rate as a function of u at firing rates above those where UHCs are detected. The detection of UHCs suggests a minimum firing rate for the system operating at a given ϕ. It can also be seen that firing rate and temperature are closely related, despite variation in equivalence ratio and inlet velocity in the combined set of data. The increase of reactor temperature with firing rate has been observed in previous studies as well [22, 68, 77].
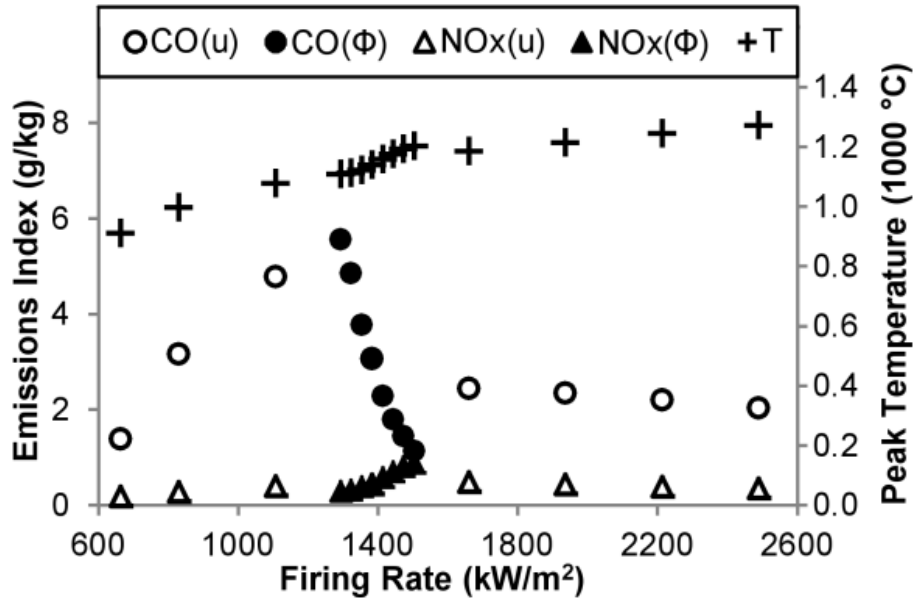
Figure 22. Emission indices of CO (EICO) and NOx (EINOx), and peak reactor wall temperature (T) over a range of tested firing rates for the variation of equivalence ratio (ϕ) and inlet velocity (*u*)

3.5   Conclusion

Experimental and analytical results were presented for the combustion of lean methane/air mixtures in a mesoscale counter-flow reactor. This reactor design has been studied previously for conversion of rich methane/air, propane/air and heptane/air mixtures; this is the first study focused on the oxidation of lean mixtures.

The analytical model, previously derived for reforming studies in the counter-flow reactor, was recalibrated for combustion of lean methane/air reactants and applied over the range of experimentally tested operating conditions. Results were in qualitative

69

agreement with reaction front location trends and temperature measurements taken along the axial position of the reactor channels during experiments. The results highlighted the stabilization mechanism of the reactor as well as modes of destabilization, and showed rich and lean behavior to be similar.

Stability was experimentally determined over a range of inlet velocities and equivalence ratios below the conventional flammability limit of methane at inlet conditions. Emissions of CO and NOx ranged from 35 to 143 ppm and 5 to 25 ppm, respectively, and CO generally decreased with increasing inlet velocity and equivalence ratio. UHCs were detected at the lowest firing rates suggesting that a minimum firing rate is necessary for optimal performance.

4   LEAN HEPTANE AND PROPANE COMBUSTION IN A NON-CATALYTIC PARALLEL-PLATE COUNTER-FLOW REACTOR

The third focus of this research expanded upon the demonstration and quantification of lean methane combustion in the counter-flow reactor to examine more complex fuels: propane and heptane. This work is described below, and was published as *E.L. Belmont, J.L. Ellzey, Combust. Flame 161(4) (2014) 1055–1062*.

4.1   Introduction

Previous studies on the counter-flow reactor have demonstrated its ability to convert fuel-rich reactants of methane [36], propane [37] and heptane [38] to hydrogen-rich syngas. The same reactor has been operated with fuel-lean mixtures of methane [39]. In this study, increasingly complex fuels are studied: propane and heptane. The latter, being a liquid fuel, has importance as a single-component, and part of a multi-component, surrogate for logistical fuels [78]. Furthermore, the demonstration of fuel-lean liquid combustion in the counter-flow reactor is an important demonstration of its fuel-flexibility for field applications because liquid fuels are generally safer and easier to transport than gaseous fuels.

Another important consideration for reactor operation in field applications is the operating points at which combustion can be sustained in the device. In order for a combustor to be widely applicable for different applications, the ability to operate over a

broad range of equivalence ratios and firing rates is desirable. As shown in the study of lean methane combustion in the counter-flow reactor, and described in Chapter 3, stable combustor operation over a broad range of equivalence ratios and inlet velocities (u) is necessary to achieve a wide range of firing rates while minimizing pollutant emissions [39].

Combustion stability as a function of reactant equivalence ratio and inlet velocity is determined for lean propane and lean heptane in the counter-flow reactor. Lean stability results are compared to previously obtained stability results for counter-flow reactor operation in the rich regimes for both fuels. Counter-flow combustor emissions measurements of carbon monoxide (CO), nitrogen oxides (NO_x) and unburned hydrocarbons (UHCs) are analyzed in this study for lean operation on propane and heptane, and results are compared to previously obtained emissions measured for lean methane combustion. Reactor channel wall temperatures are compared to adiabatic equilibrium temperatures to determine superadiabicity. The results of lean methane, propane and heptane combustion in the counter-flow reactor are examined to understand the influence of superadiabatic operation on operating range and emissions.

4.2   Materials and Methods

4.2.1   Experimental Apparatus

Premixed fuel and air are provided to the counter-flow reactor using mass flow controllers for propane and air, and a pump for heptane. Heptane is vaporized and premixed with air via a custom-designed and built vaporization and mixing chamber. Heptane is vaporized prior to entering the reactor. A detailed description of the heptane vaporization system used in this study is available in Belmont et al. [38] and described in Section 2.2.1.

Concentrations of carbon monoxide (CO), nitrogen oxides (NO_x), and unburned hydrocarbons (UHCs) were measured in the reactor exhaust using Rosemount Analytical analyzers. Samples were drawn through an uncooled quartz probe with a 2 mm inner diameter and inert tubing, and dried before analysis. A previous study [37] showed slightly lower product species concentrations from outside channels, and minimal variation of composition within a single channel except near the alumina walls. In consideration of these findings, exhaust samples in this study were taken from the center channels at the middle of the channel exit. Therefore, the data produced in this study is expected to be representative of interior channels in scaled up reactors.

4.2.2   Experimental Method

The start-up procedure began by burning a near-stoichiometric mixture of the fuel of interest at the reactor outlets at an inlet velocity of 50 cm/s. The reaction fronts propagated upstream in the channels once the reactor heads had warmed sufficiently, and stabilized downstream of the porous SiC flow straighteners. Operating conditions were

then gradually adjusted to the reference conditions for each fuel, and were maintained at those values until temperatures stabilized. References conditions for propane and heptane were $\phi = 0.41$ and $u = 125$ cm/s.

The warm-up phase took approximately 45 minutes. Experiments included the determination of stable operating conditions and the exhaust gas concentrations of CO, NO_x and UHCs for each fuel over a range of inlet velocities and equivalence ratios. Test conditions were considered stable if combustion was sustained in the main reactor section for ten minutes at constant temperatures. Reactor wall temperatures were monitored in each of the four channels throughout the experiments. Gas temperatures were not measured directly due to the tendency of thermocouples inserted into the channel to act as flame holders. Peak wall temperatures were recorded at stable reactor conditions and showed less than $\pm 5°C$ variation during that time and while exhaust gas samples were taken. Reactor temperatures were limited to less than $1300°C$ through the restriction of tested operating conditions in order to avoid damage to the reactor.

Following the warm-up phase and stabilization at the reference conditions, equivalence ratio or inlet velocity was adjusted to the desired test values. Inlet velocity was specified at standard conditions of $25°C$ and 1 atm. Emissions results were obtained over a range of inlet velocities with equivalence ratio held constant at $\phi = 0.41$, and over a range of equivalence ratios with inlet velocity held constant at 125 cm/s. Emissions concentrations in parts per million (ppm) are reported as measured on a dry basis.

Each operating point was tested twice. Total uncertainty was calculated at each point as the root-sum-square of the contributing uncertainties. The uncertainty of emissions results is due to repeatability of measurements as calculated using a student-t distribution, the calibration gases and the analyzers. Average uncertainties of CO, NO_x and UHC measurements for propane and heptane are ±13, 2 and 16 ppm and ±28, 2 and 1 ppm, respectively. Inlet velocity uncertainty is due to uncertainties of the mass flow controllers for air and propane, the pump for heptane, and the channel cross-sectional area. Equivalence ratio uncertainty is due to contributions from the flow controllers and pump. Average uncertainties of inlet velocity and equivalence ratio are ±10 cm/s and ±0.03 for propane, and average uncertainties of inlet velocity and equivalence ratio are ±10 cm/s and ±0.04 for heptane. Temperature uncertainty is attributed to contributions from repeatability of measurements, the thermocouples, and the data acquisition system. Average temperature uncertainties for propane and heptane are estimated to be $\pm16°C$ and $\pm20°C$, respectively.

4.3   Results and Discussion

4.3.1   Operating Range

4.3.1.1 Propane

Figure 23 is a stability plot for counter-flow reactor operation on propane, where operating conditions are defined in terms of inlet velocity and both standard and

normalized equivalence ratio. Normalized equivalence ratio, defined as $\phi/(1+\phi)$, permits direct comparison of rich and lean operating regimes because it compensates for the inherent asymmetry in the definition of standard equivalence ratio [66].
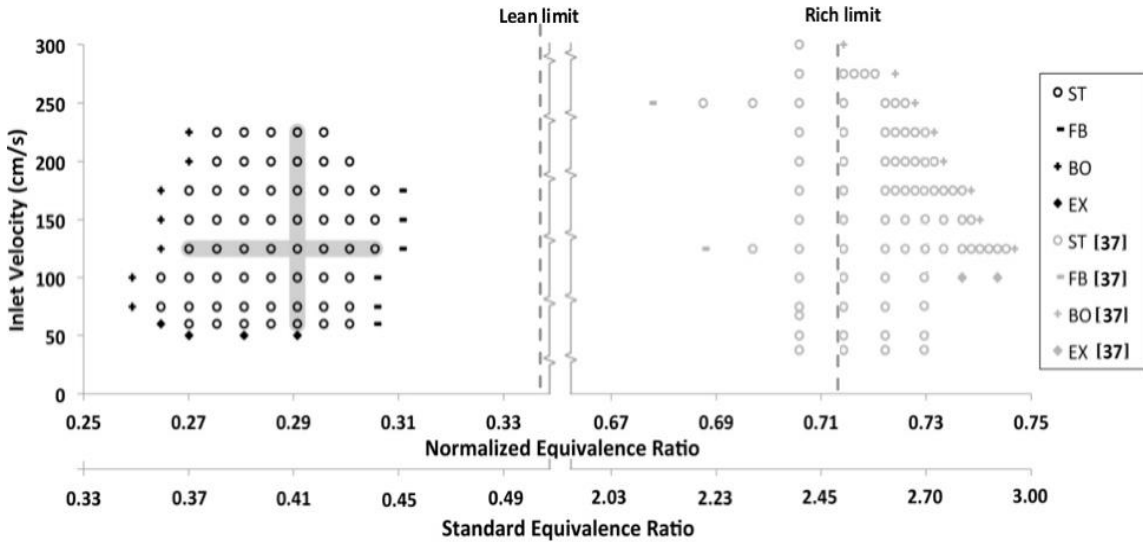
Figure 23. Stability map for counter-flow reactor operation on lean and rich [37] propane/air reactants, with stable (ST) and unstable points due to flashback (FB), blow-off (BO) and extinction (EX) shown as a function of inlet velocity and both standard and normalized equivalence ratios. Lean and rich flammability limits for propane/air reactants at inlet conditions are indicated.

The conditions where the reactor operates stably, as well as conditions where operation becomes unstable, are shown. Combustor instability can occur as flashback, in which the reaction front propagates upstream past a section of porous flow straightener in the reactor channel; blow-off, in which the reaction front propagates out of the outlet of the reactor channel; or extinction, in which the rate of heat loss exceeds the rate of heat

76

release and combustion is not sustained. In addition to stability data acquired for lean combustor operation, previously obtained data for reactor operation on fuel-rich mixtures of propane [37] are included in the plot. Taken together, a broader understanding of stable reactor operation is attained.

Some operating points were not tested at high inlet velocities in order to avoid damage to the reactor due to high temperatures. Lean operation is achieved at minimum and maximum propane standard equivalence ratios of 0.36 and 0.44, over a range of inlet velocities from 60 to 225 cm/s. These conditions correspond to Reynolds numbers of approximately 100-600 based upon inlet conditions, putting reactor operation in the laminar regime. Stable operation in the lean regime is entirely below the conventional lean flammability limit of propane, $\phi = 0.51$, while the stable rich range spans from below to above the conventional rich flammability limit, $\phi = 2.5$ [2]. In normalized form, the width of the stable rich regime is approximately 35% broader than the lean.

4.3.1.2 Heptane

Figure 24 is a stability plot for counter-flow reactor operation on heptane, where operating conditions are defined in terms of inlet velocity and both standard and normalized equivalence ratio. The operating conditions where the reactor operates stably, as well as conditions where operation becomes unstable due to flashback, blow-off or extinction, are shown. In addition to stability data acquired for lean combustor operation,

previously obtained data for reactor operation on fuel-rich mixtures of heptane [38] are included in the plot.

Lean operation is achieved at minimum and maximum heptane standard equivalence ratios of 0.37 and 0.46, over a range of inlet velocities from 100 to 225 cm/s. The minimum stable inlet velocity, 100 cm/s, is significantly higher than previously tested fuels, methane and propane, which stabilized at 60 cm/s. Destabilization by extinction at the lower velocity limit, which occurs at 75 cm/s for heptane combustion at $\phi = 0.41$ in the counter-flow reactor, has been observed in previous studies as well [36, 39]. This mode of destabilization results from the low rate of enthalpy input at low inlet velocities, while the rate of heat loss is a function of reactor temperature, which does not change proportionately. Stable operation in the lean regime is significantly below the conventional lean flammability limit of heptane, $\phi = 0.56$, while the stable rich range spans from below to slightly above the conventional rich flammability limit, $\phi = 3.8$ [2]. In both standard and normalized form, the width of the stable rich regime is significantly broader than the lean.
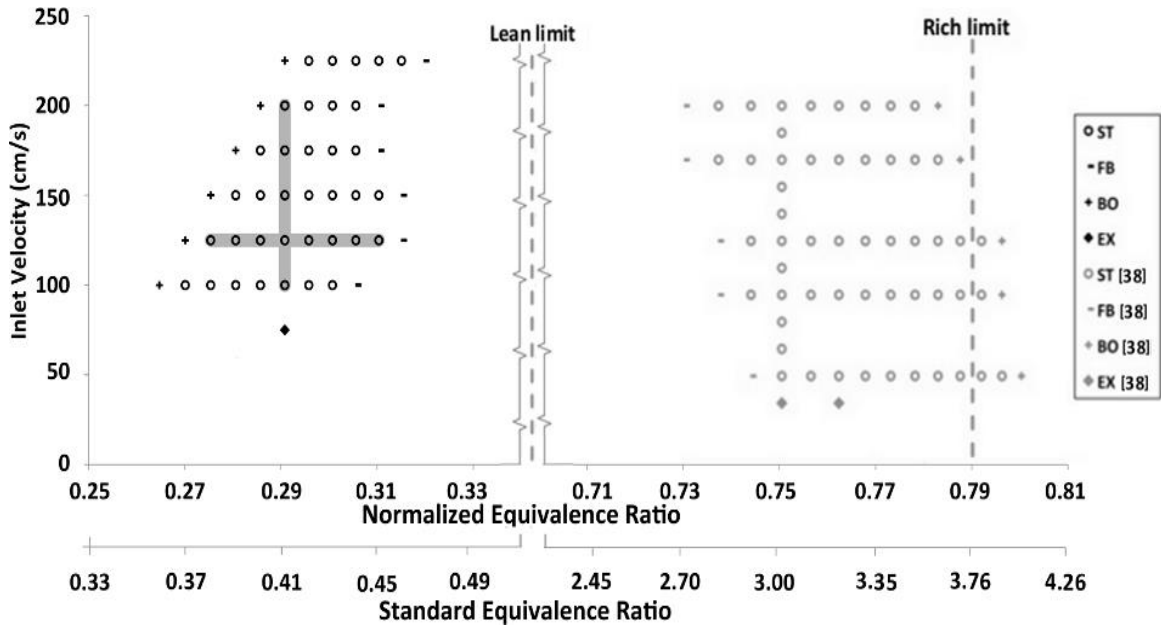
Figure 24. Stability map for counter-flow reactor operation on lean and rich [38] heptane/air reactants, with stable (ST) and unstable points due to flashback (FB), blow-off (BO) and extinction (EX) shown as a function of inlet velocity and both standard and normalized equivalence ratios. Lean and rich flammability limits for heptane/air reactants at inlet conditions are indicated.

4.3.2   Emissions

Exhaust emissions of CO, NO_x and UHCs, and peak wall temperature measurements are reported for lean reactor operation on heptane and propane, and these results are compared to previously published data for methane [39]. Results are presented for two sets of tests: variation of inlet velocity with equivalence ratio held constant, and variation of equivalence ratio with inlet velocity held constant.

4.3.2.1 Effect of Inlet Velocity

For a specified equivalence ratio, the equilibrium temperature is fixed and is not affected by volumetric flow rate. In a practical reactor, however, increasing the inlet velocity at a specified equivalence ratio increases the firing rate while altering the ratio of volumetric heat release to external heat loss, which is primarily affected by convection from the outside surface area. In addition, the residence time in the reactor decreases with increasing velocity. These two factors of temperature and residence time are important in the formation of emissions.
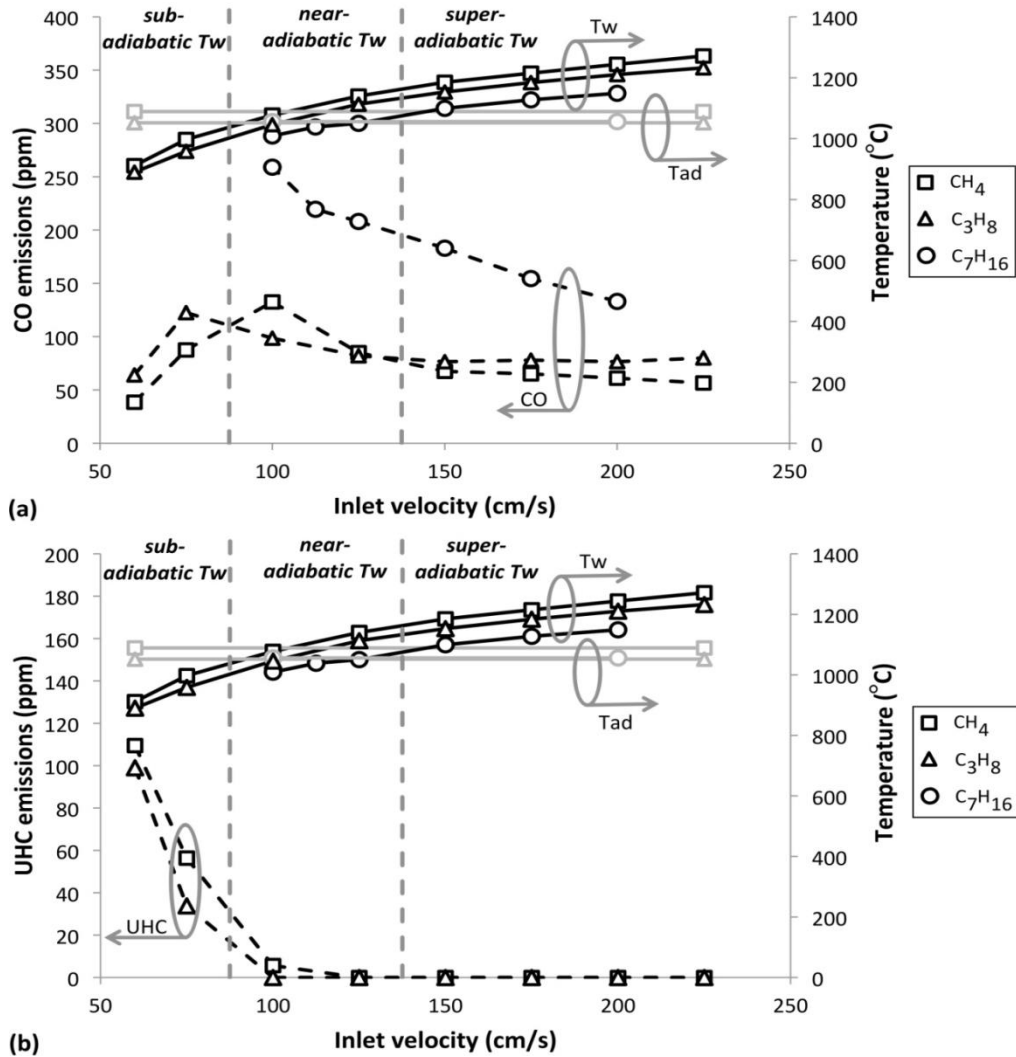
Figure 25. **(a) CO exhaust concentration and peak wall temperature (Tw) for lean counter-flow combustor operation on heptane, propane and methane [39], and (b) UHC exhaust concentration and peak wall temperature measured for lean counter-flow combustor operation on propane and methane [39] are shown. UHCs are undetected at all tested heptane operating points and are not shown. A range of inlet velocities are tested with equivalence ratio held constant at $\phi = 0.41$ for heptane and propane, and $\phi = 0.44$ for methane. Calculated adiabatic equilibrium temperatures (Tad) for the tested equivalence ratios of each fuel are shown. Subadiabatic, near-adiabatic and superadiabatic operating regions, defined in terms of peak wall temperature, are also shown.**

Figure 25a shows CO exhaust concentrations and peak measured wall temperatures for lean reactor operation on heptane, propane and methane [39] as a function of inlet velocity. Figure 25b shows UHC exhaust concentrations and peak wall temperatures for propane and methane. For heptane, UHCs were undetected at all points and are not included in Figure 25b. In order to facilitate direct comparison of the data presented in this study to other bodies of work, these results are presented in terms of standard equivalence ratio. Inlet velocity varies from 60 to 225 cm/s with equivalence ratio held constant at $\phi = 0.44$ for methane and $\phi = 0.41$ for propane, and from 100 to 200 cm/s for heptane at $\phi = 0.41$. Calculated adiabatic equilibrium temperatures for each fuel at the tested equivalence ratios are shown. Propane and heptane data were acquired at $\phi = 0.41$, as highlighted in the stability maps shown in Figure 23 and Figure 24, where broad ranges of stable inlet velocities were achieved for both fuels. In the earlier study [39], it was found that methane flames stabilized over a broad range of inlet velocities at an equivalence ratio of $\phi = 0.44$. Although this small difference in equivalence ratio complicates the comparison of the different fuels, it is still instructive to examine the trends associated with changes in inlet velocity, which significantly affect reactor temperatures. This effect is attributed to an increase in the ratio of volumetric heat release within the reactor to heat losses from the surface of the reactor as inlet velocity increases. The change in reactor temperatures strongly impacts reaction rates, and therefore emissions.

Additionally, regions of combustor operation are defined based upon peak wall temperatures, and are indicated in Figure 25a and Figure 25b. While peak gas temperatures are expected to be superadiabatic at all operating points based upon previous theoretical analyses [35, 39], peak wall temperatures are a readily measured indicator of reactor conditions. Peak wall temperatures are the lowest temperatures experienced by the reaction zone; this has significant implications for reaction chemistry and quenching, and therefore emissions. The operating regions are designated as subadiabatic, near-adiabatic, and superadiabatic depending on the value of the peak reactor wall temperature relative to the adiabatic temperature, where near-adiabatic operation is identified where peak reactor temperatures are within approximately 50°C.

Propane combustion produces peak reactor wall temperatures that vary from 890 to 1233°C at the lowest and highest tested inlet velocities, respectively, and are superadiabatic at inlet velocities above 100 cm/s. The positive correlation of peak wall temperature with inlet velocity is also shown for methane [39], as well as in previous studies [36-38]. This is a result of increased rate of heat release within the reactor with increasing velocity compared to rate of heat loss to the surroundings. Heptane combustion produces a similar temperature trend, with peak wall temperatures increasing from 1046 to 1149°C with increasing inlet velocity. Heptane has a narrower stable operating range than propane and methane at the tested equivalence ratios; instability occurs at inlet velocities below 100 cm/s and above 200 cm/s.

The CO concentration from heptane combustion decreases from 259 ppm to 133 ppm with increasing inlet velocity. CO concentration from propane also decreases with increasing inlet velocity above 75 cm/s, with minor variation at the highest tested inlet velocities that is within calculated uncertainty. At the lowest tested inlet velocity of 50 cm/s, the concentration of CO is significantly less than the peak value of 123 ppm that occurs at 75 cm/s. UHCs from propane are detected at inlet velocities of 50 and 75 cm/s.

The results of propane combustion show temperature and CO trends that are similar to methane [39]. Detection of UHCs at the lowest tested inlet velocities indicates incomplete fuel breakdown for both fuels. The absence of measured UHCs for heptane is attributed to the narrower stable operating range of heptane within the counter-flow reactor, which is limited to a minimum inlet velocity of 100 cm/s. It is anticipated that UHCs would be detected if heptane flames could be stabilized in the reactor at lower inlet velocities, following trends observed for methane and propane, however the current reactor geometry does not support heptane flames at inlet velocities below 100 cm/s at ϕ = 0.41.
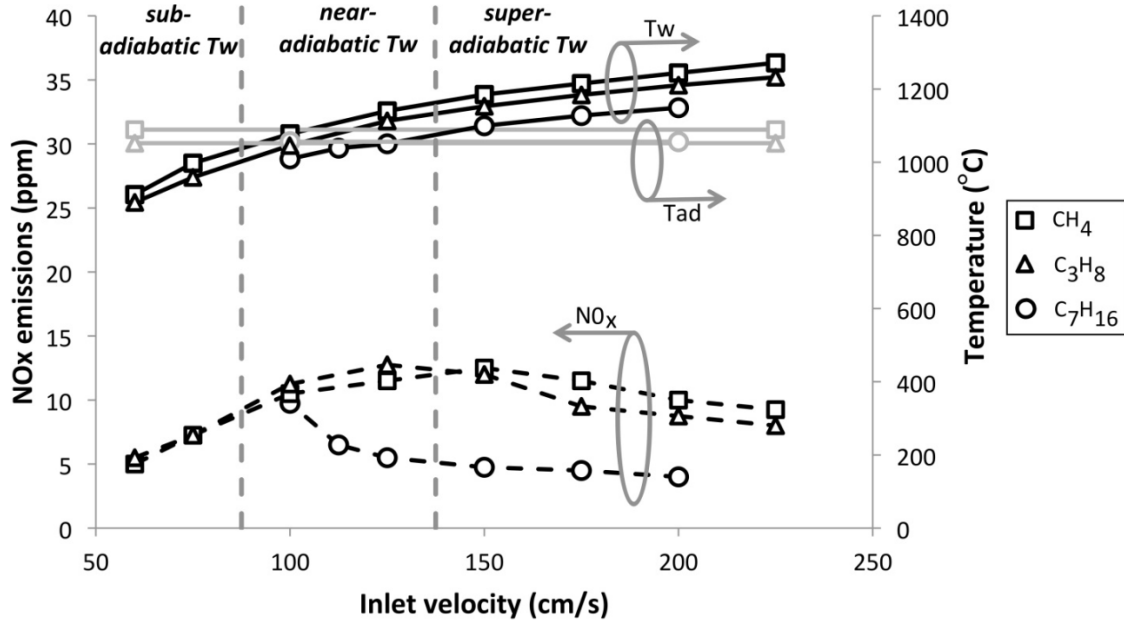
**Figure 26. NO$_x$ exhaust concentration and peak wall temperature (Tw) measured for lean counter-flow combustor operation on heptane, propane and methane [39]. Inlet velocity is varied with equivalence ratio held constant at ϕ = 0.41 for heptane and propane, and ϕ = 0.44 for methane. Adiabatic equilibrium temperatures (Tad) for the range of tested equivalence ratios of each fuel are shown. Subadiabatic, near-adiabatic and superadiabatic operating regions, defined in terms of peak wall temperature, are also shown.**

Figure 26 shows NO$_x$ exhaust concentrations for combustion of lean heptane, propane and methane [39]. Results are presented for inlet velocities from 60 to 225 cm/s with equivalence ratio held constant at ϕ = 0.41 for propane and ϕ = 0.44 for methane, and from 100 to 200 cm/s for heptane at ϕ = 0.41. Peak measured wall temperatures and calculated adiabatic equilibrium temperatures are shown. Additionally, regions of

combustor operation, defined by subadiabatic, near-adiabatic and superadiabatic peak wall temperatures, are indicated.

NO_x concentration is below 13 ppm at all tested points. The highest NO_x measurements occur at 125 cm/s for propane, and the concentrations decrease with increasing and decreasing inlet velocities from that point. The same trend is observed for methane combustion [39]. The initial increase in NO_x with inlet velocity is attributed to temperature dependence, whereas the variation at higher inlet velocities is largely within the estimated uncertainty. A slight decrease at the highest tested inlet velocities is attributed to decreased residence times at these conditions. Similar effects of inlet velocity on emissions have been observed in other studies [14, 15].

Heptane combustion produces the highest NO_x concentration at the lowest tested inlet velocity. Concentration decreases with an increase in inlet velocity, and remains constant within the estimated uncertainty over the remainder of the tested inlet velocities.

4.3.2.2 Effect of Equivalence Ratio

For a fixed inlet velocity, a change in equivalence ratio changes the reactor firing rate while maintaining an approximately constant residence time. The necessary firing rate is determined by process requirements, while environmental considerations dictate acceptable emissions levels.

86

Figure 27 shows CO exhaust concentrations and peak wall temperatures for lean reactor operation on heptane, propane and methane [39]. Equivalence ratios are varied from 0.38 to 0.45 for heptane, 0.37 to 0.44 for propane and 0.41 to 0.48 for methane, with inlet velocity held constant at u = 125 cm/s. Calculated adiabatic equilibrium temperatures for each fuel at the tested equivalence ratios are also shown. The widths of stable equivalence ratio ranges are the same for each fuel at an inlet velocity of 125 cm/s, where all emissions were measured for equivalence ratio variation. However, as can be seen in the stability maps shown in Figure 23 and Figure 24, and in the previously published lean methane investigation [39] described in Chapter 3, the upper and lower limits of these stable ranges vary between the different fuels. Methane in particular exhibits a stable range that is shifted more significantly towards stoichiometric as compared to the other two tested fuels. Because there are no flameholders in the counter-flow reactor, stable operation is obtained when the inlet flow is balanced by the burning rate, which is a function of equivalence ratio, preheat temperature, heat losses, heat recirculation, and fuel chemistry.
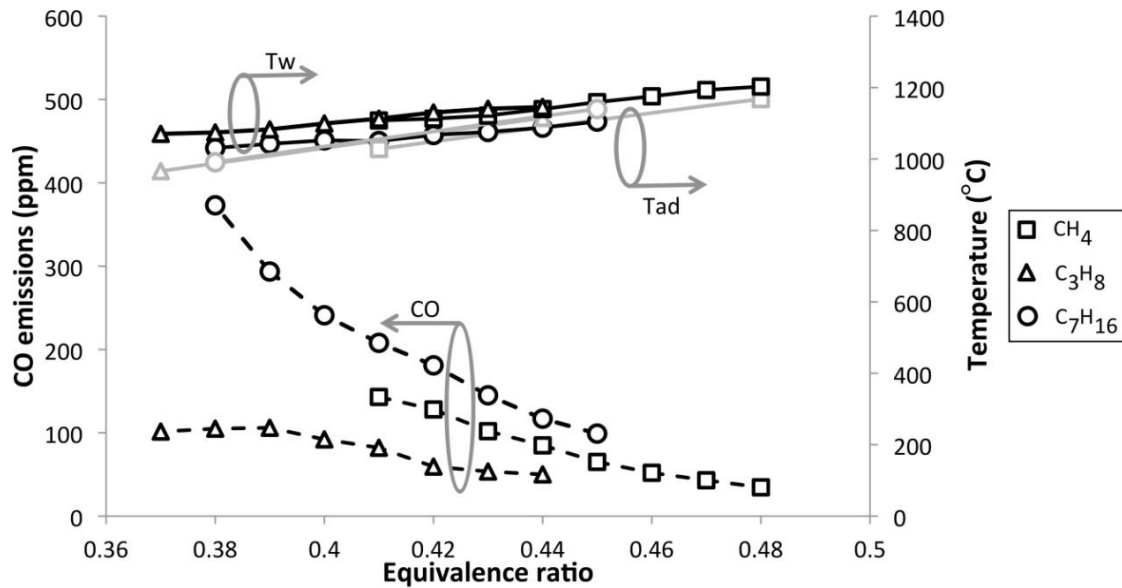
Figure 27. CO exhaust concentration and peak wall temperature (Tw) measured for lean counter-flow combustor operation on heptane, propane and methane [39] with varying φ and inlet velocity held constant at *u* = 125 cm/s are shown, as well as calculated adiabatic equilibrium temperatures (Tad) for the range of tested equivalence ratios of each fuel

Both heptane and propane combustion result in modest increases of peak wall temperatures with equivalence ratio from 1046 to 1149°C and 1071 to 1146°C, respectively. This trend is consistent with the results for methane [39]. The positive correlation of temperature with equivalence ratio for both fuels is also in agreement with trends predicted by chemical equilibrium. Comparison of measured and equilibrium temperatures shows that peak wall temperatures are superadiabatic at all tested methane and propane equivalence ratios. Peak wall temperatures for heptane are superadiabatic at equivalence ratios below 0.42, and are subadiabatic at the highest tested equivalence

ratios. Peak wall temperatures as a function of equivalence ratio are generally within 50°C of the adiabatic equilibrium temperature for all fuels, and are considered to be in the near-adiabatic regime, thus the three operating regimes identified in Figure 25 and Figure 26 are not identified in Figure 27 and Figure 28.

The measured CO concentration for propane combustion initially increases slightly with increasing equivalence ratio from $\phi = 0.37$ to $\phi = 0.39$, however the variation in this range is within calculated uncertainty. At higher equivalence ratios, CO concentration decreases with increasing equivalence ratio from a peak value of 106 ppm to 50 ppm at the highest tested equivalence ratio of 0.44. Likewise, the measured CO concentration for heptane combustion decreases from a peak value of 373 ppm at the lowest tested equivalence ratio of 0.38 to 99 ppm at the highest tested equivalence ratio of 0.45. This trend is in agreement with the results for methane, which show a decrease in CO concentration with increasing equivalence ratio across the tested range. As was previously observed with methane [39], this negative correlation is in contrast to chemical equilibrium, which indicates an increase in CO concentration as equivalence ratio approaches stoichiometry. However, the measured values for heptane and propane combustion are significantly in excess of equilibrium, which predicts less than 1 ppm of CO at all tested equivalence ratios. Mesoscale reactors are particularly prone to reaction quenching at the channel walls as compared to larger reactors due to increased surface area-to-volume ratios, which leads to incomplete combustion. An additional challenge of high surface area-to-volume ratios in mesoscale reactors is the increased heat loss at channel walls, which produces lower reaction temperatures and therefore decreased

reaction rates. Reactor temperatures and heat loss are also highly dependent on inlet conditions, including inlet velocity and equivalence ratio, which significantly impact the rate of volumetric heat release. The observed CO trend is attributed to a dependence on reactor temperature, which increases with equivalence ratio and drives the oxidation of CO toward CO_2 and equilibrium. Similar CO trends have been observed in other mesoscale combustor studies [14, 39].
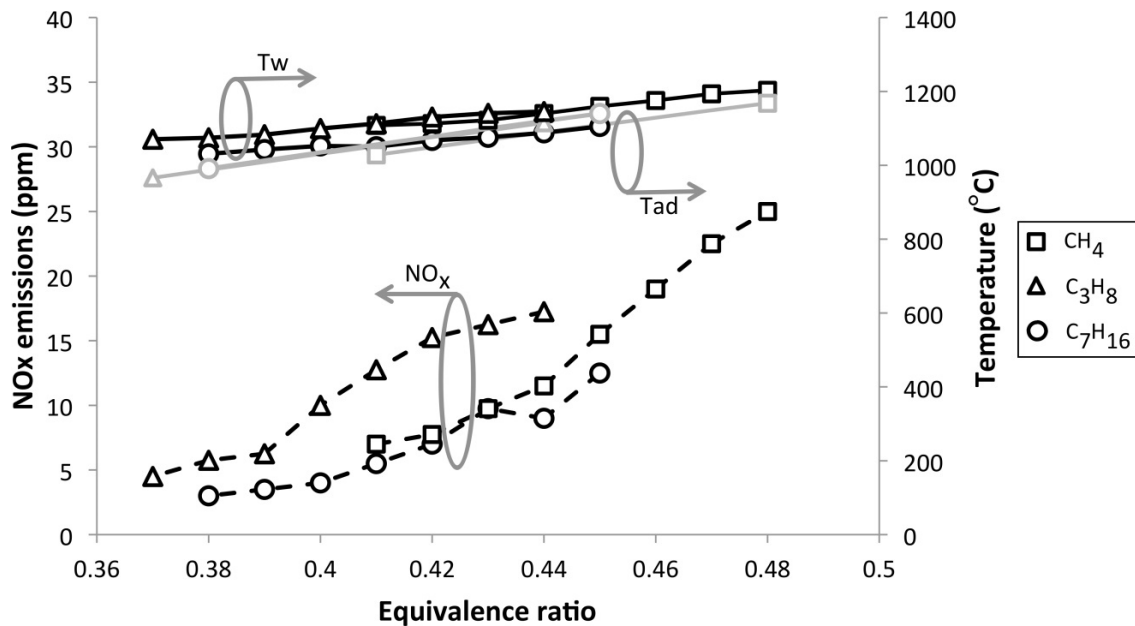

Figure 28. NO_x exhaust concentration and peak wall temperature (Tw) measured for lean counter-flow combustor operation on heptane, propane and methane [39] with varying ϕ and inlet velocity held constant at $u = 125$ cm/s are shown, as well as adiabatic equilibrium temperatures (Tad) calculated for the range of tested equivalence ratios of each fuel

Figure 28 shows NO_x exhaust concentrations for lean reactor operation on heptane, propane and methane [39]. Results are presented for varying equivalence ratio with inlet velocity held constant at $u = 125$ cm/s. Again, peak wall temperatures and calculated adiabatic equilibrium temperatures are shown. The measured NO_x concentration for heptane and propane combustion increases with increasing equivalence ratio from 5 ppm at $\phi = 0.37$ to 17 ppm at $\phi = 0.44$. The same trend is observed for methane combustion [39].

Unburned hydrocarbons are undetected at all tested equivalence ratios for lean heptane, propane and methane combustion at an inlet velocity of $u = 125$ cm/s, indicating complete fuel breakdown.

4.3.3   Effect of Superadiabatic Operation

The peak reactor wall temperatures measured during experiments are categorized as subadiabatic, near-adiabatic and superadiabatic relative to the calculated adiabatic equilibrium temperature of the unburned fuel mixture, and are labeled accordingly in Figure 25 and Figure 26. In a reactor that operates without heat recirculation, temperatures will necessarily be subadiabatic everywhere because of unavoidable heat losses from the system. In a heat-recirculating reactor, however, temperatures in excess of the adiabatic equilibrium temperature can be achieved through conduction and radiation by the solid structure of the reactor, and through convection by the gas. Previous theoretical analyses of the counter-flow reactor indicate that peak gas

temperatures within the reactor channels are significantly in excess of wall temperatures [35, 39]. Furthermore, experiments and computations of stationary flames in ducts constructed of low thermal conductivity materials show that wall temperatures in such systems are significantly less than centerline peak temperatures and adiabatic temperatures [79-81]. While peak gas temperatures at the centerlines of the reactor channels are therefore expected to be significantly higher than peak wall temperatures, the latter are more readily measured without interfering with reactor dynamics, such as by flameholding. Furthermore, reactor wall temperatures are quite important in determining quenching and heat loss rates. Therefore, peak wall temperatures provide an important and practical metric by which reactor performance can be evaluated and monitored. The results of this study reveal common trends in fuel emissions as the peak wall temperatures change with varying inlet conditions of equivalence ratio or inlet velocity. Regions of operation can be distinguished in terms of peak wall temperature, where distinct trends are noted depending on the value of the peak wall temperature relative to the calculated adiabatic equilibrium temperature. The results highlight the importance of achieving significantly superadiabatic peak temperatures within the reactor channels, which will result in near-adiabatic or superadiabatic wall temperatures due to heat losses at external surfaces, in achieving favorable emissions.

The current analysis of peak reactor wall temperature relative to calculated adiabatic equilibrium temperature is distinguished from a global definition of superadiabatic performance that is used in the discussion of heat recirculating reactors, which refers to the peak temperature in the gas phase of the reactor relative to the calculated adiabatic

equilibrium temperature. The peak wall temperatures observed in this study approach or are above the calculated adiabatic equilibrium temperatures for each fuel. Therefore, based upon previous theoretical and experimental analyses of heat recirculating reactors [2, 35, 39, 66, 79] which account for heat losses at the wall at all conditions, all reported cases in this study most likely exhibit superadiabatic temperatures at the centerline of the reactor channel, and operation would therefore be deemed superadiabatic by global definition. The current analysis, however, focuses on the categorization of peak wall temperature relative to calculated equilibrium temperature, and uses the designation of subadiabatic, near-adiabatic and superadiabatic to convey the relative magnitudes of these values.

Inlet velocity has a significant effect on the peak wall temperature, which is as much as 200°C greater than the adiabatic temperature at the conditions tested in this study. In Figure 25 and Figure 26, regions of subadiatic, near-adiabatic, and superadiabatic peak wall temperature conditions have been identified. Stable operation for heptane was not obtained at significantly subadiabatic wall temperature conditions. For methane and propane, high levels of UHCs are detected at subadiabatic wall temperature conditions, and NO_x concentrations are low. These results are consistent with incomplete combustion.

At conditions where near-adiabatic wall temperatures were measured, CO peaks and then decreases with increasing inlet velocity for all fuels and UHCs are not detected at the highest tested inlet velocities in this regime. The variation of NO_x among the different

fuels in this region is not consistent: concentrations increase for propane and methane and decrease for heptane. It should be noted, however, that all NO_x concentrations are less than 15 ppm.

At conditions where superadiabatic peak wall temperatures were measured, the emissions of all reported species are fairly constant with the exception that CO for heptane/air continues to decrease.

A negative correlation of CO with temperature is observed in all data, except those points where UHCs are detected for methane and propane (Figure 25 and Figure 27). These products are far from equilibrium values, which predict less than 1 ppm for both CO and UHCs. In contrast, no UHCs are detected for heptane combustion. Likewise, no significantly subadiabatic wall temperatures are measured at any stable heptane operating points. The stable range of inlet velocities is narrower for heptane as compared to methane and propane. Flashback occurs at a higher inlet velocity for heptane compared to the other two fuels, and the lowest stable velocity is limited to approximately where the measured peak wall temperatures become subadiabatic. In contrast, methane and propane are able to stabilize at significantly subadiabatic wall temperatures, but UHCs are measured at these points (Figure 25).

Heptane is likewise limited at the high end of the tested inlet velocity range by blow-off at 225 cm/s, whereas methane and propane are stable at this condition. Peak wall temperature values are lower for heptane than methane and propane across the tested

range of inlet velocities (Figure 25 and Figure 26). Flame temperature and speed are strongly dependent on reactant temperature; therefore peak wall temperature and burning rate within the reactor are expected to be highly dependent on the extent of counter-flow heat exchange from combustion products in order to preheat counter-flowing reactants in adjacent channels. Since the counter-flow reactor requires burning rate to equal reactant velocity in order to operate stably, insufficient preheating of reactants leads to heptane blow-off at high inlet velocities.

The results of lean methane, propane and heptane combustion suggest significant changes in stability and emissions behavior when the peak wall temperatures become subadiabatic. Emissions concentrations indicate that low wall temperatures in the subadiabatic peak wall temperature regime do not promote sufficient reaction rates for complete fuel breakdown, and increasing wall temperatures into the adiabatic and superadiabatic regimes drive reactions toward equilibrium. Emissions and stability range results suggest that combustor operation with peak wall temperatures in the near-adiabatic and superadiabatic regimes is desirable for allowing increased firing rates and decreased emissions. The most significant decline in emissions is seen in the transition from subadiabatic to near-adiabatic peak wall temperatures, while further temperature increase into the superadiabatic regime produces marginal additional advantage. The more significant advantage of operation in the superadiabatic wall temperature regime is found in extension of the stable combustor operating range, as highlighted by the absence of heptane stability in the subadiabatic wall temperature regime. This finding is in agreement with a previous investigation of preheated flames [82].

In contrast to the previous cases in which peak wall temperature was significantly affected by changes in velocity, the peak wall temperature as a function of equivalence ratio (Figure 27 and Figure 28) is generally within $50^{o}C$ of the adiabatic equilibrium temperature at the tested inlet velocity of 125 cm/s for each fuel, and is considered to be in the near-adiabatic regime. Emissions of CO decrease and NO_x increase with increasing equivalence ratio for all three fuels. Measured concentrations are significantly above equilibrium values, and the observed trends are attributed to temperature dependence.

While the data for equivalence ratio variation with an inlet velocity of 125 cm/s show peak wall temperatures in the near-adiabatic regime, Figure 25 and Figure 26 indicate that an increase or decrease in the inlet velocity may result in a shift of the peak wall temperatures into the superadiabatic or subadiabatic regimes. The effects of such a shift on stability and emissions can be anticipated based upon the results for inlet velocity variation.

4.4   Conclusions

Lean premixed combustion of heptane and propane was studied in a heat recirculating mesoscale counter-flow reactor. This reactor design has previously been used to study the oxidation of lean methane, as well as the conversion of rich heptane, propane and methane reactant mixtures to hydrogen-rich synthesis gas. The current study expands the established capability of the counter-flow reactor to operate in the lean combustion

96

regime on increasingly complex fuels. In particular, liquid fuels are generally easier and safer to transport than gaseous fuels, and are studied because of their logistical importance.

Results included reactor stability maps for heptane and propane combustion that show stable operating points, as well as points where operation became unstable due to flashback, blow-off or extinction, for rich and lean reactant mixtures. Emissions of CO, NO_x and UHCs were presented for lean heptane and propane operation and compared to previously obtained results for lean methane operation. Additionally, operating regions were defined in terms of peak reactor wall temperatures. Similarities in trends between the three tested fuels highlight the correlation of emissions with peak reactor wall temperature, and support previous findings that a minimum firing rate is necessary for optimal performance. Further analysis highlights the importance of achieving peak wall temperatures near, or in excess of, the calculated adiabatic equilibrium temperature of the fuel at inlet conditions in heat-recirculating reactors for emissions minimization and stable range extension.

5   EFFECT OF GEOMETRIC SCALE ON HEAT RECIRCULATION AND SYNGAS PRODUCTION IN A NON-CATALYTIC COUNTER-FLOW REFORMER

The fourth focus of this research examined the effect of channel reactor geometric scaling on syngas production from methane. This work is described below, and is under review by *Combustion Science and Technology*.

5.1   Introduction

A computational model of the counter-flow reactor was previously developed to study the reaction zone characteristics of rich methane combustion, in which the reactor channels were modeled in two dimensions, and the detailed GRI 2.11 kinetics mechanism was used. The model was validated against experimental results, where the impact of inlet velocity and equivalence ratio operating conditions on combustion zone characteristics was successfully modeled [81].

This study utilizes the computational model to study the impact of geometric scaling on rich methane reforming in the counter-flow reactor. Scalability is an important consideration for portable power applications, as well as for large-scale, stationary applications. In either case, reactor scaling may be achieved by changing the geometry of

the individual channels or by altering the number of parallel channels [83]. This study focuses on geometry at the individual channel scale.

Many experimental heat recirculation reactors used in research are mesoscale, in which the flame scale is on the order of a few millimeters. This scale is convenient for laboratory use and manufacturability. The optimal size for a given application, however, may depend on other factors including portability and stable operating range requirements.

Previous research has found significant effects of geometric parameters on reactor stability. Studies of parallel-plate reactors examined the effect of channel width and length, as well as wall thickness [84-86]. Findings suggest that there is a tradeoff involved in varying these parameters, and that, in turn, suggests the potential for optimization. One example of this tradeoff is recognized with regard to varying channel width. Operating under an assumption of a constant Nusselt number of approximately 4, convective heat transfer between gases and channel wall is inversely proportional to the channel width. Conversely, the increase in the surface area-to-volume ratio with decreasing channel width leads to increased heat losses to the environment. Similarly, when considering the variation of channel length, increased length translates to increased residence time, which may permit increased fuel conversion to combustion product species. Increased length, however, also increases surface area from which heat losses to the surroundings can occur.

Several studies have examined the effects of geometric scaling on the combustion stability and performance of mesoscale, heat-recirculating combustors [87]. The parameters that have been examined include channel wall thickness and material in Swiss-roll and parallel-channel reactors [84, 85, 88, 89], as well as channel length [90] and channel width [84, 89, 91-94]. Kaisare and Vlachos [86] numerically studied the effect of reactor length, wall thickness and reactor opening size on flame stability in micro- and mesoscale channel reactors.

The effect of scaling the counter-flow reactor on non-catalytic fuel reforming is the focus of this computational study, where reactor channel length or height are varied from the original dimensions examined in previous experimental [36-40] and analytical investigations [35, 39]. The impact of scaling on methane reforming is quantified in a number of ways: reactor operating range, efficiency of reactant conversion to hydrogen and carbon monoxide, efficiency of methane fuel conversion, efficiency of heat recirculation from hot combustion products to incoming cold reactants, and degree of superadiabicity, defined as the ratio of peak temperatures to equilibrium temperatures, achieved in the reactor. Computational investigation of reactor operating range and chemical species conversion provides an efficient means of testing numerous reactor geometries. Quantification of heat recirculation efficiency and degree of superadiabicity provides insights into reactor operation that are not readily measured during experimentation. Heat recirculation efficiency in the counter-flow reactor is compared to that achieved in a porous reactor [95].

5.2   Numerical Model

The data presented in this study were obtained from simulations performed using the computational fluid dynamics (CFD) code Fluent 14.5.   The CFD code solves conservation of mass, energy and species equations and the low Mach-number Navier-Stokes equations. The conservation of mass is given by

$$\frac{\partial \rho_f}{\partial t} + \nabla \cdot \left(\rho_f \boldsymbol{v} \right) = 0 \tag{9}$$

and the conservation of momentum is given by

$$\frac{\partial (\rho_f \boldsymbol{v})}{\partial t} + \nabla \cdot \left(\rho_f \boldsymbol{v} \boldsymbol{v} \right) = -\nabla p + \nabla \cdot \bar{\tau} + \boldsymbol{F} \tag{10}$$

where ρ_f is fluid density, $\boldsymbol{v}$ is the velocity vector, and p is the static pressure. The stress tensor, $\bar{\tau}$, represents viscous forces. The effect of the sections of porous media within the reactor channels on fluid dynamics is accounted for by the momentum source term, $\boldsymbol{F}$, in Equation 10. The momentum source representation of porous media is modeled in Fluent as including two components, viscous and inertial losses, where the former is dominant in laminar flows such as those in the current investigation. The viscous resistance of the porous media is specified as 3.846e7 m^-2. The fluid is approximated by the ideal gas law, thus fluid density is given by $\rho_f = p/(RT/M_w)$ where R is the ideal gas constant, T is temperature and M_w is the molecular weight of the gas.

101

Conservation of energy for the fluid phase is given by

$$\frac{\partial(\rho_f E)}{\partial t} + \nabla \cdot \left(\boldsymbol{v}(\rho_f E + p)\right) = \nabla \cdot \left(k_f \nabla T - \sum_i h_i \boldsymbol{J}_i\right) + S_{h,f} \tag{11}$$

where $E = h - p/\rho_f + v^2$ and h is sensible enthalpy, defined for incompressible fluid as $h = \sum_i Y_i h_i$ with Y_i as the mass fraction of species i. Thermal conductivity is given by k, $\boldsymbol{J}$ represents Fickian species diffusive flux, and $S_{h,f}$ is a volumetric source term that includes the heat of chemical reactions.

Conservation of energy for the solid phase is given by

$$\frac{\partial(\rho_s h_s)}{\partial t} = \nabla \cdot (k_s \nabla T) + S_{h,s} \tag{12}$$

where $S_{h,s}$ represents user-defined sources that account for volumetric external ambient heat losses, and radiation between gray surface channel walls and porous zones. Solid thermal conductivity, k_s, is defined as 50 W/m-K using manufacturer specifications of the silicon carbide used in experimental counter-flow reactors. Net radiative heat flux, q_k, at a channel surface includes incoming and outgoing fluxes, $q_{k,i}$ and $q_{k,o}$ respectively, where the incoming and outgoing fluxes are given by

$$q_{k,o} = \epsilon \sigma T_k^4 + (1 - \epsilon) q_{k,i} \tag{13a}$$

102

$$q_{k,i} = \sum_j \int q_{j,o} dF_{dk-dj} \tag{13b}$$

where solid emissivity, ϵ, is defined as 0.85, σ is the Stefan-Boltzmann constant, T_k is the surface temperature, and $F_{dk\text{-}dj}$ is the view factor between surfaces k and j.

Conservation of species is given by

$$\frac{\partial(\rho_f Y_i)}{\partial t} + \nabla \cdot \left(\rho_f \boldsymbol{v} Y_i\right) = -\nabla \cdot \boldsymbol{J}_i + R_i \tag{14}$$

where the net rate of production of species i, R_i, is the sum of Arrhenius reaction rates for N reactions. Combustion chemistry is modeled using detailed reaction chemistry mechanism GRI 2.11. Further details about the numerical model can be found in [81].

5.2.1   Model Geometry

Figure 29a is a schematic of the four-channel reactor used in previous experimental investigations [36-40]. Figure 29b is a schematic of the computational domain of the original reactor geometry, with dimensions of the counter-flow reactor used in previous experimental reforming and thermal oxidation studies. The domain is reduced to one half-channel, which lessens the computational load significantly, through the use of symmetry and a user-defined function (UDF). Channel plane symmetry in the y-direction is imposed at $y = 0$, and temperature symmetry in the x-direction is imposed by a UDF at

$x = 0$. External losses are accounted for by radiative wall ends and convective losses from the wall in the direction perpendicular to the x-y plane. Therefore, the computational model approximates the reactor as an infinite number of parallel channels in the y-direction.
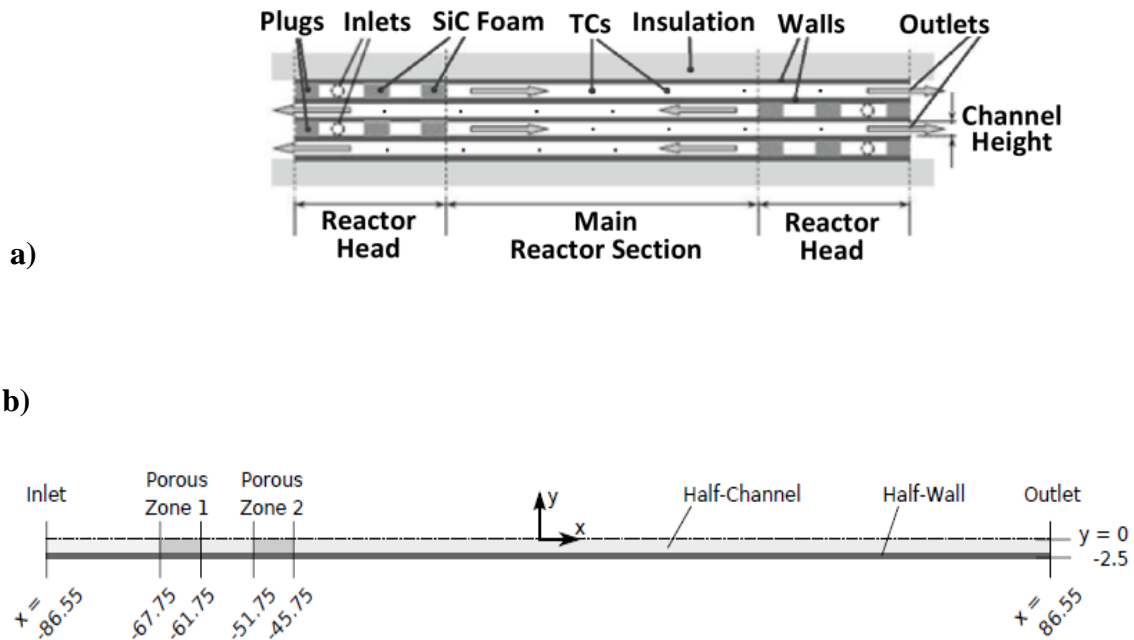
Figure 29. (a) A schematic of the four-channel reactor and (b) the computational domain of the original reactor geometry (VR=1.0)

The reactors modeled in this study are scaled relative to the volume of the original reactor (122 cm^3) by a volume ratio, defined as

$$Volume\ Ratio(VR) = \frac{Volume\ of\ scaled\ reactor}{Volume\ of\ original\ reactor} \qquad (15)$$

104

where the scaled reactor volume is achieved by varying either channel height or main reactor section length, while maintaining the other dimension at the reference, original reactor value. Geometry is additionally constrained by maintaining the original reactor head length, and channel wall thickness is maintained at the original value of 1 mm. Volume ratios of 0.75, 1.0 and 1.25 are investigated, where volume ratio 1.0 (VR=1.0) corresponds to the original reactor design and dimensions. Table 3 shows the dimensions of each scaled reactor.

Table 3. Counter-flow reactor dimensions for volume ratios (VR) 0.75, 1.0 and 1.25, obtained by varying channel height (h) or channel length (L) with the other dimension held constant at its original, reference value

Volume Ratio (VR)	Reactor ID	Channel height (mm)	Total channel length (mm)
1.0	VR=1.0	4.0	173.1
0.75	VR(h)=0.75	2.7	173.1
1.25	VR(h)=1.25	5.3	173.1
0.75	VR(L)=0.75	4.0	129.8
1.25	VR(L)=1.25	4.0	216.4

5.2.2 Solution Approach

Scaled reactors were modeled in ANSYS ICEM CFD. The initial model grids had axial and transverse spacing equal to that used in Schoegl and Ellzey [81]. A base case of each reactor model was run for 20k time steps of size 2e-5 seconds at inlet conditions of $\phi = 2.2$ and $u = 125$ cm/s in order to achieve ignition and initial stabilization of the flame front in the main reactor section of the channel. The solution of the base case was then used as an initial solution for each tested equivalence ratio and inlet velocity operating point. Solutions were continued until steady state was achieved, where steady state was determined to occur when the flame front velocity within the main section of the reactor model was less than 0.5 mm/s. Flame front location was determined by the location of peak H radical concentration.

After steady state was achieved, the mesh for each case was refined in a three phase process. Each mesh was locally refined in regions of high concentrations of specific chemical species, following Schoegl and Ellzey [81]. This process effectively increased the mesh resolution up to 64-fold around the combustion zone by partitioning quadrilateral elements into four sub-elements. Following each stage of mesh refinement, simulations were continued for a total of 5k additional time steps of size 1e-5 seconds. After the third refinement, the spatial discretization solution technique was changed from first-order upwind to second-order upwind, and the final result was obtained after an additional 3k time steps of size 1e-5 seconds. The Semi-Implicit Method for Pressure

Linked Equations (SIMPLE) algorithm was used for pressure-velocity coupling during the transient calculations.

5.3 Results and Discussion

Results are presented below for each of the five scaled reactors over the range of tested inlet velocities and equivalence ratios. Data include operating conditions where a stationary reaction zone was achieved in the main section of the reactor at steady state, as well as heat recirculation efficiency, gas and wall temperature ratios, and hydrogen, carbon monoxide and methane conversion efficiencies at those steady state points.

5.3.1 Operating Range

Each of the five reactor geometries were tested over a range of inlet velocities and equivalence ratios to determine which operating points produce a stationary flame front solution in the main section of the reactor channel, which corresponds to stable reactor operating points in experimental studies. Inlet velocity was varied from 50-200 cm/s in increments of 25 cm/s at $\phi = 2.2$, and equivalence ratio was varied from $\phi = 1.4$-2.6 in increments of 0.2 at $u = 125$ cm/s. Figure 30 shows the operating limits within these ranges for the three reactor geometries that were scaled by channel height. Beyond the limits of operating range, the flame front is either upstream of the main reactor section at the porous media flow straightener, which corresponds to flashback in experimental

investigations, or the flame front propagates out of the channel exit, which corresponds to blow-off in experimentation.

In the case of equivalence ratio variation, the computations indicate flashback and blow-off at equivalence ratios below and above the lowest and highest tested equivalence ratios, respectively, for which solutions are obtained in the main reactor section. When the volume ratio is increased by increasing channel height, the equivalence ratio at which flashback occurs decreases. For VR(h)=0.75, flashback occurred at $\phi = 1.8$. For VR=1.0 and VR(h)=1.25, flashback occurred at $\phi = 1.6$ and $\phi = 1.4$, respectively. The results show a shift in equivalence ratio operating range towards stoichiometric as channel height is increased. Nearly all of the tested equivalence ratios are above the flammability limit of $\phi = 1.67$ for methane at inlet conditions, and preheating of reactants is required to achieve the observed extension of flammability limits [96]. Therefore, the operating range results suggest that preheating through internal heat recirculation within the reactor becomes more effective with decreasing channel height. As channel height increases, axial convection begins to dominate over transverse heat and mass diffusion, where the latter are required for conversion of fuel at the channel plane of symmetry.

In the case of inlet velocity variation, the two lower volume ratio reactors (VR(h)=0.75 and VR=1.0) produced stationary flame fronts in the main reactor section over the entire tested inlet velocity range, while the VR(h)=1.25 solution did not result in a flame within the reactor, indicating blow-off, at $u = 150$ cm/s. Therefore the largest volume ratio reactor, VR(h)=1.25, is the only one of the three reactors scaled by height that is limited

over the tested inlet velocity range. Blow-off occurred at $u = 150$ cm/s because the reactants were insufficiently preheated to raise the burning rate to equal the reactant feed rate, which is the criterion for operation in the counter-flow reactor. Similar results were observed in Oh et al. [88] and Norton et al. [84], where larger channel widths resulted in lower reaction rates due to slow heat transfer from the wall where ignition starts [23] towards the reactants at the channel plane of symmetry. In contrast, smaller separation distances between channel walls produce thinner reaction zones with larger temperature and composition gradients.
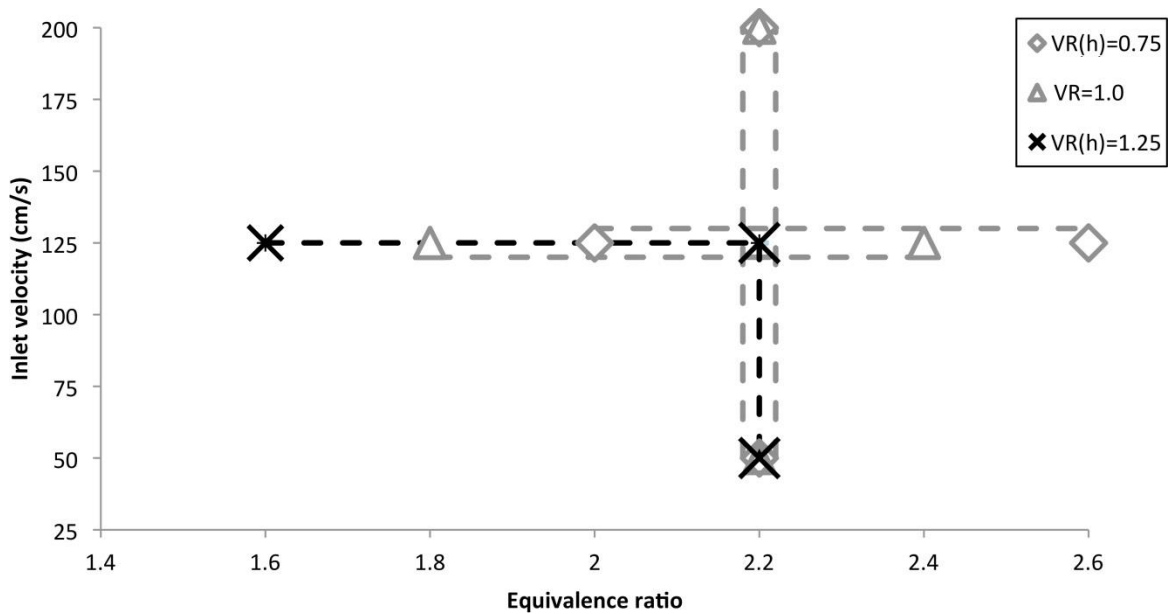
Figure 30. Operating limits for counter-flow reactors scaled to smaller and larger volume ratios by varying channel height (VR(h)=0.75 and VR(h)=1.25) and original reactor geometry (VR=1.0) over the tested range of inlet velocities, $u = 50$-200 cm/s at $\phi = 2.2$, and the tested range of equivalence ratios, $\phi = 1.4$-2.6 at $u = 125$ cm/s.

Figure 31 shows the operating limits within the ranges of tested inlet velocities and equivalence ratios for the three reactor geometries scaled by channel length. In the case of equivalence ratio variation, flashback occurred at decreasing equivalence ratios as volume ratio increased: $\phi = 1.8$ for VR(L)=0.75, $\phi = 1.6$ for VR=1.0 and $\phi = 1.4$ for VR(L)=1.25. Blow-off occurred at $\phi = 2.4$ for the reactor with the shortest length, VR(L)=0.75, whereas a solution was obtained at the upper end of the tested equivalence ratio range for the longer reactors VR=1.0 and VR(L)=1.25. In the case of inlet velocity variation, the two longer reactors, VR(L)=1.25 and VR=1.0, produced solutions throughout the tested range of $u = 50$-200 cm/s. The lowest volume ratio reactor with shortest channel length, VR(L)=0.75, had an operating range of $u = 100$-150 cm/s, due to flashback at 75 cm/s and blow-off at 175 cm/s.

The results suggest that operating range increases with channel length, however VR(L)=0.75 and VR=1.0 produced operating points throughout the tested inlet velocity range and therefore the extents of inlet velocity operating range were not tested. It is likely that there is an optimal channel length for maximum operating range; as channel length increases, surface area and thus heat loss also increase, however there is also increased axial distance for the reaction front to stabilize. Since there is no predetermined combustion zone location in the main section of the reactor, the flame front is free to stabilize at the point where the burning velocity equals the local inlet velocity. For example, increasing the equivalence ratio from $\phi = 2.0$ to $\phi = 2.2$ at a fixed inlet velocity

results in lower heat release. The flame front will then stabilize further downstream, where the heat recirculation is more significant and the reactants can be further preheated prior to combustion. Likewise, the flame front location will adjust to changes in inlet velocity at a fixed equivalence ratio; the flame front will shift downstream in response to an increase in inlet velocity, where additional heat recirculation will provide sufficient preheating for the burning velocity to equal the reactant feed rate. The reactor scaled down by channel length, VR(L)=0.75, has the most limited axial distance within the main section for the reaction front to adjust to changes in operating conditions before blow-off or flashback will occur, thus its operating range is significantly narrower than longer reactors VR=1.0 and VR(L)=1.25.
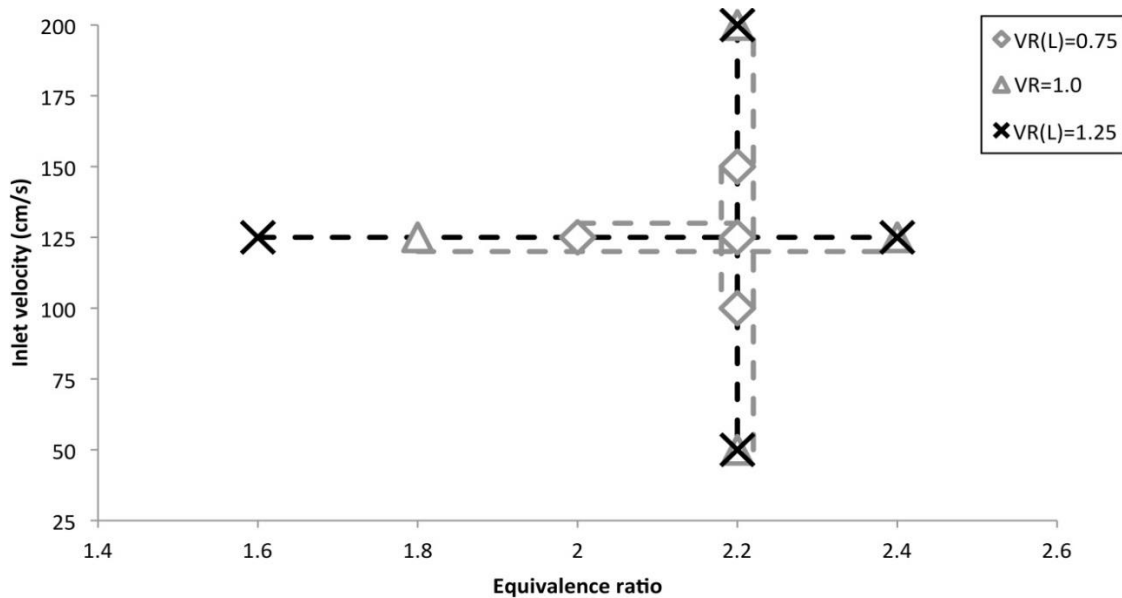

Figure 31. Operating range for counter-flow reactors scaled to smaller and larger volume ratios by varying channel length, VR(L)=0.75 and VR(L)=1.25, and original reactor geometry, VR=1.0, over the tested range of inlet velocities, u = 50-200 cm/s at ϕ = 2.2, and the tested range of equivalence ratios, ϕ = 1.4-2.6 at u = 125 cm/s.

5.3.2 Heat Recirculation Efficiency

The counter-flow reactor transfers heat by conduction and radiation upstream from hot combustion products in the post-flame region to cold reactants in the preheat region. Heat is also transferred through the channel walls to the unburned reactants counter-flowing in the adjacent channels, thereby preheating the reactants. Figure 32 shows temperature profiles for the channel wall and gas at the reactor channel plane of symmetry, obtained for the original reactor geometry (VR=1.0) at operating conditions of ϕ = 2.2 and u = 125 cm/s. The preheat zone is identified as the region between the channel inlet and the point where wall and gas temperatures are equal. Upstream of this point, the wall temperature exceeds the gas temperature and heat is transferred to the gas. The two sections of porous media flow straighteners (PM) are identified, and the impact of these conductive inserts on increasing the gas temperature can be seen. Downstream of the preheat zone, the reaction zone occurs and gas temperatures exceed wall temperatures. Heat is then transferred from the gas to the wall, where it conducts and radiates upstream and preheats reactants in adjacent channels.
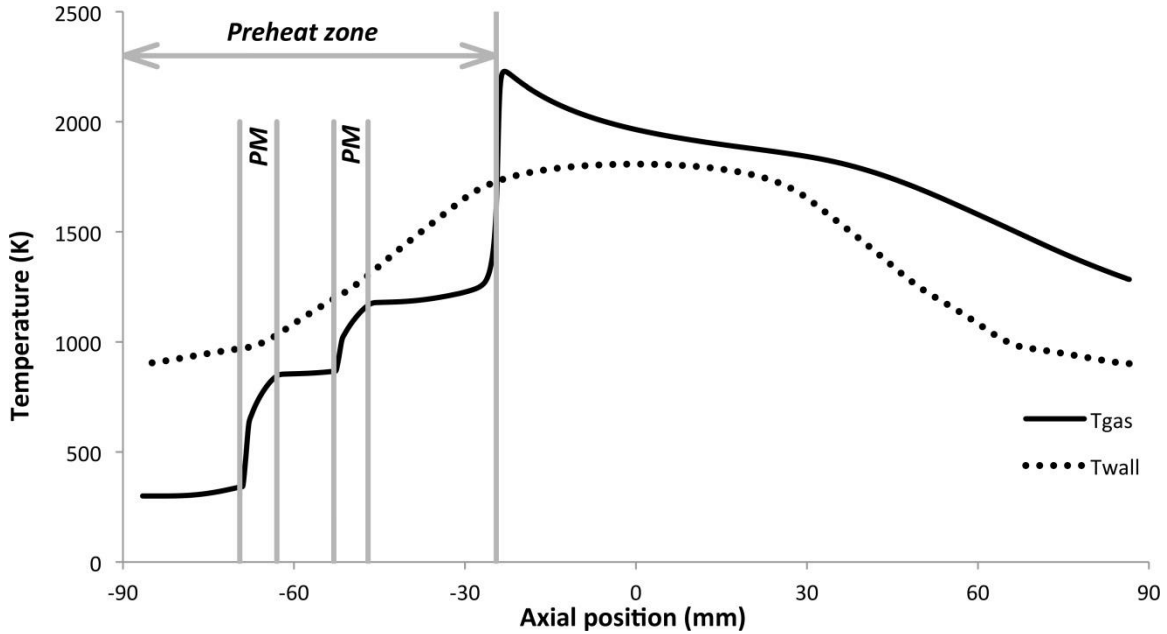
Figure 32. Gas (Tgas) and wall (Twall) temperature profiles along the axial length of a counter-flow reactor channel, obtained from the original reactor geometry (VR=1.0) with inlet conditions of ϕ = 2.2 and u = 125 cm/s. The preheat zone is identified, as well as the locations of the two sections of porous media flow straighteners (PM), the high thermal conductivity of which contributes to preheating the reactants.

The amount of heat transferred to the reactants in the preheat zone is obtained by integrating the heat flux into the channel upstream of the reaction zone, from the inlet to the point where the gas and solid temperatures are equal and the flux equals zero. Heat recirculation efficiency is a measure of this heat transfer and is defined as

$$Heat\ recirculation\ efficiency = \frac{Heat\ transfer\ to\ reactants}{Firing\ rate} \qquad (16)$$

where firing rate is calculated based upon the lower heating value of methane.

Figure 33 shows the calculated heat recirculation efficiency for each of the five scaled reactors as a function of equivalence ratio. All reactors show a decrease in heat recirculation efficiency with increasing equivalence ratio. A significant increase in efficiency is found with decreasing channel height, where the smallest channel height VR(h)=0.75 shows approximately 30% and 26% heat recirculation efficiency at $\phi = 2.0$ and $\phi = 2.2$, respectively, versus 19% and 18% efficiency produced by the largest channel height VR(h)=1.25. The increase in heat recirculation efficiency with decrease in volume ratio is attributed to the increase in wall surface area for heat transfer per unit of gas volume as channel height decreases. The shift of equivalence ratio operating range towards progressively richer equivalence ratios with decrease in channel height, shown in Figure 30 and discussed in Section 5.3.1, is attributed to this increased heat recirculation efficiency; the more effective preheating provided by increased heat recirculation efficiency permits the combustion of progressively richer reactant mixtures.
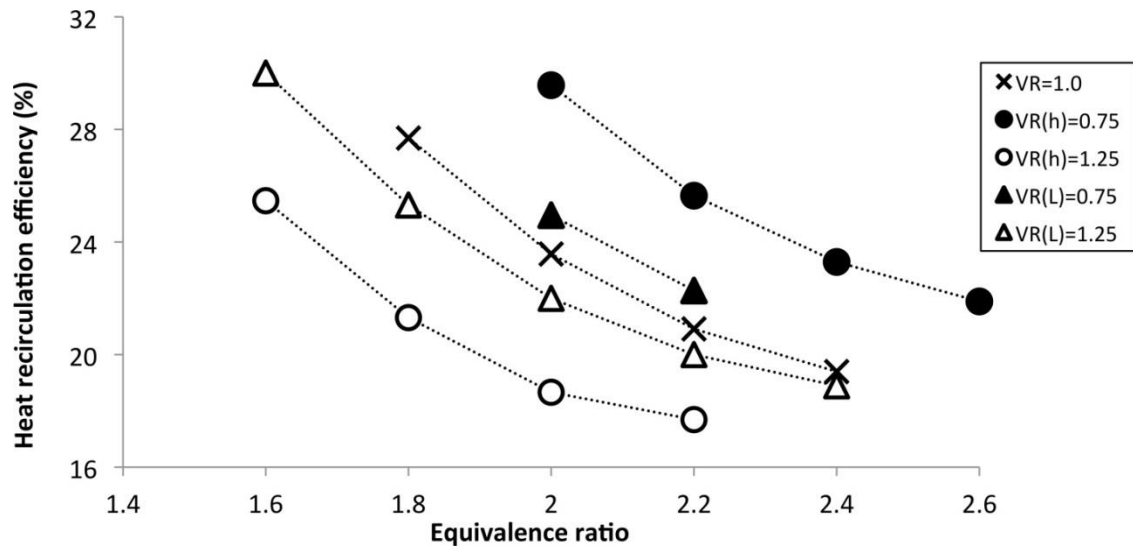
Figure 33. Heat recirculation efficiency is shown for each of the scaled reactors, including those scaled by channel height (VR(h)=0.75 and VR(h)=1.25) and those scaled by channel length (VR(L)=0.75 and VR(L)=1.25), as a function of equivalence ratio at $u = 125$ cm/s.

Heat recirculation efficiency decreases slightly with increasing channel length, where the shortest reactor length VR(L)=0.75 produced efficiencies of 25% and 22% versus 22% and 20% observed for the longest reactor length VR(L)=1.25 at $\phi = 2.0$ and $\phi = 2.2$. This trend is attributed to greater amounts of heat loss from longer reactors with larger external surface area. Additionally, flame fronts shift further downstream with increase in equivalence ratio. This brings the locations of peak gas temperatures in adjacent channels closer to the longitudinal center, which minimizes heat loss and temperature decrease of hot combustion gases prior to preheating reactants in adjacent channels. Thus the heat recirculation efficiency of the longest reactors, VR(L)=1.25 and VR=1.0, appear to converge with increasing equivalence ratios, where the flame fronts in both reactors are

approaching the channel center along the axial length. The shortest reactor channel length, VR(L)=0.75, has limited equivalence ratio operating range, but the peak reactor temperatures are in close axial proximity to the preheat zones of adjacent channels at the points where operation is attained.

Figure 34 shows the calculated heat recirculation efficiency for each of the five scaled reactors as a function of inlet velocity. A decrease in efficiency with increasing inlet velocity is observed for all reactors except that with the smallest channel height, VR(h)=0.75, which shows a peak efficiency at $u = 150$ cm/s. The decrease in efficiency exhibited by most reactors is attributed to the decrease in residence time with increasing inlet velocity, which impacts fuel conversion and heat release. A similar trend was observed in Barra et al. [95]. The different trend exhibited by VR(h)=0.75 is likewise attributed to fuel conversion efficiency and peak temperatures in this reactor.

As was observed in Figure 33 for the variation of equivalence ratio, heat recirculation efficiency is observed to increase with decreasing channel height and channel length, with the largest difference observed between VR(h)=0.75 and VR(h)=1.25.

116
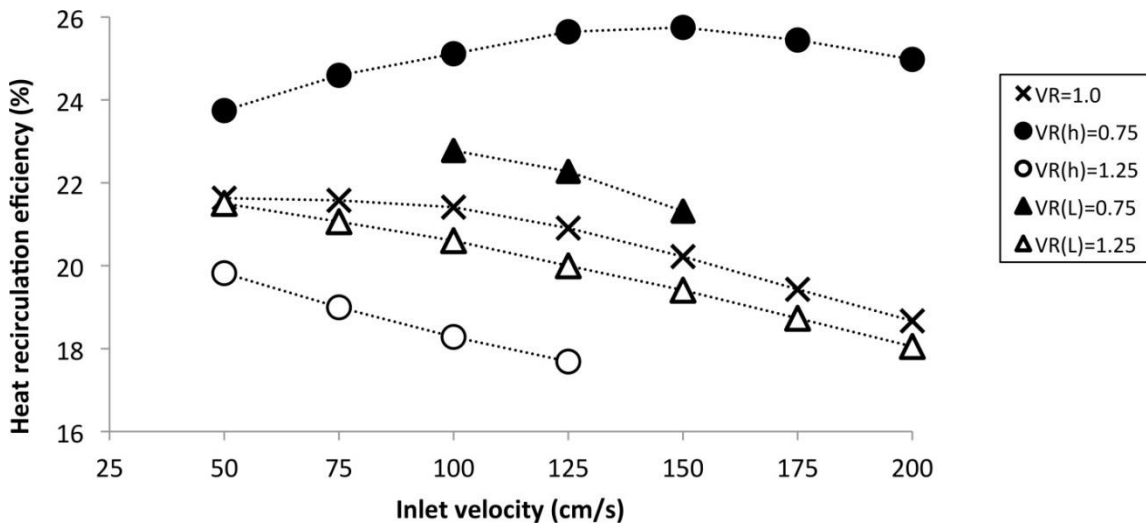
Figure 34. Heat recirculation efficiency is shown for each of the scaled reactors, including those scaled by height (VR(h)=0.75 and VR(h)=1.25) and those scaled by length (VR(L)=0.75 and VR(L)=1.25), as a function of inlet velocity at $\phi = 2.2$.

5.3.3 Temperature Ratio

Excess enthalpy reactors recirculate energy from hot combustion products to preheat incoming reactants, which increases the enthalpy of the reaction zone. This can permit the combustion of reactant mixtures at equivalence ratios beyond the flammability limits of those mixtures at inlet conditions, as shown in Figure 30 and Figure 31 where the majority of stable points tested in the scaled reactors are above the methane rich flammability limit of $\phi = 1.67$ [2]. The preheating of reactants through internal heat recirculation will also result in higher peak temperatures within the reactor than those that would occur with non-preheated reactants at inlet conditions. The peak temperatures achieved in the counter-flow reactor simulations are compared to two values that are

characteristic of a rich methane flame: peak temperature in the spatially-resolved temperature history of an adiabatic flame, calculated here using Cantera, and the adiabatic equilibrium temperature. In the case of non-preheated rich combustion at ambient reactor inlet conditions, the peak flame temperature exceeds the equilibrium temperature because endothermic reforming reactions cause a decrease in temperature from the peak flame value as the flame composition approaches equilibrium. For example, a numerically-simulated methane/air flame of ϕ=1.6 and initial reactant temperature of 300 K will produce a peak flame temperature of 1858 K and a final equilibrium temperature of 1832 K. The computational model utilized in this study allows the determination of the gas preheat temperature within the reactor channel, including the maximum preheat temperature that is achieved prior to combustion. Spatially-resolved flame calculations performed for reactants at those maximum preheat temperatures provide the peak flame temperature that can be expected as a result of heat recirculation and chemistry effects. The scaled reactors tested in this study at inlet conditions of ϕ=1.6, VR(h)=1.25 and VR(L)=1.25, achieved maximum preheat temperatures of 1290 K and 1450 K, respectively. Spatially-resolved flame calculations performed using Cantera reveal peak flame temperatures of 2550 K and 2649 K for these initial reactant temperatures, respectively. By comparison, maximum temperatures within the scaled reactors tested in this study at inlet conditions of ϕ=1.6 and initial reactant temperature 300 K are 2539 K for reactor VR(h)=1.25 and 2642 K for reactor VR(L)=1.25. These temperatures significantly exceed the characteristic temperatures of the non-preheated adiabatic flame, indicating significant heat recirculation and preheating

within the reactor, but nearly achieve the theoretical maximum flame temperatures predicted as a result of the achieved preheating. Thus, both heat recirculation and chemistry effects contribute to the maximum flame temperatures observed in the reactors. The other tested reactors supported steady-state flames at inlet conditions of $\phi \geq 1.8$, which is above the flammability limit of methane at 300 K. Therefore, a similar temperature comparison is not done for other conditions and reactors.

The comparison of maximum reactor temperatures to maximum and equilibrium temperatures calculated for adiabatic flames highlights the effect of internal heat recirculation on raising the peak reactor temperature above adiabatic flame values, in addition to permitting the extension of flammability limits. The extent to which temperatures may exceed the adiabatic flame and equilibrium temperatures depends upon the preheat temperature achieved by the reactants, and therefore the amount of heat recirculated as well as the amount of heat loss from the reactor. Peak reactor temperatures are therefore reflective of the effectiveness of heat recirculation. A temperature ratio is defined as a measure of superadiabicity, or extent of temperature increase above the adiabatic equilibrium temperature, as

$$Temperature\ ratio = \frac{Peak\ gas\ or\ wall\ temperature}{Adiabatic\ equilibrium\ temperature} . \qquad (17)$$

Temperature ratio is defined in terms of both peak gas and peak wall temperatures, where the latter is more readily measured during experimentation.
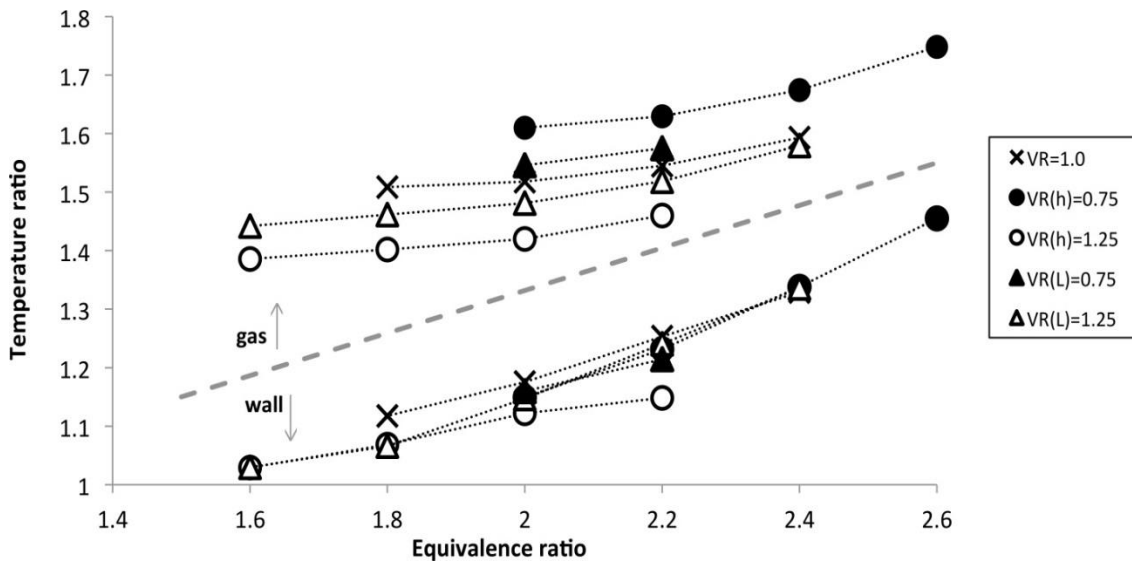
Figure 35. Separated by a dashed line, gas (above) and wall (below) temperature ratios are shown for each of the scaled reactors, including those scaled by height (VR(h)=0.75 and VR(h)=1.25), those scaled by length (VR(L)=0.75 and VR(L)=1.25), and original reactor geometry (VR=1.0), as a function of equivalence ratio at u = 125 cm/s.

Figure 35 shows gas and wall temperature ratios for each of the five scaled reactors as a function of equivalence ratio. All temperature ratios are above unity, indicating superadiabatic peak gas and wall temperatures at all equivalence ratios. Gas temperature ratios are also significantly higher than wall temperature ratios at all points, where the latter are the temperatures typically measured during experimentation. Both gas and wall temperature ratios increase with equivalence ratio, suggesting that higher levels of preheat, and therefore increasingly superadiabatic conditions, are required to achieve

120

reactor operation at equivalence ratios increasingly above the conventional flammability limit. Gas temperature ratios are highest in the reactors with decreased channel height and length, VR(h)=0.75 and VR(L)=0.75, and lowest in the reactors with increased channel height and length, VR(h)=1.25 and VR(L)=1.25.
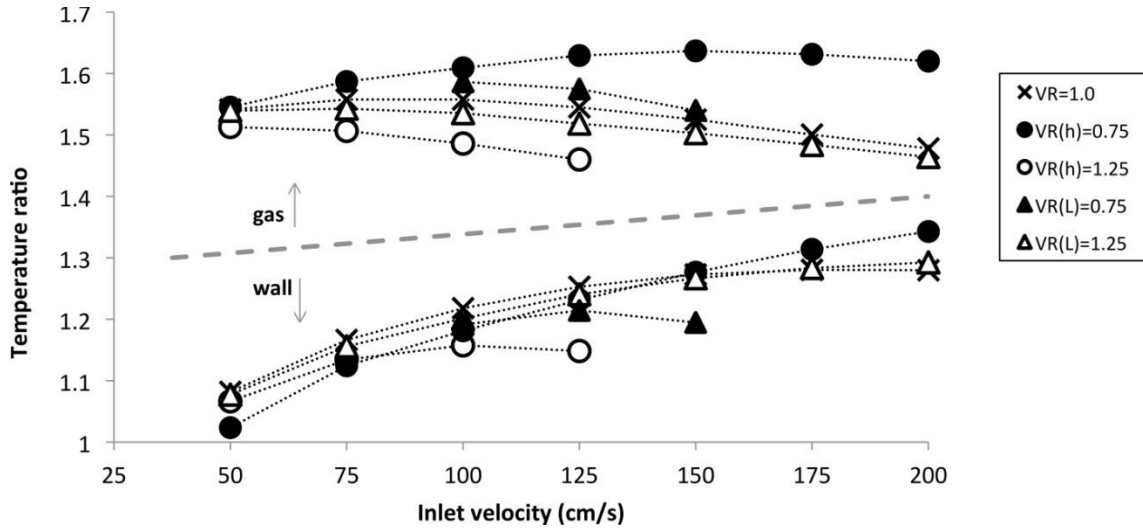
Figure 36. Separated by a dashed line, gas (above) and wall (below) temperature ratios are shown for each of the scaled reactors, including those scaled by height (VR(h)=0.75 and VR(h)=1.25), those scaled by length (VR(L)=0.75 and VR(L)=1.25), and original reactor geometry (VR=1.0), as a function of inlet velocity at $\phi = 2.2$.

Figure 36 shows gas and wall temperature ratios for each of the five scaled reactors as a function of inlet velocity. All temperature ratios are above unity, indicating superadiabatic peak gas and wall temperatures at all inlet velocities. Gas temperature ratios are also significantly higher than wall temperature ratios at all points. Gas

temperature ratios are highest in the reactors with decreased channel height and length, VR(h)=0.75 and VR(L)=0.75, and lowest in the reactors with increased channel height and length, VR(h)=1.25 and VR(L)=1.25. This correlates with heat recirculation efficiency trends observed in Figure 34 and discussed in Section 5.3.2. Gas temperature ratios generally show a slight increase with inlet velocity at the lowest tested inlet velocities, and a decrease with inlet velocity at the highest tested values. This is attributed to a low rate of heat release at the lowest firing rates, where heat losses may have a significant impact on reactor temperatures, and incomplete fuel conversion at the highest firing rates due to decreased residence time.

5.3.4 *Hydrogen Conversion Efficiency*

The goal of hydrocarbon reforming is the production of syngas consisting primarily of hydrogen and carbon monoxide, of which hydrogen is often the higher valued product. Hydrocarbon reforming is carried out at rich conditions, where partial oxidation will occur due to oxidizer deficiency of the reactants. Equilibrium predicts an increase in hydrogen product concentration with increasing reactant equivalence ratio. The equilibrium yield is not necessarily achievable in a practical reactor, however, due to limited residence time for reaction. Hydrogen production in the counter-flow reactor is defined in terms of hydrogen conversion efficiency as

$$H_2 \, conversion \, efficiency = \frac{H_2 \, product \, concentration}{H_2 \, equilibrium \, concentration} \tag{18}$$

where thermodynamic equilibrium provides a theoretical maximum concentration, and hydrogen conversion efficiency quantifies the actual hydrogen yield relative to this value.
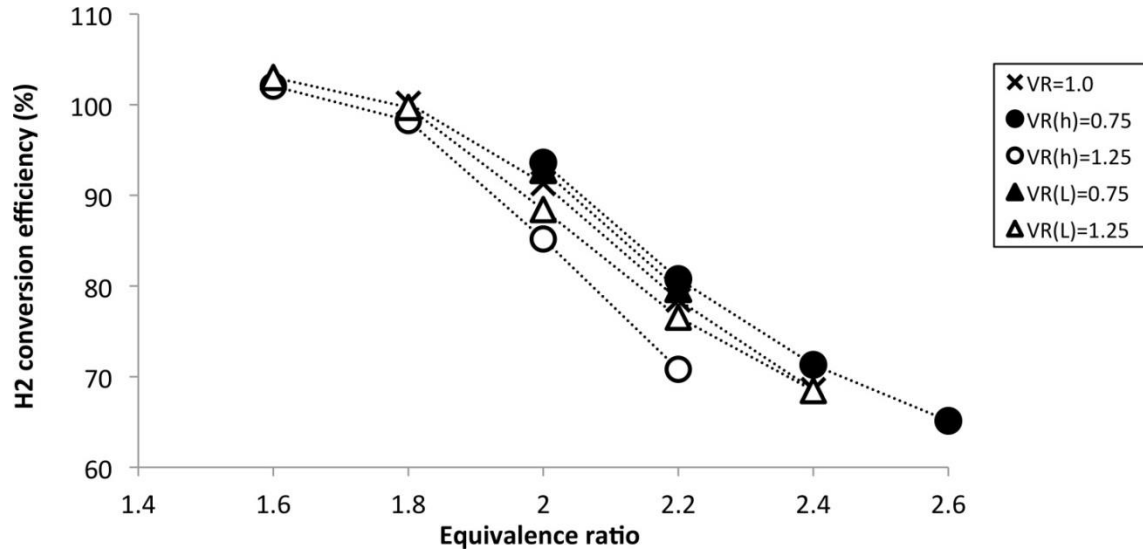
Figure 37. Hydrogen conversion efficiencies are shown for each of the scaled reactors, including those scaled by height (VR(h)=0.75 and VR(h)=1.25) and those scaled by length (VR(L)=0.75 and VR(L)=1.25), as a function of equivalence ratio at _u_ = 125 cm/s.

Figure 37 shows hydrogen conversion efficiencies for each of the five scaled reactors as a function of equivalence ratio. All reactors show a decrease in conversion efficiency with increasing equivalence ratio. The results for the original reactor geometry, VR=1.0, are in agreement with experiment findings that hydrogen conversion efficiency, as defined above, decreases from approximately 95% to 75% as equivalence ratio is increased from $\phi = 1.8$ to $\phi = 2.4$ [36]. Computational reactor conversion efficiencies exceed 100% at the

lowest tested equivalence ratios, where hydrogen product concentration exceeds the yield predicted by equilibrium for reactants at 300 K. Equilibrium predicts a shift in primary hydrogen-containing products from water towards diatomic hydrogen as reactant temperature is increased. Since reactants are preheated within the counter-flow reactor, hydrogen production in excess of that predicted by equilibrium for 300 K products, and therefore conversion efficiencies above 100%, are reasonable.

Trends observed in hydrogen conversion efficiencies are similar to those observed in temperature ratio and heat recirculation efficiency variation with height and length scaling: hydrogen conversion efficiencies are slightly higher in the reactors with decreased channel height and length, VR(h)=0.75 and VR(L)=0.75, as compared to original reactor geometry, VR=1.0, and lowest in the reactors with increased channel height and length, VR(h)=1.25 and VR(L)=1.25. Overall, however, there is little difference in hydrogen conversion efficiency between the reactors at most tested equivalence ratios. This suggests that heat recirculation and reactant preheating are necessary for flammability limit extension, but do not significantly impact product composition in many cases. This finding is in agreement with a study of burner-stabilized flames of preheated, premixed methane and air [96]. The lack of significant impact of reactor length on product composition is also suggested by the previous findings of Kaisare and Vlachos [86], who concluded that burner length is unlikely to impact reactor operation significantly because homogeneous combustion is largely localized.

Figure 38 shows hydrogen conversion efficiencies for each of the five scaled reactors as a function of inlet velocity. All reactors except for VR(L)=0.75 show an increase in conversion efficiency with inlet velocity at low firing rates, and all except VR(h)=0.75 show a decrease in conversion efficiency with inlet velocity at high firing rates. This suggests that optimal operation occurs around the middle of the tested inlet velocity range, where firing rate is sufficiently high to dominate over external losses but not high enough to limit conversion by decreased residence time. The results for VR(h)=0.75 suggest that this reactor may be able to operate at higher inlet velocities beyond the tested range.
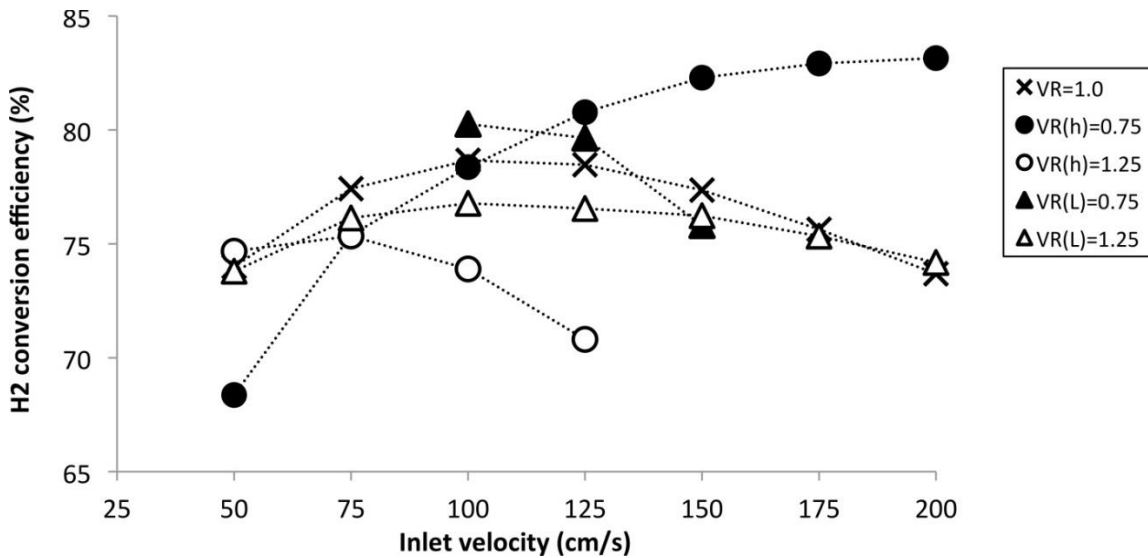
Figure 38. Hydrogen conversion efficiencies are shown for each of the scaled reactors, including original reactor geometry (VR=1.0), those scaled by height (VR(h)=0.75 and VR(h)=1.25) and those scaled by length (VR(L)=0.75 and VR(L)=1.25), as a function of inlet velocity at ϕ = 2.2.

5.3.5   Carbon Monoxide and Methane Conversion Efficiencies

Carbon monoxide is a major component of syngas and, like hydrogen, is valued for its heating value and utility in industrial applications. CO is produced in high concentrations under rich combustion conditions where partial oxidation of carbon will occur due to the oxidizer deficiency of the reactants. Equilibrium predicts an increase in carbon monoxide concentration with increasing reactant equivalence ratio, and carbon monoxide production in the counter-flow reactor is defined relative to equilibrium by the CO conversion efficiency as

$$CO\ conversion\ efficiency = \frac{CO\ product\ concentration}{CO\ equilibrium\ concentration}. \qquad (19)$$

Hydrogen (Eq. 18) and carbon monoxide (Eq. 19) conversion efficiencies indicate reaction progress towards theoretical completion, where theoretical completion is defined by product equilibrium composition based upon inlet conditions. An additional important measure of reactor performance is efficiency of fuel utilization within the reactor. Fuel conversion efficiency is defined as

$$CH_4\ conversion\ efficiency = \frac{\dot{n}_{CH_4,in} - \dot{n}_{CH_4,out(actual)}}{\dot{n}_{CH_4,in} - \dot{n}_{CH_4,out(equilibrium)}} \qquad (20)$$

where $\dot{n}_{CH_4}$ is the molar flow rate of methane, the subscripts *in* and *out* indicate reactants into and products out of the reactor, respectively, and the subscripts *actual* and

equilibrium indicate the molar flow rate in the simulation reactor products and the predicted molar flow rate in a theoretical equilibrium product composition, respectively.

Figure 39 shows CO and CH_4 conversion efficiencies for each of the five scaled reactors as a function of equivalence ratio. CH_4 conversion efficiency shows a decrease in fuel conversion with increasing equivalence ratio. CH_4 conversion efficiency is 100% at the lowest tested equivalence ratios, and decreases with increasing equivalence ratios above $\phi = 1.8$. This decrease is attributed to a decrease in peak reactor temperature; the temperature ratios in Figure 35 show an increase in superadiabicity with equivalence ratio, but these temperature ratios indicate a decrease in gas and wall temperatures with increasing equivalence ratios because of the significant decrease in equilibrium temperature over this range. This decrease in reactor temperature slows reaction progress towards equilibrium, including fuel breakdown.

Peak CO conversion efficiency was found to occur between $\phi = 1.8$ and $\phi = 2.0$ in Figure 39, with a decrease in efficiency at higher and lower equivalence ratios. A significant decrease in CO conversion efficiency is observed at the highest tested equivalence ratios, which is attributed to low reactor temperatures and incomplete fuel conversion at these operating points.
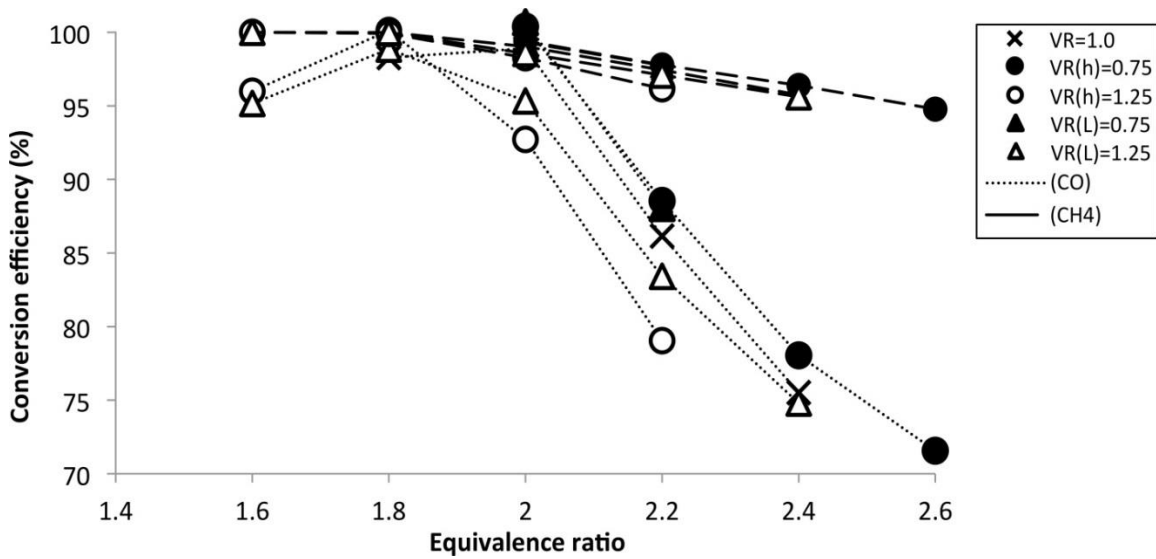
Figure 39. CO and CH₄ conversion efficiencies are shown for each of the scaled reactors, including original reactor geometry (VR=1.0), those scaled by height (VR(h)=0.75 and VR(h)=1.25) and those scaled by length (VR(L)=0.75 and VR(L)=1.25), as a function of equivalence ratio at u=125 cm/s.

Figure 40 shows CO and CH₄ conversion efficiencies for each of the five scaled reactors as a function of inlet velocity. CH₄ conversion efficiency generally shows little change across the range of tested inlet velocities, however slight changes and trends can be observed. These same trends are observed, with much greater differences between data values, in CO conversion efficiencies of the five scaled reactors. It is noteworthy that the trends observed in CO conversion efficiency closely resemble those observed in H₂ conversion efficiency in Figure 38. All reactors except for VR(L)=0.75 show an increase in conversion efficiency with inlet velocity at low velocities, and all reactors except VR(h)=0.75 show a decrease in conversion efficiency with inlet velocity at high

128

velocities. CO conversion efficiency results, like H_2 conversion efficiencies, suggest that optimal operation may occur around the middle of the tested inlet velocity range.
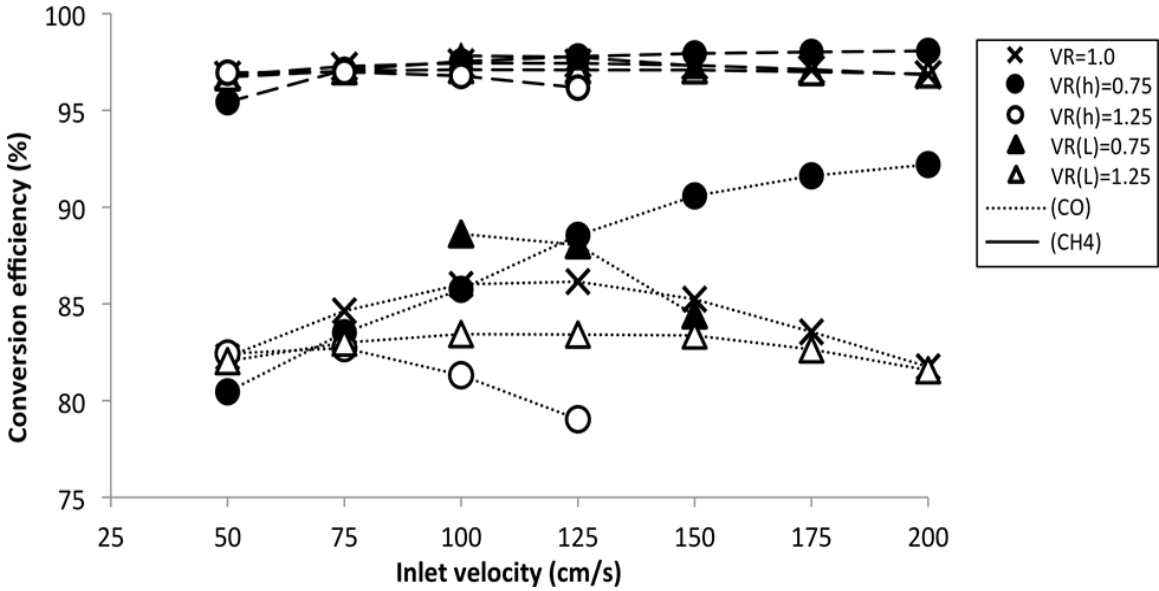
Figure 40. CO and CH$_4$ conversion efficiencies are shown for each of the scaled reactors, including original reactor geometry (VR=1.0), those scaled by height (VR(h)=0.75 and VR(h)=1.25) and those scaled by length (VR(L)=0.75 and VR(L)=1.25), as a function of inlet velocity at ϕ = 2.2.

5.4   Conclusions

A computational study was undertaken to determine the effect of geometric scale on fuel reforming in a meso-scale parallel-plate counter-flow reactor. Length and height of the reactor channels were scaled relative to the original dimensions of the counter-flow

reactor that has been used in previous analytical and experimental investigations. Results were quantified in terms of operating range, heat recirculation efficiency, temperature ratio, and hydrogen, carbon monoxide and methane fuel conversion efficiencies.

Reactor operating range was found to be strongly impacted by channel scaling. Decreasing channel height resulted in a shift in operating range towards higher equivalence ratios. Decreasing channel length resulted in a significant narrowing of the equivalence ratio and inlet velocity operating ranges. Most operating points were above the conventional rich flammability limit and adiabatic flame speed of methane/air combustion based upon inlet conditions, which highlights the importance of heat recirculation in achieving operation of the counter-flow reformer at these conditions.

Heat recirculation efficiency and temperature ratios were found to be significantly higher for reactors with decreased channel height. These findings indicate more effective heat recirculation with smaller channel height, where channel wall surface area-to-gas volume ratio is increased and the transverse distance for mass and heat diffusion is reduced. Channel length showed a less significant impact on heat recirculation, with shorter channel lengths producing slightly higher heat recirculation efficiencies and temperature ratios than longer lengths.

Hydrogen conversion efficiency decreased with increasing equivalence ratio for all reactors, with slightly higher conversion efficiencies found for reduced channel height and length. Carbon monoxide efficiency decreased with increasing equivalence ratio over the majority of the tested range, with a slight increase in efficiency with equivalence ratio

observed at the lowest tested equivalence ratios. Methane equivalence ratio decreased with equivalence ratio from 100% at the lowest tested equivalence ratios to approximately 95% at the highest tested equivalence ratios.

Hydrogen conversion efficiency initially increased with inlet velocity at the lowest tested firing rates, and decreased at the highest tested inlet velocities, suggesting that an optimal firing rate exists. Carbon monoxide and methane conversion efficiency trends closely resembled those of hydrogen conversion efficiency. Methane conversion efficiency varied little between 95-98% over the tested range of inlet velocities.

Scaled down reactors were achieved by decreasing reactor channel height and length, although the latter resulted in a significantly narrowed operating range. The results of this study highlight the effectiveness of small scale reactor channels in achieving heat recirculation and significantly superadiabatic temperatures. These, in turn, permit the effective extension of flammability limits to operation at rich equivalence ratios. While increasing heat recirculation may be required to significantly extend the reactor operating range, the results of this study suggest that superadiabatic temperatures serve to extend the flammable range of operating points but otherwise do not strongly impact hydrogen conversion efficiencies.

6   CONCLUSIONS AND RECOMMENDATIONS

The effect of key operating condition and reactor geometry parameters on excess enthalpy combustion of fuels was investigated experimentally and numerically in this research. Operating condition parameters that were tested include inlet reactant equivalence ratio and inlet velocity, and reactor geometry parameters that were tested include reactor channel height and length. The impact of variation of these parameters on combustion stability, fuel conversion and product composition was examined. Premixed fuel and air reactants were examined at lean and ultra-lean equivalence ratios, and rich and ultra-rich conditions.

Lean combustion produces hot product gases that can be used for thermomechanical energy production, and ultra-lean thermal oxidation can facilitate the conversion of low heating value reactants. Rich and ultra-rich combustion produces product gases that contain significant amounts of hydrogen and carbon monoxide, called synthesis gas or syngas, which can be used as a fuel, converted to another high value product, or purified for the hydrogen that it contains. Despite the differences in the compositions and applications of reactant mixtures on the lean and rich sides of stoichiometry, there are common challenges in their chemical conversion that can be met through the use of superadiabatic combustion. Two key challenges that are common to lean and rich combustion, including ultra-lean and ultra-rich, is the limitation of flammability limits, beyond which a reactant mixture will not readily combust, and reaction rates, which

decrease dramatically as equivalence ratio deviates from stoichiometry towards lean or rich conditions.

Heat recirculating reactors can be utilized to address these challenges, in which energy can be recirculated from hot combustion products to preheat cold reactants, thereby increasing the enthalpy of the reaction zone with no net addition of energy to the system. The preheated reactants and increased enthalpy of the reaction zone permit the extension of flammability limits, when the limits are defined in terms of incoming reactant conditions, and an increase in burning rate as compared to the adiabatic flame speed based upon inlet conditions. A particular type of heat recirculating reactor, known as a counter-flow reactor, was used in this research.

There are a number of parameters that are characteristic of reactor design and operation, and which have the potential to strongly impact combustion stability, fuel conversion and product composition. This research examines several of these critical parameters, including reactant equivalence ratio and inlet velocity, and reactor channel height and length.

The experimental portions of this research included the first demonstrations of liquid fuel reforming, and lean combustion of gaseous and liquid fuels, in the counter-flow reactor. The demonstration of reactor operation under these conditions is critical to establishing the fuel and application flexibility of the counter-flow reactor. The variation of inlet conditions, including inlet velocity and reactant equivalence ratio, was found to have a similar impact on combustion stability for all tested fuels, and in both the rich and lean

regimes. When inlet velocity was varied, an increase in inlet velocity shifted the stable equivalence ratio range towards stoichiometry, while a decrease in inlet velocity shifted the stable equivalence ratio range away from stoichiometry towards leaner or richer equivalence ratios. When equivalence ratio was varied, a change in equivalence ratio away from stoichiometry resulted in a decrease in stable inlet velocities, while a change in equivalence ratio towards stoichiometry lead to an increase in stable inlet velocities. These trends, common between rich and lean combustion of gaseous and liquid fuels, highlight a requirement of combustion stability in the counter-flow reactor: the local inlet velocity must be equal to the burning rate. The burning rate of rich and lean reactant mixtures is significantly influenced by reactant temperature, which is dependent upon the amount of heat recirculation achieved in the reactor.

Heptane reforming, with the goal of syngas production, was performed in the counter-flow to study the impact of inlet velocity and reactant equivalence ratio on syngas yield. When the maximum hydrogen production was achieved in the combustion of rich heptane reactants, 42% of the hydrogen bound in the heptane fuel was converted to diatomic hydrogen, H_2. The maximum amount of energy originally bound in the incoming heptane fuel that became bound in H_2 product in the reactor exhaust was 18%, while the maximum total energy bound in the product species was 75% of the energy bound in the incoming reactants. The presence of high energy hydrocarbon species in the exhaust, significantly in excess of levels predicted by equilibrium, contributed to the high total energy conversion efficiency and indicates incomplete fuel conversion. Inlet velocity was found to have little impact on product composition except at the lowest

tested inlet velocities, where a significant decrease in H_2 production and an increase in unburned hydrocarbons were observed; this effect is attributed to an increased ratio of external heat loss to chemical heat release at low firing rates. The variation of reactant equivalence ratio did show a strong impact on product composition.

Lean combustion of methane, propane and heptane in the counter-flow reactor also showed a greater impact of equivalence ratio variation on exhaust pollutant species production as compared to the variation of inlet velocity. The exception to this was observed at the lowest tested inlet velocities, where measured temperatures within the reactor decreased below the calculated adiabatic equilibrium temperature based upon reactant conditions, dubbed subadiabatic temperatures, and fuel conversion became incomplete as indicated by the detection of unburned hydrocarbons. The effects of low inlet velocity operation are attributed to the increased ratio of external heat losses to chemical energy release within the reactor, as was observed in heptane reforming. The variation of equivalence ratio showed a significant and consistent effect on measured product species for all three tested fuels: CO decreased and NO_x increased as equivalence ratio approached stoichiometry. The observed trends are attributed to strong temperature dependence of the formation of both product species.

The computational portion of this study investigated the impact of reactor geometric scaling on combustion stability and syngas production in the counter-flow reactor. Based upon results of experimental rich and lean combustion, the trends observed in the computational study are expected to have implications for lean combustion in scaled reactors as well. Similar to the results of experimental counter-flow investigations, the

135

variation of equivalence ratio was found to have a more significant effect on product composition as compared to the variation of inlet velocity. A decrease in product yields with increasing equivalence ratio, channel height and channel length was observed in the computational study of methane reforming, and a similar effect of equivalence ratio variation on product yield was observed in the experimental study of heptane reforming in the counter-flow reactor. The computations, which permit the quantification of characteristic quantities that are not readily measured in the reactor, indicate a decrease in heat recirculation efficiency with increasing equivalence ratio, as well as increasing channel height and length. Thus, the computations highlight the importance of effective heat recirculation for combustion stability and product species composition.

Based upon the results of this work, recommendations for future study include the characterization of preheated flames for the development of accurate chemical kinetics mechanisms at equivalence ratios near and beyond ambient-condition flammability limits. By utilizing experimental setups that are simpler than the counter-flow reactor, such as a flat flame burner that can be approximated as a one-dimensional system, the two- and three-dimensional effects that are present in heat-recirculating reactors can be eliminated, and the chemistry of combustion at extreme equivalence ratios can be isolated. The results of such studies will allow for increased accuracy in the modeling of combustion in heat recirculating reactors, which operate largely beyond the conditions where chemical kinetics mechanisms are validated. The study of one-dimensional preheated flames will also permit the quantification of soot formation through the use of laser diagnostic tools, such as laser extinction or laser induced incandescence, which

136

would permit the carbon balance on rich combustion, such as the rich reforming in the counter-flow reactor performed in this study, to be closed.

BIBLIOGRAPHY

1. Weinberg, F.J., *Combustion Temperatures: The Future?* Nature, 1971.
    233: p. 239-241.

2. Zabetakis, M.G., *Flammability Characteristics of Combustible Gases and
    Vapors*, B.o.M. US Dept. of the Interior, Editor. 1965: Washington, DC.

3. Aldushin, A.P., *New Results in the Theory of Filtration Combustion.*
    Combust. Flame, 1993. **94**: p. 308-320.

4. Hustad, J.E. and O.K. Sonju, *EXPERIMENTAL STUDIES OF LOWER
    FLAMMABILITY LIMITS OF GASES AND MIXTURES OF GASES AT
    ELEVATED-TEMPERATURES.* Combustion and Flame, 1988. **71**(3): p.
    283-294.

5. Wierzba, I. and Q. Wang, *The flammability limits of H-2-CO-CH4 mixtures
    in air at elevated temperatures.* International Journal of Hydrogen
    Energy, 2006. **31**(4): p. 485-489.

6. Fan, Y., Y. Suzuki, and N. Kasagi, *Experimental study of micro-scale
    premixed flame in quartz channels.* Proceedings of the Combustion
    Institute, 2009. **32**: p. 3083-3090.

7.   Maruta, K., et al., *Characteristics of Microscale Combustion in a Narrow Heated Channel.* Combust. Explos. Shock Waves, 2004. **40**(5): p. 516-523.

8.   Ahn, J., et al., *Gas-phase and catalytic combustion in heat-recirculating burners.* Proc. Combust. Inst., 2005. **30**: p. 2463-2472.

9.   Shebeko, Y.N., et al., *BURNING VELOCITIES AND FLAMMABILITY LIMITS OF GASEOUS-MIXTURES AT ELEVATED-TEMPERATURES AND PRESSURES.* Combustion and Flame, 1995. **102**(4): p. 427-437.

10.   Gu, X.J., et al., *Laminar burning velocity and Markstein lengths of methane-air mixtures.* Combustion and Flame, 2000. **121**(1-2): p. 41-58.

11.   Elia, M., M. Ulinski, and M. Metghalchi, *Laminar burning velocity of methane-air-diluent mixtures.* Journal of Engineering for Gas Turbines and Power-Transactions of the Asme, 2001. **123**(1): p. 190-196.

12.   Konnov, A.A., *The effect of temperature on the adiabatic laminar burning velocities of CH4-air and H-2-air flames.* Fuel, 2010. **89**(9): p. 2211-2216.

13.   Wood, S. and A.T. Harris, *Porous burners for lean-burn applications.* Progress in Energy and Combustion Science, 2008. **34**(5): p. 667-684.

14.   Marbach, T.L. and A.K. Agrawal, *Heat-recirculating combustor using porous inert media for mesoscale applications.* Journal of Propulsion and Power, 2006. **22**(1).

15.   Keramiotis, C., et al., *Porous burners for low emission combustion: An experimental investigation.* Energy, 2012. **45**(1): p. 213-219.

16.   Bubnovich, V., et al., *Flame stabilization between two beds of alumina balls in a porous burner.* Applied Thermal Engineering. **30**(2â€"3): p. 92-95.

17.   Kennedy, L.A., et al., *Chemical Structures of Methane-Air Filtration Combustion Waves for Fuel-Lean and Fuel-Rich Conditions.* Proc. Combust. Inst., 2000. **28**: p. 1431-1438.

18.   Bingue, J.P., A.V. Saveliev, and L.A. Kennedy, *Optimization of hydrogen production by filtration combustion of methane by oxygen enrichment and depletion.* Int. J. Hydrogen Energy, 2004. **29**(13): p. 1365-1370.

19.   Babkin, V.S., I. Wierzba, and G.A. Karim, *The phenomenon of energy concentration in combustion waves and its applications.* Chemical Engineering Journal, 2003. **91**: p. 279-285.

20.   Drayton, M.K., et al., *Syngas Production Using Superadiabatic Combustion of Ultra-Rich Methane-Air Mixtures.* Proc. Combust. Inst., 1998. **27**: p. 1361-1367.

21. Al-Hamamre, Z. and A. Al-Zoubi, *The use of inert porous media based reactors for hydrogen production.* International Journal of Hydrogen Energy, 2010. **35**(5): p. 1971-1986.

22. Mathis, W.M. and J.L. Ellzey, *Flame Stabilization, Operating Range, and Emissions for a Methane/Air Porous Burner.* Combust. Sci. Tech., 2003. **175**(5): p. 825-239.

23. Pedersen-Mjaanes, H., L. Chan, and E. Mastorakos, *Hydrogen Production from Rich Combustion in Porous Media.* Int. J. Hydrogen Energy, 2005. **30**: p. 579-592.

24. Vourliotakis, G., et al., *Detailed kinetic modelling of the T-POX reforming process using a reactor network approach.* International Journal of Hydrogen Energy, 2008. **33**(11): p. 2816-2825.

25. Al-Hamamre, Z., S. Voß, and D. Trimis, *Hydrogen production by thermal partial oxidation of hydrocarbon fuels in porous media based reformer.* International Journal of Hydrogen Energy, 2009. **34**(2): p. 827-832.

26. Pereira, J.M.C., et al., *Quasi-1D and 3D TPOX porous media diffuser reformer model.* Fuel, 2010. **89**(8): p. 1928-1935.

27. Lloyd, S.A. and F.J. Weinberg, *A Burner for Mixtures of Very Low Heat Content.* Nature, 1974. **251**: p. 47-49.

28. Lloyd, S.A. and F.J. Weinberg, *Limits to Energy Release and Utilisation From Chemical Fuels.* Nature, 1975. **257**: p. 367-370.

29. Chen, C.-H. and P.D. Ronney, *Three-dimensional effects in counterflow heat-recirculating combustors.* Proceedings of the Combustion Institute, 2010. **33**(2): p. 3285-3291.

30. Ju, Y. and B. Xu, *Theoretical and experimental studies on mesoscale flame propagation and extinction.* Proc. Combust. Inst., 2005. **30**: p. 2445-2453.

31. Ju, Y. and C.W. Choi, *An Analysis of Sub-Limit Flame Dynamics Using Opposite Propagating Flames in Mesoscale Channels.* Combust. Flame, 2003. **133**: p. 483-493.

32. Ronney, P.D., *Analysis of Non-Adiabatic Heat-Recirculating Combustors.* Combust. Flame, 2003. **135**: p. 421-439.

33. Il Kim, N., et al., *Development and scale effects of small Swiss-roll combustors.* Proceedings of the Combustion Institute, 2007. **31**(2): p. 3243-3250.

34. Fursenko, R.V., S.S. Minaev, and a.V.S. Babkin, *Thermal Interaction of Two Flame Fronts Propagating in Channels with Opposing Gas Flows.* Combust. Explos. Shock Waves, 2001. **37**(5): p. 493-500.

35.   Schoegl, I. and J.L. Ellzey, *Superadiabatic Combustion in Conducting Tubes and Heat Exchangers of Finite Length.* Combust. Flame, 2007. **151**: p. 142-159.

36.   Schoegl, I. and J.L. Ellzey, *A mesoscale fuel reformer to produce syngas in portable power systems.* Proceedings of the Combustion Institute, 2009. **32**(2): p. 3223-3230.

37.   Schoegl, I., S.R. Newcomb, and J.L. Ellzey, *Ultra-rich combustion in parallel channels to produce hydrogen-rich syngas from propane.* International Journal of Hydrogen Energy, 2009. **34**: p. 5152-5163.

38.   Belmont, E., S.M. Solomon, and J.L. Ellzey, *Syngas Production from Heptane in a Non-catalytic Counter-flow Reactor.* Combustion and Flame, 2012. **159**: p. 3624-3631.

39.   Belmont, E.L., I. Schoegl, and J.L. Ellzey, *Experimental and analytical investigation of lean premixed methane/air combustion in a mesoscale counter-flow reactor.* Proceedings of the Combustion Institute, 2013. **34**(2): p. 3361-3367.

40.   Belmont, E.L. and J.L. Ellzey, *Lean heptane and propane combustion in a non-catalytic parallel-plate counter-flow reactor.* Combustion and Flame, 2014. **161**(4): p. 1055-1062.

41. Schoegl, I., *Superadiabatic Combustion in Counter-Flow Heat Exchangers*, in *Mechanical Engineering*. 2009, The University of Texas at Austin.

42. Krumpelt, M., et al., *Fuel processing for fuel cell systems in transportation and portable power applications.* Catalysis Today, 2002. **77**(1–2): p. 3-16.

43. Dunn-Rankin, D., *Lean Combustion: Technology and Control*. 2007: Focal Press.

44. Fernandez-Pello, A.C., *Micro-Power Generation Using Combustion: Issues and Approaches.* Proc. Combust. Inst., 2002. **29**: p. 883-899.

45. Weinberg, F.J., et al., *On Thermoelectric Power Conversion from Heat Recirculating Combustion Systems.* Proc. Combust. Inst., 2002. **29**: p. 941-947.

46. Vican, J., et al., *Development of a Microreactor as a Thermal Source for MEMS Power Generation.* Proc. Combust. Inst., 2002. **29**: p. 909-916.

47. Weinberg, F.J., et al., *On thermoelectric power conversion from heat recirculating combustion systems.* Proceedings of the Combustion Institute, 2002. **29**: p. 941-947.

48. Chen, C.-H. and P.D. Ronney, *An Active Gas Mask Using a Heat-Recirculating Burner*, in *Spring Technical Meeting, Combustion Institute, Western States Section*. 2008: Los Angeles, CA.

49. Kaisare, N.S. and D.G. Vlachos, *A review on microcombustion: Fundamentals, devices and applications.* Progress in Energy and Combustion Science, 2012. **38**(3): p. 321-359.

50. Lattin, W.C. and V.P. Utgikar, *Transition to hydrogen economy in the United States: A 2006 status report.* International Journal of Hydrogen Energy, 2007. **32**(15): p. 3230-3237.

51. Romm, J., *The Hype About Hydrogen: Fact and Fiction in the Race to Save the Climate*. 2004, New York: Island Press.

52. Sehested, J., *Four challenges for nickel steam-reforming catalysts.* Catalysis Today, 2006. **111**(1–2): p. 103-110.

53. Ahmed, S. and M. Krumpelt, *Hydrogen from Hydrocarbon Fuels for Fuel Cells.* Int. J. Hydrogen Energy, 2001. **26**: p. 291-301.

54. Zhdanok, S., L.A. Kennedy, and G. Koester, *Superadiabatic Combustion of Methane Air Mixtures under Filtration in a Packed Bed.* Combust. Flame, 1995. **100**: p. 221-231.

55.   Dhamrat, R.S. and J.L. Ellzey, *Numerical and Experimental Study of the Conversion of Methane to Hydrogen in a Porous Media Reactor.* Combustion and Flame, 2006. **144**: p. 698-709.

56.   Fay, M., R. Dhamrat, and J.L. Ellzey, *Effect of Porous Reactor Design on Conversion of Methane to Hydrogen.* Combustion Science and Technology, 2005. **177**(11): p. 2171-2189.

57.   Sileghem, L., et al., *Laminar burning velocity of gasoline and the gasoline surrogate components iso-octane, n-heptane and toluene.* Fuel, 2013. **112**(0): p. 355-365.

58.   Kalghatgi, G.T., et al., *Surrogate fuels for premixed combustion in compression ignition engines.* International Journal of Engine Research, 2011. **12**(5): p. 452-465.

59.   Kukkadapu, G., et al., *Autoignition of gasoline and its surrogates in a rapid compression machine.* Proceedings of the Combustion Institute, 2013. **34**: p. 345-352.

60.   Cancino, L.R., et al., *Autoignition of gasoline surrogate mixtures at intermediate temperatures and high pressures: Experimental and numerical approaches.* Proceedings of the Combustion Institute, 2009. **32**: p. 501-508.

61.   Dixon, M.J., et al., *Experimental and numerical conversion of liquid heptane to syngas through combustion in porous media.* Combustion and Flame, 2008. **154**(1-2): p. 217-231.

62.   Pastore, A. and E. Mastorakos, *Rich n-heptane and diesel combustion in porous media.* Experimental Thermal and Fluid Science, 2010. **34**(3): p. 359-365.

63.   Al-Hamamre, Z., *Thermodynamic and kinetic analysis of the thermal partial oxidation of n-heptane for the production of hydrogen rich gas mixtures.* International Journal of Hydrogen Energy, 2013. **38**(26): p. 11458-11469.

64.   Yajima, S., T. Satow, and T. Hirai, *Mechanism of the pyrolytic graphite formation.* Journal of Nuclear Materials, 1965. **17**(2): p. 116-126.

65.   Hull, C.B., *Numerical Simulation of Conversion of n-Heptane to Hydrogen in an Inert, Porous Medium*. 2007, The University of Texas at Austin.

66.   Law, C.K., *Combustion Physics*. 2006: Cambridge University Press.

67.   Henneke, M.R. and J.L. Ellzey, *Modeling of Filtration Combustion in a Packed Bed.* Combust. Flame, 1999. **117**: p. 832-840.

68.   Smucker, M.T. and J.L. Ellzey, *Computational and Experimental Study of a Two-section Porous Burner.* Combustion Science and Technology, 2004. **176**(8): p. 1171 - 1189.

69. Newburn, E.R., A.K. Agrawal, and Asme, *Liquid fuel combustion using heat re-circulation through annular porous media*. Proceedings of the ASME Turbo Expo 2005, Vol 2. 2005, New York: Amer Soc Mechanical Engineers. 435-441.

70. Matkowsky, B.J. and G.I. Sivashinsky, *An Asymptotic Derivation of Two Models in Flame Theory Associated with the Constant Density Approximation.* SIAM J. Appl. Math., 1979. **37**(3): p. 686-699.

71. Goodwin, D.G. *An Open-Source Extensible Software Suite for CVD Process Simulation*. in *Chemical Vapor Deposition XVI and EUROCVD 14*. 2003. The Electrochemical Society.

72. Smith, G.P., et al., *GRI-Mech 3.0 URL http://www.me.berkeley.edu/gri-mech/version30/*. 1999.

73. Xu, K., M. Liu, and P. Zhao, *Stability of lean combustion in mini-scale porous media combustor with heat recuperation.* Chemical Engineering and Processing: Process Intensification, 2011. **50**(7): p. 608-613.

74. Francisco, R.W., et al., *On the Combustion of Hydrogen-Rich Gaseous Fuels with Low Calorific Value in a Porous Burner.* Energy & Fuels, 2010. **24**(2): p. 880-887.

75.   Gosiewski, K., et al., *A study on thermal combustion of lean methane-air mixtures: Simplified reaction mechanism and kinetic equations.* Chemical Engineering Journal, 2009. **154**(1-3): p. 9-16.

76.   Bouma, P.H. and L.P.H. de Goey, *Premixed Combustion on Ceramic Foam Burners.* Combust. Flame, 1999. **119**: p. 133-143.

77.   Brenner, G., et al., *Numerical and Experimental Investigation of Matrix-Stabilized Methane/Air Combustion in Porous Inert Media.* Combust. Flame, 2000. **123**: p. 201-213.

78.   Curran, H.J., et al., *A Comprehensive Modeling Study of n-Heptane Oxidation.* Combustion and Flame, 1998. **114**(1-2): p. 149-177.

79.   Zamashchikov, V. and E. Tikhomolov, *Sub-critical stable hydrogen-air premixed laminar flames in micro gaps.* International Journal of Hydrogen Energy, 2011. **36**(14): p. 8583-8594.

80.   Evans, C.J. and D.C. Kyritsis, *EXPERIMENTAL INVESTIGATION OF THE EFFECTS OF FLAME PHENOMENOLOGY ON THE WALL TEMPERATURE DISTRIBUTION OF MESOSCALE NONADIABATIC DUCTS.* Combustion Science and Technology, 2011. **183**(9): p. 847-867.

81.   Ellzey, J.L. and I. Schoegl, *Numerical Investigation of Ultra-Rich Combustion in Counterflow Heat Exchangers.* Combustion Science and Technology, 2010. **182**.

82.   Smith, C.H., D.I. Pineda, and J.L. Ellzey, *Syngas Production from Burner-stabilized Methane/Air Flames: The Effect of Preheat.* Combustion and Flame, 2012. **Preparing Minor Revisions for Resubmission**.

83.   Mettler, M.S., G.D. Stefanidis, and D.G. Vlachos, *Scale-out of Microreactor Stacks for Portable and Distributed Processing: Coupling of Exothermic and Endothermic Processes for Syngas Production.* Industrial & Engineering Chemistry Research, 2010. **49**(21): p. 10942-10955.

84.   Norton, D.G. and D.G. Vlachos, *Combustion characteristics and flame stability at the microscale: a CFD study of premixed methane/air mixtures.* Chemical Engineering Science, 2003. **58**(21): p. 4871-4882.

85.   Norton, D.G. and D.G. Vlachos, *A CFD study of propane/air microflame stability.* Combustion and Flame, 2004. **138**(1-2): p. 97-107.

86.   Kaisare, N.S. and D.G. Vlachos, *Optimal reactor dimensions for homogeneous combustion in small channels.* Catalysis Today, 2007. **120**(1): p. 96-106.

87.   Shirsat, V. and A.K. Gupta, *A review of progress in heat recirculating meso-scale combustors.* Applied Energy, 2011. **88**(12): p. 4294-4309.

88.   Kim, Y., et al. *Effect of Scale and Fuel Type on Heat-Recirculation Combustor Performance*. in *U. S. National Meeting, Combustion Institute*. 2007. La Jolla, CA.

89. Lee, M.J., et al., *Scale and material effects on flame characteristics in small heat recirculation combustors of a counter-current channel type.* Applied Thermal Engineering, 2010. **30**: p. 2227-2235.

90. Vijayan, V. and A.K. Gupta, *Combustion and heat transfer at meso-scale with thermal recuperation.* Applied Energy, 2010. **87**(8): p. 2628-2639.

91. Pizza, G., et al., *Dynamics of premixed hydrogen/air flames in microchannels.* Combustion and Flame, 2008. **152**(3): p. 433-450.

92. Pizza, G., et al., *Dynamics of premixed hydrogen/air flames in mesoscale channels.* Combustion and Flame, 2008. **155**(1-2): p. 2-20.

93. Daou, J. and M. Matalon, *Influence of Conductive Heat-Loses on the Propagation of Premixed Flames in Channels.* Combust. Flame, 2002. **128**: p. 321-339.

94. Li, J., et al., *A numerical study on premixed micro-combustion of CH4-air mixture: Effects of combustor size, geometry and boundary conditions on flame temperature.* Chemical Engineering Journal, 2009. **150**(1): p. 213-222.

95. Barra, A.J. and J.L. Ellzey, *Heat Recirculation and Heat Transfer in Porous Burners.* Combust. Flame, 2004. **137**: p. 230-241.

96.   Smith, C.H., D.I. Pineda, and J.L. Ellzey, *Syngas production from burner-stabilized methane/air flames: The effect of preheated reactants.* Combustion and Flame, 2013. **160**(3): p. 557-564.